University of Liège

Faculty of Medicine

Laboratory of Tumour and Development Biology

Promoter: Pr. Didier Cataldo

Impact of exposure to diesel particles on the development of lung cancer

Marie-Laure Delhez

Thesis submitted for the Degree of Doctorate in Biomedical and Pharmaceutical Sciences

Academic year 2024-2025

University of Liège

Faculty of Medicine

Laboratory of Tumour and Development Biology

Promoter: Pr. Didier Cataldo

Impact of exposure to diesel particles on the development of lung cancer

Marie-Laure Delhez

Thesis submitted for the Degree of Doctorate in Biomedical and Pharmaceutical Sciences

Academic year 2024-2025

REMERCIEMENTS

Avant de remercier celles et ceux qui ont accompagné cette aventure, je voudrais dire quelques mots sur ce que cette thèse a représenté pour moi. Une thèse de doctorat, bien au-delà de l'accumulation de savoirs, est une véritable leçon de vie.

Comme dans la vie, on commence avec des certitudes, des plans tracés, des méthodes. Puis on se trompe, on échoue. On persiste parfois dans des voies sans issue, on s'entête. Et puis, on apprend. On réajuste sa méthode, on reformule ses questions, on recommence ses expériences. Peu à peu, on comprend que l'erreur n'est pas un échec, mais une étape. Faire une thèse, c'est apprendre la persévérance. C'est apprendre à transformer ses erreurs en tremplins plutôt qu'en regrets. C'est un travail lent et exigeant qui demande patience et parfois renoncement, mais c'est aussi une aventure profondément formatrice.

Faire une thèse, c'est aussi une formidable aventure humaine, qui se construit au fil des échanges, des conseils, des critiques constructives et des encouragements de celles et ceux qui rendent le chemin plus riche et infiniment plus supportable dans les moments de doute.

Je tiens à remercier Professeur Didier Cataldo pour m'avoir accueillie et donné l'opportunité d'entreprendre cette thèse. Son optimisme inébranlable et sa confiance m'ont permis de garder le cap, même quand les résultats se font attendre. J'aimerais aussi remercier les membres de mon comité de thèse pour leurs contributions lors des différents comités.

Je remercie chaleureusement Marie-Julie, dont l'aide m'a fourni des repères précieux pour avancer et affiner ma démarche. Son professionnalisme et sa rigueur m'ont poussée à me dépasser et pour cela je lui suis sincèrement reconnaissante.

Je remercie tout particulièrement Alison avec qui j'ai commencé ce long périple. Son soutien et son aide concrète pour l'utilisation du FACS ainsi que pour la mise en page du manuscrit ont largement contribué à ce que cette thèse voit le jour. Au-delà de ça, notre relation née dans un cadre professionnel s'est transformée en une amitié qui a marqué mon parcours.

Merci à Lucia Rodriguez-Rodriguez. J'ai eu beaucoup de chance de pouvoir bénéficier de son aide précieuse pour la maîtrise du FACS. Son intelligence, sa rigueur et la passion qu'elle met dans son travail m'ont toujours inspirée. J'ai énormément appris à ses côtés, et je suis convaincue que je ne serais pas arrivée au bout de cette thèse sans son soutien.

Je tiens également à remercier Perrine, ma petite collègue de bureau. Au fil des années, nous nous sommes soutenues mutuellement et épaulées dans les moments de découragement. Je suis heureuse d'avoir traversé ce long chemin en sa compagnie. A nous deux, on en aura bu du café ! Qu'elle n'oublie jamais de croire en elle, je resterai sa plus fidèle supportrice.

Un grand merci à Laura, dont le tempérament de feu, si différent du mien, a pourtant donné naissance à une belle amitié. Je me sens privilégiée d'avoir partagé avec elle de grandes étapes de sa vie (son mariage, ses 30 ans,…), mais aussi des souvenirs inoubliables liés au labo : le congrès à Séville, nos sorties aux Granges, les réunions du club de lecture,… Autant de moments forts, professionnels ou personnels, que je garderai longtemps en mémoire.

Je remercie de tout cœur Maelle, ma super binôme de la team « PMN ». Sa douceur et son professionnalisme ont été pour moi une véritable source d'apaisement et de motivation au quotidien. Son aide pour la réalisation de mes FACS « 3 panels » était plus que précieuse. Je souhaite à tout le monde d'avoir une collègue comme elle.

Merci à Fabienne et Alicia, nos super techniciennes, toujours présentes avec efficacité et bonne humeur. Elles sont les piliers du labo et je suis heureuse d'avoir pu travailler avec elles tout au long de mon parcours. Alicia est un peu le petit clown de la team, souvent à son insu. Je lui souhaite de continuer à perfectionner son anglais, surtout quand je repense à son niveau « par rapport » à celui du début, qu'elle ne lâche rien !

Merci à Benedetta pour nos conversations partagées autour d'un thé/café. Sa présence chaleureuse brillait comme le soleil d'Italie au labo. Nous formions la meilleure team lors des cleaning days ! Je voudrais la remercier pour toutes ses petites attentions.

Merci à Laurine et Marine, alias les *pioupious* ou encore les *sœurs pleureuses* pour leur gentillesse et leur bonne humeur. Elles ont apporté un vrai coup de fraicheur à l'équipe et pourtant, leur présence à rendu l'ambiance bien plus chaleureuse.

Merci à nos voisins du LBTC, Louis et Esther. C'est comme s'ils faisaient partie de l'équipe. Esther a été une formidable étudiante que j'ai eu le plaisir d'encadrer lors de son mémoire. J'ai été très triste de la voir partir, mais heureusement, elle n'est pas allée très loin. Depuis, elle est devenue une confidente précieuse qui a été d'un réel soutien dans une multitude de choses qu'elle seule connait… Merci pour tout.

Après ces sept années de thèse, marquées par tant de rencontres, je sais que vous allez tous inévitablement me manquer. Particulièrement nos rires pendant les temps de midi, qui illuminaient mes journées.

Enfin, un immense merci à ma famille : mes parents, ma sœur, mon « bauf » et les petits, pour le soutien inconditionnel dont ils ont toujours fait preuve. Ils sont mes murs porteurs, ceux qui m'ont tenue à l'abri quand tout semblait s'écrouler. Leur présence m'a permis de tenir debout. Cette thèse, je la leur dois aussi.

ACKNOWLEDGMENTS

Before thanking those who accompanied me throughout this journey, I would like to say a few words about what this thesis has meant to me. A doctoral thesis, far beyond the accumulation of knowledge, is a true life lesson.

Just like in life, you begin with certainties, well-drawn plans, and solid methods. Then come the mistakes, the failures. Sometimes you persist down dead ends, stubbornly hanging on. And then, you learn. You adjust your method, reformulate your questions, redo your experiments. Little by little, you realize that mistakes are not failures, they are steps forward. Doing a PhD means learning perseverance. It means learning to turn your mistakes into steppingstones rather than regrets. It's a slow and demanding process that requires patience and sometimes renunciation, but it is also a deeply formative adventure.

A PhD is also a wonderful human experience, built through exchanges, advice, constructive criticism, and the encouragement of those who made the path richer and infinitely more bearable during moments of doubt.

I would like to thank Pr. Didier Cataldo for welcoming me and giving me the opportunity to undertake this thesis. His unwavering optimism and trust helped me stay the course, even when results were slow to come. I would also like to thank the members of my thesis committee for their contributions throughout the different meetings.

My warmest thanks go to Marie-Julie, whose support gave me valuable guidance to move forward and refine my approach. Her professionalism and rigor pushed me to go beyond my limits, and for that I am sincerely grateful.

A very special thanks to Alison, with whom I began this long journey. Her support and practical help from mastering the FACS to formatting this manuscript were instrumental in bringing this thesis to life. Beyond all that, our professional relationship turned into a true friendship that marked my path in a lasting way.

Many thanks to Lucia Rodriguez-Rodriguez. I was very lucky to benefit from her invaluable help in mastering FACS. Her intelligence, precision, and the passion she puts into her work have always been a great source of inspiration. I learned so much

by her side, and I am convinced I wouldn't have reached the end of this thesis without her support.

I also want to thank Perrine, my dear office mate. Over the years, we supported and encouraged each other through moments of discouragement. I'm grateful to have walked this long road with her. I hope she never stops believing in herself. I will always be her most loyal supporter.

A huge thank-you to Laura, whose fiery temperament, so different from mine, nevertheless gave birth to a beautiful friendship. I feel truly privileged to have shared with her some major moments of her life (her wedding, her 30th birthday…), as well as unforgettable memories from the lab: the congress in Seville, our outings to *Les Granges*, the big Télévie evening… So many personal and professional highlights that I'll carry with me for a long time.

My heartfelt thanks to Maëlle, my partner in the "PMN team." Her calm nature and professionalism were a true source of comfort and motivation every day. Her help with setting up my 3 panel FACS was truly invaluable. I genuinely hope everyone gets the chance to work with someone like her.

Thank you to Fabienne and Alicia, our amazing technicians, always there with efficiency and good humor. They are the pillars of the lab, and I'm grateful to have worked with them throughout my journey. Alicia was a bit like the team's little clown, often without even realizing it. I hope she keeps working on her English, especially when I think back to her level "par rapport à" when she started… Don't give up, you're getting there!

Thank you to Benedetta for our conversations shared over tea or coffee. Her warm presence lit up the lab like the Italian sun. We made the best team during cleaning days! Thank you for all the little thoughtful gestures, they truly meant a lot.

Thanks to Laurine and Marine, the *pioupious*, or sometimes the *weeping sisters* for their kindness and good humor. They brought a real breath of fresh air to the team and yet made the atmosphere even warmer and more welcoming.

Thank you to our LBTC neighbors, Louis and Esther. It felt like you were part of our team. Esther, you were a brilliant student, and it was a pleasure to supervise your master's thesis. I was very sad to see you leave, but thankfully, you didn't go far. Since

then, you’ve become a trusted confidante and a real source of support in countless ways… most of which only you know. Thank you for everything!

After these seven years of doctoral work, marked by so many meaningful encounters, I know I will inevitably miss you all, especially our lunchtime laughs, which never failed to brighten my days.

Finally, my deepest thanks go to my family: my parents, my sister, my “bauf,” and my godchildren, for their constant and unconditional support. They are my pillars, the ones who held me up when everything seemed to fall apart. Their presence kept me standing. This thesis belongs to them.

TABLE OF CONTENTS

LIST OF ABBREVIATIONS

AhR	Aryl hydrocarbon Receptor
ALK	Anaplastic Lymphoma Kinase
AMs	Alveolar Macrophages
APC	Antigen Presenting Cells
ARG-1	Arginase 1
CLP	Common Lymphoid Progenitor
CMP	Common Myeloid Progenitor
COPD	Chronic Obstructive Pulmonary Disease
COX2	Cyclooxygenase-2
CSC	Cancer Stem Cell
CTL	Cytotoxic T lymphocyte
CTLA-4	T-lymphocyte associated protein 4
DAMPs	Damage Associated Molecular Patterns
DEP	Diesel Exhaust Particle
DNA	Deoxyribonucleic acid
EC	Elemental Carbon
EGFR	Epidermal Growth Factor
EMT	Epithelial to Mesenchymal Transition
G-CSF	Granulocyte Colony Stimulating Factor
GMP	Granulocyte Monocyte Progenitor
GSH	Glutathion
GZM	Granzymes
H_2O_2	Hydrogen peroxide
HO-1	Heme-Oxygenase 1
HSC	Hematopoietic Stem Cell
HSPC	Hematopoietic Stem and Progenitor cell
IARC	International Agency for Research on Cancer
ICAM-1	Intercellular Adhesion Molecule 1
IFN-γ	Interferon gamma
IL-10	Interleukin 10
iNOS	Inducible Nitric Oxide Synthase
LCINS	Lung Cancer In Never Smokers
MHC	Major Histocompatibility Complex
MPO	Myeloperoxidase
MPP	Multipotent Progenitor
NE	Neutrophil Elastase
NeP	Neutrophil Progenitors
NETs	Neutrophil Extracellular Traps
NK	Natural Killer
NO	Nitric Oxide

NOX2	NADPH oxidase 1
NSCLC	Non-Small Cell Lung Cancer
O_2-	Superoxide anion
O_3	Ozone
•OH	Hydroxyl radical
OC	Organic Carbon
PAD4	Protein Arginine Deaminase 4
PAH	Polycyclic Aromatic Hydrocarbons
PAMPs	Pathogen Associated Molecular Patterns
PD-1	Programmed cell Death protein 1
PD-L1	Programmed cell Death Ligand 1
PGE2	Prostaglandin E2
PM	Particulate Matter
PMN-MDSC	Polymorphonuclear Myeloid-Derived Suppressor Cells
PMNs	Polymorphonuclear Neutrophils
preNeus	Neutrophil precursors
PSGL-1	P-selectin Glycoprotein Ligand 1
ROS	Reactive Oxygen Species
RTLF	Respiratory Tract Lining Fluid
SCID	Severe Combined Immunodeficiency
SCLC	Small Cell Lung Cancer
SiglecF	Sialic acid binding immunoglobulin-like lectin F
TCR	T cell Receptor
TGFβ	Transofrming Growth Factor beta
TLRs	Toll-Like Receptors
Treg	Regulatory T cell
VEGF	Vascular Endothelial Growth F
WHO	World Health Organization

RESUMÉ-ABSTRACT

RESUMÉ

Les polluants environnementaux tels que les particules de diesel (DEP) sont reconnus pour modifier l'immunité pulmonaire et favoriser la progression de tumeurs. Dans cette étude, nous avons examiné comment l'exposition aux DEP façonne le paysage immunitaire pulmonaire, en mettant particulièrement l'accent sur la régulation immunitaire médiée par les neutrophiles et l'état fonctionnel des populations lymphocytaires. Nous avons également examiné comment ces altérations peuvent contribuer à l'établissement d'un microenvironnement immunitaire favorable au développement des tumeurs.

L'exposition aiguë au DEP chez la souris a entraîné un recrutement important de polymorphonucléaires neutrophiles (PMN) dans les poumons, avec l'émergence d'un sous-ensemble distinct de PMN $CD14^{pos}$, absent de la rate. Ces neutrophiles $CD14^{pos}$ présentent les caractéristiques des cellules suppressives polymorphonucléaires dérivées des myéloïdes (PMN-MDSC), notamment une formation accrue de NETs, une expression augmentée des gènes immunosuppresseurs (ex. : Arg1, Nos2, Cd274, Ptgs2, Il10, Tgfb) et des marqueurs de surface tels que PD-L1 et Siglec-F. Sur le plan fonctionnel, ils entravent la prolifération des cellules T $CD8^{+}$ ex vivo.

Dans un modèle d'exposition chronique au DEP, ce profil immunosuppresseur est amplifié, avec une accumulation persistante de PMN $CD14^{pos}$ exprimant des niveaux élevés de CD73 et de SIRPα, ce qui suggère un renforcement de l'immunosuppression et de l'évasion immunitaire médiées par l'adénosine. Alors que le nombre total de cellules T est resté inchangé, les cellules T $CD4^{+}$ et $CD8^{+}$ résidant dans le poumon ont montré des signes d'épuisement fonctionnel, notamment une expression élevée de PD-1, CD39 et LAG3, ainsi qu'une augmentation marquée des cellules T régulatrices (Tregs).

En utilisant un modèle murin d'adénocarcinome pulmonaire $Kras^{LSL\text{-}G12D/+}$-$Trp53^{lox/lox}$, nous montrons que l'exposition chronique au DEP favorise la progression tumorale, comme en témoignent l'augmentation de la taille des nodules tumoraux, une prolifération cellulaire plus élevée (Ki67), des signes d'épuisement fonctionnel des cellules T et une expansion des Tregs. Ce phénomène s'accompagne d'une

augmentation du nombre total de PMN et des populations de PMN CD14^{pos} dans les poumons des souris exposées au DEP. Ces résultats démontrent que le DEP modifie le paysage immunitaire en favorisant un phénotype suppressif des neutrophiles et en altérant la fonction lymphocytaire antitumorale, ce qui contribue finalement à créer un microenvironnement propice au développement des tumeurs pulmonaires.

ABSTRACT

Environmental pollutants such as diesel exhaust particles (DEP) are recognized to modify lung immunity and promote tumour progression. In this study, we investigated how DEP exposure reshapes the pulmonary immune landscape, with a particular focus on neutrophil-mediated immune regulation and the functional state of lymphocyte populations. We also examined how these alterations may contribute to the establishment of an immune microenvironment permissive to tumour development.

Acute DEP exposure in mice led to significant recruitment of polymorphonuclear neutrophils (PMNs) in the lungs, with the emergence of a distinct $CD14^{pos}$ PMN subset absent from the spleen. These $CD14^{pos}$ neutrophils exhibited features of polymorphonuclear myeloid-derived suppressor cells (PMN-MDSCs), including increased NET formation, upregulation of immunosuppressive genes (e.g., Arg1, Nos2, Cd274, Ptgs2, Il10, Tgfb), and surface markers such as PD-L1 and Siglec-F. Functionally, they impair $CD8^{+}$ T cell proliferation ex vivo.

Chronic DEP exposure further amplified this immunosuppressive profile, with persistent accumulation of $CD14^{pos}$ PMNs expressing high levels of CD73 and SIRPα, suggesting enhanced adenosine-mediated suppression and immune evasion. While total T cell numbers were unchanged, lung-resident $CD4^{+}$ and $CD8^{+}$ T cells exhibited signs of functional exhaustion, including elevated expression of PD-1, CD39, LAG3, and a marked increase in regulatory T cells (Tregs).

Using a $Kras^{LSL\text{-}G12D/+}$-$Trp53^{lox/lox}$ (KP) mice lung adenocarcinoma mouse model, we show that chronic DEP exposure promotes tumour progression, as evidenced by increased tumour size, higher proliferation (Ki67), signs of functional T cell exhaustion and Treg expansion. This was accompanied by an increase in both total PMN counts and $CD14^{pos}$ PMN populations in the lungs of DEP-exposed mice. These findings demonstrate that DEP reshapes the immune landscape by promoting a suppressive neutrophil phenotype and impairing anti-tumour lymphocyte function, ultimately contributing to a microenvironment permissive to lung tumour growth.

INTRODUCTION

INTRODUCTION

1. Air pollution

Air pollution is defined as the contamination of the atmosphere by any substances that are harmful to humans and other living organisms. These pollutants can be solid, liquid, or gaseous and are released in concentrations higher than normal, significantly diminishing environmental quality and causing serious health risks (Manisalidis et al., 2020).

Human activities, particularly since the onset of the Industrial Revolution, have led to the emission of huge quantities of pollutants into the air. Anthropogenic air pollution has emerged as one of the most significant public health threats globally. Both outdoor (ambient) and indoor air pollution contribute significantly to disease and premature death worldwide. Outdoor pollution originates from sources such as industrial facilities, motor vehicles, and combustion of fossil fuels, while natural events like volcanic eruptions and forest fires also play a role. Indoor air pollution, on the other hand, is mainly present in developing regions, where polluting fuels such as kerosene, wood, animal dung and coal are still widely used for cooking and heating, often in poorly ventilated spaces. Whether indoors or outdoors, air pollution can cause a wide range of health issues, including strokes, heart disease, lung cancer, and both acute and chronic respiratory diseases. According to the World Health Organization (WHO), the combined effects of ambient and household air pollution are estimated to result in approximately 7 million premature deaths each year making it the 4th leading risk factor for early death worldwide (WHO, 2025).

WHO identifies five major air pollutants: particulate matter (PM), ground-level ozone (O_3), carbon monoxide (CO), sulfur oxides (SO_2), and nitrogen oxides (NO_2). Among them, O_3 and PM are the most prevalent and hazardous. PM, especially in its fine and ultrafine forms, is among the most dangerous pollutants.

2. Particulate matter (PM)

2.1 Guidelines

As reported by WHO data from 2019, 99% of the world's population lived in areas where air quality failed to meet recommended guidelines. Low- and middle-income countries were the most affected with highest exposures and most premature deaths linked to air pollution.

The World Air Quality Report 2024, published by IQAir, provides an extensive global review of air quality data, focusing on $PM_{2.5}$ concentrations as a key indicator of air pollution. Scientists analysed data from 40,000 air quality monitoring stations across 954 locations in 138 countries. Alarmingly, only seven countries met the WHO's average concentration guideline for $PM_{2.5}$, fixed at 5 µg/m³: Australia, the Bahamas, Barbados, Estonia, Grenada, Iceland, and New Zealand. The five most polluted countries in 2024 were Chad (91,8 µg/m³), Bangladesh (78 µg/m³), Pakistan (73,7 µg/m³), the Democratic Republic of Congo (58,2 µg/m³), and India (50,6 µg/m³). In Belgium, the $PM_{2.5}$ annual average concentration was 8,89 µg/m³, 1,8 times higher than the WHO recommended threshold (IQAir, 2024).

2.2 Classification and source of PM

PM refers to a complex mixture of solid and liquid particles suspended in the air, varying widely in size, origin, and chemical composition. PM is commonly classified based on its aerodynamic diameter. Coarse particles (PM_{10}) have diameters of 10 µm or less, fine particles ($PM_{2.5}$) are 2,5 µm or smaller, and ultrafine particles are defined as having diameters below 0,1 µm (**Fig. 1**). Due to their small size, fine and ultrafine particles can remain suspended in the atmosphere for extended periods (ranging from days to weeks) and travel over long distances, sometimes spanning hundreds of kilometres (L. Wang et al., 2021). $PM_{2.5}$ represents one of the most widespread forms of air pollution.

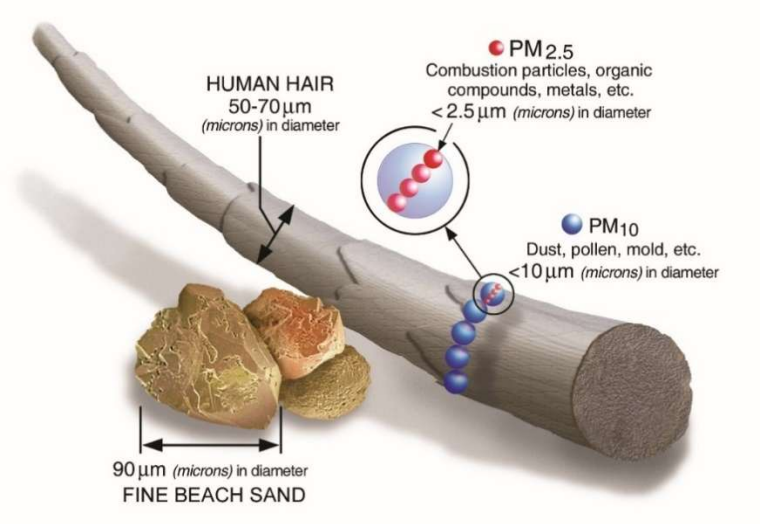

Figure 1. Size of $PM_{2.5}$ and PM_{10} in comparison to the average diameter of a human hair (~70µm) and fine beach sand (~90µm) (Guaita et al., 2011)

The sources, size, and physicochemical as well as toxicological properties of $PM_{2.5}$ particles vary considerably, with their chemical composition being highly heterogeneous and strongly dependent on their origin. PM may contain a wide array of components, including elemental carbon (EC) and organic carbon (OC), inorganic ions (e.g., nitrates, sulfates, ammonium, sodium, potassium, calcium, magnesium, and chloride), polycyclic aromatic hydrocarbons (PAHs), biological materials (such as allergens and microbial agents), as well as trace metals (e.g., iron, copper, nickel, zinc, and vanadium) (Thangavel et al., 2022). Recent evidence highlights that the adverse health effects of $PM_{2.5}$ are not uniform but depend strongly on their chemical composition. For instance, a large nation-wide Danish study including 678,465 deaths reported that primary emitted $PM_{2.5}$ components such as dust, EC and OC were associated with increased mortality from natural causes, respiratory disease and lung cancer, but paradoxically with lower cardiovascular mortality. In contrast, secondary inorganic components of $PM_{2.5}$, including sulfate (SO_4), nitrate (NO_3) and ammonium (NH_4), were linked to higher risks of natural cause and cardiovascular mortality, but to reduced respiratory disease mortality (Raaschou-Nielsen et al., 2023).

These airborne particles can originate from both anthropogenic and natural sources, while others develop from precursor compounds via atmospheric chemical reactions. Human activities such as the combustion of solid fuels, industrial and agricultural

practices, road traffic (including pavement erosion and the abrasion of brakes and tires) are significant contributors to $PM_{2.5}$ emissions. In parallel, natural phenomena including volcanic eruptions, dust storms, and forest fires also play a role in $PM_{2.5}$ release (Ryou et al., 2018). For instance, a study in Bangkok reported that $PM_{2.5}$ included vehicular exhaust (43,7%), biomass burning (24%), sea salt aerosol (10,5%), power plant (6,48%) and industrial emissions (4,46%) (ChooChuay et al., 2020). This suggests that the majority of $PM_{2.5}$ sources originate from human activities and can significantly influence local air quality.

Among the various sources of $PM_{2.5}$, this study will focus on diesel exhaust particles (DEP), which are primarily emitted by transportation activities. Road traffic, especially vehicles powered by diesel engines, represents a major contributor to urban atmospheric pollution. DEPs are a significant component of $PM_{2.5}$ in cities and are known for their complex composition and potent adverse health effects (Popovicheva et al., 2015).

For our experiments, we used SRM 1650b, a standardized reference diesel particulate matter developed by the National Institute of Standards and Technology (NIST). This material is derived from real diesel exhaust generated under controlled conditions, providing a reproducible and well-characterized mixture of carbonaceous particles and organic compounds including PAHs. SRM 1650b is widely used for calibrating analytical assays, comparing results across laboratories, and as a benchmark in toxicological studies of diesel exhaust. Its detailed Certificate of Analysis (**Annex 1**) includes information on particle size distribution, surface area, certified concentrations of various PAHs, and physical characteristics.

2.3 Diesel exhaust particles (DEP)

Diesel engine emissions are among the most widespread human-made pollutants worldwide. Originally developed in the late 19th century, diesel engines quickly became central for heavy-duty applications in industries such as manufacturing, marine transport, railways, and military sectors. It wasn't until the late 1980s that advancements in diesel systems made their use practical in lighter vehicles and personal transportation. Since then, diesel engines have gained popularity thanks to their long-lasting performance and superior fuel economy compared to gasoline-powered vehicles.

Diesel exhaust is a complex mixture made of solid, liquid, and gaseous components. The solid portion contains primary particles, typically 10-30 nanometers in diameter, composed of elemental carbon. These primary particles often cluster into larger agglomerates. Beyond carbon, this fraction includes metals introduced in fuel additives, such as zinc, magnesium, iron, manganese, platinum, and copper. Under the high temperatures within the combustion chamber, these metals can vaporize, condense, and nucleate, becoming embedded into the carbon core (Steiner et al., 2016).

Elemental carbon itself is highly biopersistent, but the overall harmful effects of the particles are largely determined by toxic substances adhered to their surfaces. During combustion, polycyclic aromatic hydrocarbons (PAHs) undergo oxidation, forming quinones that bind to carbon particles, chemically activating them. These activated particles can engage in redox reactions that generate reactive oxygen species (ROS), including hydrogen peroxide (H_2O_2). Additionally, the embedded metals may catalyse Fenton-type reactions, contributing further to oxidative stress (Antiñolo et al., 2015).

The composition of diesel exhaust depends on factors such as engine design, the use of after-treatment systems, and the makeup of fuels and lubrication additives. Technologies to reduce particulate emissions have evolved, including diesel particulate filters, selective catalytic converters, optimized combustion techniques, and the adoption of cleaner fuels like biodiesel (Khalek et al., 2015). While many countries have improved air quality through these innovations and the rise of electric vehicles, severe pollution remains in several developing regions. This is largely due to older

diesel vehicles still in operation and the lack of stringent emissions regulations, as seen in countries like India (McClellan et al., 2012).

The Euro classification system, established by the European Union, sets emission standards for vehicles, particularly targeting pollutants like nitrogen oxides (NOx) and PM from diesel engines. Introduced in the early 1990s and regularly updated (Euro 1 to Euro 6 and beyond), these standards have progressively tightened limits on vehicle emissions. This classification allowed European cities to identify and regulate high-polluting vehicles, especially older diesel cars. Many urban areas implemented Low Emission Zones (LEZs), restricting or banning vehicles below a certain Euro standard (European Commission, n.d.). As a result, cities reduced air pollution and encouraged the adoption of cleaner, more efficient diesel technologies.

2.4 Impact of PM on health

Ambient particulate air pollution is a major environmental health issue with a wide range of negative effects on human health including cardiovascular, respiratory diseases and lung cancers. The severity of these effects is supported by epidemiological studies conducted across various regions of the world, which have consistently demonstrated a positive correlation between increased mortality and exposure to ambient particulate air pollution (Liu et al., 2019; Lelieveld et al., 2020). Particle induced biological effects will depend on particles properties such as size and composition.

The respiratory tract, with an internal surface area of approximately 100 m², is specialized for gas exchange between inhaled air and the bloodstream. It is anatomically divided into three main regions: the nasopharyngeal, the tracheobronchial, and the alveolar regions. The tracheobronchial region includes the trachea, bronchi (main, lobar, and segmental), and bronchioles. The alveolar region consists of alveolar bronchioles and alveoli, the only sites where gas exchange occurs (Xia et al., 2016).

The health impacts of PM are closely linked to particle size. Defence mechanisms against inhaled particles vary by region. In the upper respiratory tract, larger particles (>10 μm) are typically trapped in the mucus and expelled via reflexes like sneezing and coughing. Mucociliary clearance, which helps move trapped particles upward, decreases progressively toward the alveolar region. In the alveoli, where mucociliary

action is absent, alveolar macrophages provide the primary defence by engulfing inhaled particles. However, this clearance is slower, and some particles may translocate across the epithelium into the bloodstream or lymphatic system. Finer particles, particularly $PM_{2.5}$ and ultrafine particles, can evade upper airway defences and reach the alveoli. There, they may disrupt respiratory function and enter systemic circulation, contributing to serious health outcomes (Xia et al., 2016) (**Fig. 2**).

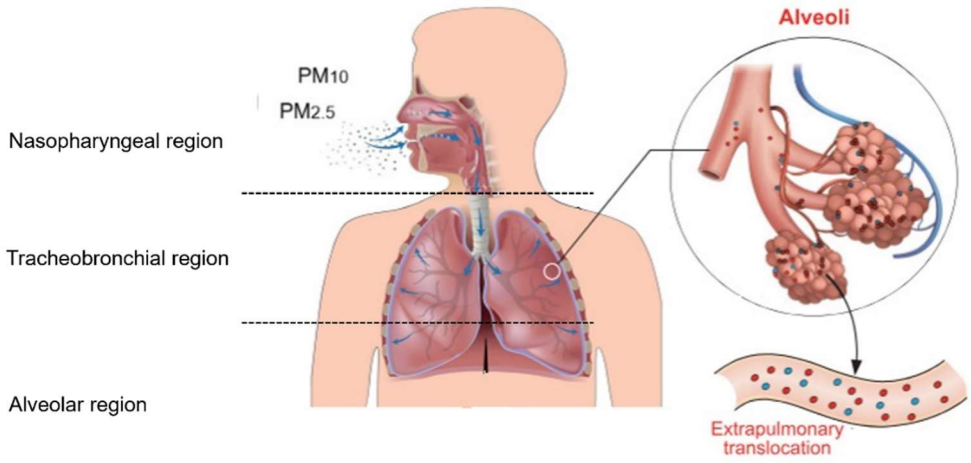

Figure 2. Deposition of inhaled particles in the human respiratory tract. *Adapted from Xia et al., 2016.*

Both in vitro and in vivo studies have sought to elucidate the biological mechanisms underlying the adverse health effects associated with PM exposure. Among these mechanisms, oxidative stress has emerged as a central pathway of PM-induced toxicity. This process is initiated by the excessive generation of ROS, which overwhelms the endogenous antioxidant defence systems, thereby shifting the cellular redox balance toward a pro-oxidant state (Santibáñez-Andrade et al., 2023). Free radicals are highly reactive molecules with a very short half-life, owing to the presence of an unpaired electron in their outer orbital. This instability drives them to rapidly interact with surrounding molecules, leading to oxidative damage (Martemucci et al., 2022). ROS include all metabolites of molecular oxygen (O_2) that are reduced to different intermediate species such as superoxide anion (O_2^-) and hydroxyl radical (•OH) as well as non-radicals such as hydrogen peroxide (H_2O_2). The resulting oxidative stress can lead to direct molecular damage, including DNA strand breaks, protein carbonylation, and lipid peroxidation (Czerska et al., 2015).

The toxic potential of PM is also closely related to its physicochemical composition. The induction of oxidative stress by PM is thought to be caused by both heavy metal and organic compound components of PM. Transition metals such as iron or copper can catalyse the formation of •OH through the Fenton reaction, further exacerbating oxidative damage. Additionally, organic compounds like PAHs can generate ROS via the quinone redox cycle, a process mediated by biotransformation enzymes such as cytochrome P450. These enzymes transfer electrons to O_2, producing O_2^- that substantially increase intracellular ROS levels (Bolton and Dunlap, 2017).

2.4.1 PM-associated respiratory diseases

Lung is the first entrance of PM explaining that both acute and chronic exposure to PM lead to respiratory symptoms. Exposure to air particulate matter is particularly problematic for children, elderly people or adult with pre-existing chronic diseases.

Emerging evidence shows that exposure to PM begins as early as the first trimester of pregnancy. Black carbon particles have been detected in the placenta, with the potential to migrate toward the foetus's liver, lungs, and brain (Bongaerts et al., 2022). Maternal exposure to air pollution has been associated with adverse birth outcomes, including preterm birth, low birth weight, and long-term health complications in children (X. Li et al., 2017; Klepac et al., 2018).

Beyond birth, several studies have reported the detrimental effects of PM on children's lung development and function (Garcia et al., 2021), along with increased rates of hospitalization due to respiratory conditions such as pneumonia, asthma, and bronchitis (Ünal et al., 2022). Traffic-related air pollution has been clearly linked to both the onset and aggravation of childhood asthma (Boogaard et al., 2022) as well as allergic diseases (Bowatte et al., 2015). Animal studies further have demonstrated that *in utero* exposure to PM at concentrations near WHO guideline levels has been shown to suppress early immune responses to allergens, predisposing neonates to respiratory infections and impairing long-term lung health (Rychlik et al., 2019)

Elderly individuals are also particularly vulnerable to the harmful effects of air pollution. Long-term exposure to PM has been linked to an increased risk of hospital admissions for both cardiovascular and respiratory diseases (Danesh Yazdi et al., 2021). This increased susceptibility may be partly due to an age-related decline in immune defence mechanisms. Specifically, older adults tend to accumulate more particulate matter in

the macrophages of lung-associated lymph nodes, leading to reduced macrophage activation and phagocytic activity (Ural et al., 2022), thereby compromising their ability to respond to pathogens effectively.

Chronic obstructive pulmonary disease (COPD) is a chronic inflammatory lung condition characterized by a persistent and progressive airflow limitation due to remodeling of the bronchi causing respiratory symptoms. Individuals with pre-existing conditions such as COPD are particularly vulnerable to the adverse effects of air pollution, facing higher risks of hospital readmission and increased mortality rates following exposure to polluted air (Heinrich and Schikowski, 2018).

2.4.2 PM-associated cardiovascular diseases

Cardiovascular effects of inhaled PM account for a significant proportion of the morbidity and mortality associated with air pollution. Epidemiological studies have demonstrated clear associations between air pollution and a range of cardiovascular diseases, including atherosclerosis (Jilani et al., 2020), elevated blood pressure due to vascular constriction (Qin et al., 2021), cardiac arrhythmias (Feng et al., 2019), heart failure (Yang et al., 2022), and venous thromboembolism (Renzi et al., 2020).

Pulmonary exposure to PM in rodent models of atherosclerosis has supported these epidemiological studies that link traffic-related air pollution to increased hospital admissions for acute myocardial infarction (Miller et al., 2015). Other experimental evidence shows that PM exposure enhances coagulation by elevating blood levels of fibrinogen, thrombin, von Willebrand factor, and platelet activity, while simultaneously shortening ex vivo coagulation times (Robertson and Miller, 2018; Lei et al., 2021).

Several biological mechanisms have been proposed to explain the cardiovascular effects of PM exposure. One such mechanism is “particle translocation”, in which ultrafine particles are small enough to cross the pulmonary epithelial barrier and enter the bloodstream. Once in circulation, these particles can be transported to distant sites within the cardiovascular system, potentially exerting harmful effects (Oberdörster et al., 2002). Traffic-related PM, particularly DEP, is rich in redox-active organic compounds such as PAHs and quinones. These components can generate ROS, thereby inducing oxidative stress upon cellular contact. DEP can trigger a cascade of oxidative responses through multiple cellular pathways, leading to the oxidation of key cellular structures, including lipids, proteins and DNA. In addition, the activation of

inflammatory cells in the lungs by inhaled pollutants can result in the release of pro-inflammatory mediators. These mediators not only sustain local inflammation but may also enter the circulation, contributing to systemic inflammation and subsequently affecting cardiovascular homeostasis (Miller and Newby, 2020).

A further proposed mechanism involves the activation of alveolar receptors by inhaled pollutants, which stimulates sensory afferent pathways and alters cardiovascular regulation through changes in autonomic nervous system balance and endocrine release. Exposure to PM has been associated with changes in heart rate variability (HRV) (Lee et al., 2020), indicating a shift from decreased parasympathetic to enhanced sympathetic activity, both of which are linked to increased cardiovascular risk.

Many of the cardiovascular effects of PM could exacerbate the pathophysiology of diseases such chronic kidney disease through elevated blood pressure, impaired renal perfusion or inflammation. Vascular effects of air pollution are also linked to stroke for which atherosclerosis is a plausible mechanism by which PM could induce stroke. It has also been described that PM is associated with extrapulmonary effects such as impacts on cognitive development and neurodegenerative disorders (Lin et al., 2022; Calderón-Garcidueñas et al., 2023).

2.4.3 PM-associated lung cancer

DEP has been classified as a Group 1 carcinogen by the International Agency for Research on Cancer (IARC), based on converging evidence from epidemiological studies, animal models, and in vitro genotoxicity assays (IARC, 2014). Since this classification, an expanding body of research has further strengthened the link between PM exposure and lung cancer incidence.

Among these studies, a landmark prospective cohort analysis, part of the European Study of Cohorts for Air Pollution Effects (ESCAPE), pooled data from 17 cohorts across 9 European countries, encompassing an average follow-up of 12.8 years. The findings confirmed a significant association between long-term exposure to $PM_{2.5}$ and the incidence of lung cancer (Raaschou-Nielsen et al., 2013). More recently, a multi-center study which include England, South Korea, and Taiwan demonstrated a consistent relationship between ambient $PM_{2.5}$ levels and the estimated incidence of EGFR-driven lung cancer across different populations and $PM_{2.5}$ concentration ranges.

Strikingly, this study also found that just three years of exposure to air pollution could be sufficient to initiate this association (Hill et al., 2023). Additionally, $PM_{2.5}$ exposure has been associated not only with an increased risk of lung cancer, but also with elevated mortality from other types of cancer of extrapulmonary organs (Kim et al., 2018).

In addition to epidemiological evidence, experimental studies offer compelling mechanistic insights into the biological effects of $PM_{2.5}$. Both in vitro and in vivo models have substantiated its oncogenic potential. These mechanisms will be explored in greater detail in the section dedicated to the effects of particulate matter on cancer hallmarks.

3. Lung cancer

3.1 Overview

Lung cancer remains the leading cause of cancer-related mortality worldwide, accounting for approximately 18% of all cancer deaths. It is the second most common cancer diagnosis by gender, behind prostate cancer for men and breast cancer for women. Over recent decades, a decline in lung cancer incidence has been observed, largely attributed to changes in smoking behaviours influenced by public health campaigns and the implementation of governmental tobacco control policies. Lung cancer may originate within the lungs (primary lung cancer) or result from metastasis of malignancies elsewhere in the body (secondary lung cancer). Unfortunately, diagnosis frequently occurs at an advanced stage, contributing to a persistently poor prognosis (Thandra et al., 2021).

Survival

Lung cancer is among the malignancies with the poorest survival outcomes, comparable to those of liver and pancreatic cancers. Significant regional disparities exist across Northern, Southern, Eastern, and Central Europe. This poor prognosis is largely attributed to the fact that the disease is often diagnosed at an advanced stage. (van Meerbeeck and Franck, 2021). Nonetheless, survival rates have shown a modest but steady improvement in recent years, largely due to earlier detection, particularly through recommended low-dose computed tomography (CT) screening for individuals with a significant smoking history, and significant advances in treatment. The

development of targeted therapies (e.g., EGFR, ALK, ROS1, and BRAF inhibitors) and immune checkpoint inhibitors (targeting PD-1, PD-L1, and CTLA-4) has markedly expanded therapeutic options and contributed to improved clinical outcomes (Schabath and Cote, 2019).

Histological classification

Lung cancer is highly heterogeneous histologically. According to the WHO classification, is broadly divided into two major categories: non-small cell lung carcinoma (NSCLC) and small-cell lung carcinoma (SCLC).

NSCLC represents around 85% of all lung cancers which regroup several histological subtypes including adenocarcinoma (40%), squamous cell carcinoma (25-30%) and large cell carcinoma (10-15%). Adenocarcinoma is the most prevalent subtype, particularly among non-smokers, and typically arises in the peripheral regions of the lung. It is subdivided into five distinct subtypes: lepidic, acinar, papillary, micropapillary and solid. It is frequently associated with driver mutations such as epidermal growth factor (EGFR), anaplastic lymphoma kinase (ALK) rearrangements, KRAS and BRAF. In contrast, squamous cell carcinoma is strongly linked to tobacco exposure and generally originates in the central airways, characterized histologically by keratinization and intercellular bridges. Large cell carcinoma represents a poorly differentiated NSCLC subtype that lacks glandular or squamous features and is often diagnosed by exclusion (Schabath and Cote, 2019; WHO, 2021).

The remaining 15% of lung cancer are classified as small cell lung carcinoma (SCLC), an aggressive neuroendocrine tumour with rapid progression, early metastatic spread, poorly responsive to therapy and poor prognosis. SCLC is highly associated with smoking and typically presents as a centrally located mass (Kalemkerian et al., 2013).

Risk factors

Tobacco smoking is unequivocally the leading risk factor in the development of lung cancer, with up to 90% of cases attributed to this behaviour. However, only approximately 15% of smokers ultimately develop lung cancer, reflecting the interplay of additional risk factors and individual susceptibility (Schabath and Cote, 2019). Tobacco smoke contains more than 7,000 chemicals, including at least 69 known

carcinogens and numerous other toxic substances associated with a broad range of diseases (Hiscock et al., 2012). The relative risk of developing lung cancer among smokers is estimated to be up to 20 times higher than that of individuals who have never smoked, and this risk is directly correlated with smoking intensity and duration (the number of cigarettes smoked per day and the total years of smoking).

In addition to behavioural risk factors such as tobacco use, several environmental exposures contribute significantly to lung cancer pathogenesis. Among these, radon, a naturally occurring radioactive gas resulting from uranium decay in the soil, has mutagenic properties and is recognized as the second leading cause of lung cancer, responsible for an estimated 10% of cases. Asbestos, a material historically used in construction, is another well-documented risk factor; it can deposit persistent fibres in the lungs, triggering inflammatory and carcinogenic responses. Chronic respiratory infections, such as those caused by tuberculosis, HIV, or COPD, have also been implicated due to their potential to induce sustained inflammation and cellular damage. Furthermore, exposure to airborne particulate matter, whether from outdoor pollution, indoor biomass combustion, or occupational environments, poses an additional risk (Schabath and Cote, 2019).

As smoking prevalence has declined, an increasing proportion of lung cancers are now being diagnosed in individuals who have never smoked, a subset known as lung cancer in never smokers (LCINS). This trend is particularly evident among women and younger populations (Pelosof et al., 2017). LCINS is characterized by distinct histopathological and epidemiological features, being predominantly composed of adenocarcinomas and more frequently observed in female patients, with a higher incidence rate among women in east Asia (Ha et al., 2015; Devarakonda et al., 2021). Moreover, mounting evidence indicates that LCINS is genomically and molecularly distinct from smoking-related lung cancers, with a high prevalence of targetable oncogenic alterations such as EGFR mutations, ALK rearrangements, and other less common genomic events. These differences necessitate tailored diagnostic and therapeutic strategies. Data have also highlighted the role of genetic susceptibility and its interaction with environmental factors in the aetiology of LCINS, underscoring the complexity of lung cancer pathogenesis (LoPiccolo et al., 2024).

3.2 Effect of particulate matter on cancer hallmarks

The concept of the "hallmarks of cancer" was first articulated by Hanahan and Weinberg in 2000, providing an organizing principle to understand the complex and multifactorial nature of cancer development. These hallmarks represent a set of functional capabilities that are commonly acquired during the multistep transformation of normal cells into malignant ones. Initially, six core hallmarks were identified: sustaining proliferative signalling, evading growth suppressors, resisting cell death, enabling replicative immortality, inducing angiogenesis, and activating invasion and metastasis. Together, these features allow cancer cells to grow uncontrollably, avoid regulatory signals that limit proliferation, resist programmed cell death, bypass normal cellular aging, recruit blood vessels to supply the tumour with nutrients, and invade surrounding tissues and distant organs (Hanahan and Weinberg, 2000).

In 2011, the original organizing principle was expanded to include two additional hallmarks capabilities: deregulating cellular energetics and avoiding immune destruction. In parallel, two enabling characteristics were added: genome instability and mutation, which facilitates the acquisition of other hallmark traits, and tumour-promoting inflammation, which creates a supportive microenvironment for tumour progression. These additions reflected advances in cancer biology and recognized the broader biological context in which tumours evolve (Hanahan and Weinberg, 2011).

Further refinement of the model came in 2022, with the proposal of additional emerging traits that contribute to tumour development and progression. These include non-mutational epigenetic reprogramming, the influence of polymorphic microbiomes and the presence of senescent cells. Together, these insights underscore the dynamic and adaptable nature of cancer and highlight the importance of both intrinsic cellular mechanisms and extrinsic environmental factors in its pathogenesis (Hanahan, 2022).

PM actively contributes to tumour development by promoting the acquisition of key biological capabilities involved in the cancer continuum. To explore its role in lung carcinogenesis, the hallmarks of cancer will serve as a framework to illustrate how PM facilitates the emergence of specific cellular traits associated with each hallmark.

3.2.1 Sustained proliferative signalling

Chronic proliferation is by far the main feature of cancer cells necessary to start malignant transformation. In vitro, $PM_{2.5}$ such as DEP has been shown to enhance

proliferation of human lung cancer cell lines, including A549 (adenocarcinomic alveolar basal cells) and H1299 (non-small cell lung carcinoma) by upregulating IL1β and MMP1 expression (Yang et al., 2016) or by inducing autophagy-related genes (Niranjan et al., 2021). In addition $PM_{2.5}$ is also described to induce cell proliferation of A549 in vitro and in vivo via the Wnt3a/β-catenin pathway through the release of exosomes (Xu et al., 2019).

3.2.2 Cell death resistance

The anti-apoptotic effects induced by PM have been extensively studied, revealing the involvement of several signalling pathways. These include mechanisms that promote apoptosis evasion through STAT3 activation (Reyes-Zárate et al., 2016), as well as pro-survival pathways such as the PI3K-Akt signalling cascade (Merk et al., 2020). In the same study, Merk et al. also demonstrated that $PM_{2.5}$ exposure triggers antioxidant responses that may contribute to chemoresistance. Notably, long-term exposure to $PM_{2.5}$ was shown to activate the transcription factor Nrf2 via the JNK1/2 pathway, leading to an enhanced antioxidant response. This response involves increased intracellular glutathione (GSH) levels and the nuclear accumulation of heme oxygenase-1 (HO-1), a key antioxidant enzyme (Merk et al., 2020).

Autophagy is another cell-physiological response involved in apoptotic resistance. As an example, the long non-coding RNA LCPAT1 is induced following exposure of human lung adenocarcinoma cell line (H1299) and squamous cell carcinoma cell line (H520) to $PM_{2.5}$ which up-regulates autophagy and promotes lung cancer progression (Lin et al., 2018).

3.2.3 Induction of angiogenesis

PM has been shown to promote the formation of multiple microvessels and a dense inflammatory infiltrate in the chick embryo chorioallantoic membrane (CAM) assay (Catino et al., 2017). Furthermore, using a microfluidic system designed to mimic the alveolar microenvironment, where BEAS-2B (bronchial epithelial cells) and HPMEC (human pulmonary microvascular endothelial cells) were cultured in separate channels, it has been demonstrated that exposure to $PM_{2.5}$ activates signalling pathways that support angiogenesis (Zheng et al., 2019).

In tumour-bearing mice, exposure to $PM_{2.5}$ was associated with accelerated tumour progression and increased expression of vascular endothelial growth factor (VEGF).

Additionally, analysis of blood serum using an angiogenesis antibody array revealed elevated levels of 12 angiogenic factors following $PM_{2.5}$ exposure (Yang and Xiao, 2018). $PM_{2.5}$ has also been shown to activate macrophages, which upregulate angiogenic cytokines that promote angiogenesis in lung cancer (R. Li et al., 2020).

3.2.4 Activation of invasion and metastasis

$PM_{2.5}$ has been implicated in promoting cancer cell invasion through the induction of epithelial-to-mesenchymal transition (EMT), a key process in cancer progression. Studies have shown that $PM_{2.5}$ exposure can trigger EMT in various lung cell lines, including A549 and H292 cells (Marchetti et al., 2021; Wei et al., 2017; Yang et al., 2017). In particular, $PM_{2.5}$-treated A549 cells exhibited more than a twofold increase in migratory capacity compared to untreated controls (Colín-Val et al., 2024). Chronic exposure to $PM_{2.5}$ has also been shown to enhance the invasive behaviour of multiple human lung adenocarcinoma cell lines such as H1299, HCC827, and A549, as well as BEAS-2B bronchial epithelial cells in vitro. Furthermore, this invasive phenotype was accompanied by the upregulation of cancer stem cell (CSC)-related genes, suggesting that $PM_{2.5}$ may contribute not only to enhanced invasiveness but also to the acquisition of stem-like properties (Pan et al., 2022; Wei et al., 2017). Data from toxicological in vitro assays and global transcriptome profiling have shown that cells exposed to PM exhibit both an upregulation and increased activity of metalloproteases, leading to enhanced ability of invasion (Morales-Bárcenas et al., 2015; Taş et al., 2019).

In vivo studies corroborate these findings. $PM_{2.5}$ has been shown to promote tumorigenesis and metastasis of lung adenocarcinoma cells in severe combined immunodeficiency (SCID) mouse models (Yang and Xiao, 2018; Pan et al., 2022). However, recent evidence indicates that the presence of a competent immune system is critical for PM-enhanced tumour development. DEP-induced neutrophilic inflammation, for instance, has been implicated in promoting lung tumour metastasis (Li et al., 2018). In addition, Liu at al. demonstrated the central role of PM-induced neutrophil recruitment in promoting lung cancer metastasis. They found that ROS-mediated alveolar epithelial autophagy initiate neutrophil chemotaxis and pre-metastatic niche formation (Liu et al., 2022). Furthermore, PM exposure has been shown to trigger the recruitment of macrophages into lung tissue, an essential event in the promotion of EGFR-driven adenocarcinoma (Hill et al., 2023).

3.2.5 Inflammation and oxidative stress

Under physiological conditions, ROS, including free radicals such as O_2^-, •OH, and H_2O_2, are naturally produced as by cellular metabolism. These molecules are tightly regulated by endogenous antioxidant defences, including antioxidant enzymes, which help maintain redox homeostasis. However, when ROS production exceeds the neutralizing capacity of these antioxidant mechanisms, due to their depletion, dysfunction, or sustained stimulation, oxidative stress occurs. This imbalance can lead to damage of critical cellular components such as lipids, proteins, carbohydrates, enzymes, and DNA, thereby contributing to a range of pathological conditions.

$PM_{2.5}$ exposure, is a significant environmental source of oxidative stress. PM can generate ROS directly through its chemical constituents, including transition metals with redox activity, redox-cycling quinones, and PAHs. Cells have specific mechanisms for sensing PAHs, namely the aryl hydrocarbon receptor (AhR) which is a cytosolic environmentally sensing receptor. Binding of PAH ligands activates the nuclear translocation of the AhR, leading to the induction of xenobiotic-metabolising enzymes, such as the cytochrome P450 enzymes CYP1A1 and CYP1B1. These enzymes contribute to the detoxification of PAHs but can also bioactivate them into reactive intermediates, which in turn generate cytotoxic and genotoxic products (den Hartigh et al., 2010).

Beyond this direct effect, PM exposure also promotes immune cell recruitment and activation, particularly macrophages, which further amplifies oxidative stress through secondary ROS production. For instance, airway macrophages, normally involved in respiratory defence, release substantial amounts of ROS upon phagocytosing inhaled particles. Inflammatory cells also produce different mediators, such as cytokines and chemokines, to further recruit more inflammatory cells, as well as to activate signalling pathway which modulate important immediate cellular stress response. This creates a positive feedback loop, where oxidative stress and inflammation reinforce each other, especially under conditions of chronic PM exposure.

Nrf2 is a key transcription factor that enhances the expression of antioxidant genes by binding to antioxidant-responsive element (ARE) sequences. Its activity is tightly regulated by Keap1, which sequesters Nrf2 in the cytoplasm and prevents its nuclear translocation. Oxidative stress, a major consequence of PM exposure, acts as a

danger signal in epithelial cells, promoting activation of the NLRP3 inflammasome and subsequent IL-1β production (Vilas-Boas et al., 2024). Persistent oxidative stress induced by PM further drives the activation of intracellular signalling cascades such as MAPK and PI3K/Akt and modulates transcription factors like NF-κB and AP-1 (Wang et al., 2017; Hu et al., 2020). These molecular events regulate key processes involved in carcinogenesis, including cell proliferation, apoptosis, angiogenesis, and metastasis.

3.2.6 Genome instability

Lung cancer can develop when the DNA in cells is damaged or altered, a process known as genotoxicity. This damage may be caused by oxidative stress, disruptions in the enzymes that repair DNA, or epigenetic changes such as gene methylation, post-translational histones modifications and non-coding RNAs synthesis (miRNAs, lncRNAs, circRNAs) which will shape gene expression, driving phenotypic variation beyond the DNA sequence. These effects have been linked to exposure to PM or its components, and are thought to contribute to genome instability, which plays a role in the development of cancer (Santibáñez-Andrade et al., 2023).

The impairment of DNA, such as oxidative DNA damage, is considered as one of the major mechanisms of carcinogenesis. Forms of DNA damage include modifications to the DNA base, DNA adducts or occurrence of single and double strand breaks.

Accumulating evidence from cell culture experiments, animal models and even human studies has indicated that $PM_{2.5}$ might induce oxidative DNA damage through oxidative stress caused by the elevated generation of ROS (Niu et al., 2020). Indeed, an increase in the levels of DNA damage marker 8-hydroxy-2'-deoxyguanosine, tail DNA, and micronucleus frequency has been reported after occupational exposure to $PM_{2.5}$, suggesting a negative effect of long-term exposure to air pollution on DNA integrity (Tan et al., 2017). $PM_{2.5}$ components such PAHs and heavy metals can also directly interact with DNA to cause DNA strand breaks (Wang et al., 2025).

A complicated signalling network including DNA repair and cell cycle checkpoint pathways also referred to as the DNA damage response (DDR) is activated in response to DNA damage. If inappropriately restored by DDR, genomic mutations and other irreversible damage occur subsequently leading to severe consequences such as malignant progression. $PM_{2.5}$ could possibly decreases the DNA repair capacity by inducting mutations or inactivation of DNA repair genes like BRCA1/2, ATM and ATR,

which impairs the ability to repair damaged DNA further exacerbating genomic instability (Niu et al., 2020; Fedak et al., 2021). It has been demonstrated that PM exposure led to PAH-DNA adducts and alter nucleotide excision repair pathway (NER) components in A549 cells, liking PM-induced DNA damage to potential carcinogenesis (Quezada-Maldonado et al., 2022).

DNA hypermethylation or hypomethylation profiles represent silenced or activated target genes, respectively, and thus can repress or increase gene expression. $PM_{2.5}$ exposure is able to induce alterations in the DNA methylation pattern, especially in the promoter regions of oncogenes (Parida et al., 2023). It has been found that continuous exposure of BEAS-2B cells to $PM_{2.5}$ can methylate the p53 promoter, leading to p53 inactivation, and the ROS/Akt signalling pathway is also involved in methylation (Zhou et al., 2016). Analysis of DNA methylation alterations has been performed in lung cancer tissues of patients from regions with severe air pollution, providing evidence of global hypomethylation, accompanied by a reduction in the expression of DNA methyltransferases (DNMT3A and DNMT3B) (Jiang et al., 2016).

Histones modifications can affect histone DNA interactions and alter chromatin structure and function, which can lead to genomic instability and altered gene expression. A small cohort study found that H3 modifications were related to traffic derived PM exposure (Zheng et al., 2017).

Oncogenic driver mutations are present in over 50% of lung cancer, including mutations in EGFR, KRAS, BRAF, PI3K, MEK-1, HER2, MET, ALK and RET and inactivation of tumour suppressor genes (such as p53, PTEN, LKB-1) (Cooper et al., 2013).

3.2.7 Avoiding immune destruction

The immune system plays a crucial role in recognizing and eliminating cancer cells throughout tumour development, from initial transformation to metastatic progression. However, solid tumours like lung cancer can develop strategies to evade immune surveillance. Given that PM significantly influence inflammatory and immune responses in the lung, their potential contribution to immune evasion mechanisms deserves further investigation. This work will therefore focus on how PM exposure alters lung immunity and how these changes may facilitate lung cancer progression,

particularly by impairing immune-mediated tumour control, a relatively underexplored aspect of PM-related carcinogenesis.

4. Immunity

The immune system constitutes an intricate and highly organized network of cells, tissues, and molecular mediators that collaborate to protect the body from a wide array of harmful agents, including bacteria, viruses, parasites, and tumour cells. It is functionally divided into two major branches: innate immunity and adaptive (or acquired) immunity.

Innate immunity represents the first line of defence, offering immediate but non-specific responses to invading pathogens. This system encompasses physical barriers such as the skin and mucosal surfaces, as well as a range of cellular components including macrophages, neutrophils, natural killer (NK) cells, and dendritic cells. These innate immune cells are capable of recognizing conserved molecular structures on pathogens, termed pathogen-associated molecular patterns (PAMPs), and can also detect endogenous signals from damaged or stressed cells, known as damage-associated molecular patterns (DAMPs). Upon recognition of these signals, innate immune cells rapidly initiate defence mechanisms, notably phagocytosis, the release of antimicrobial agents, and the production of pro-inflammatory cytokines, which collectively serve to recruit and activate additional immune effectors. Innate responses are essential for controlling infections during the early stages and for shaping the quality and magnitude of subsequent adaptive immune responses (Abbas et al., 2014, pp. 23–48).

In contrast, ***adaptive immunity*** is characterized by high specificity and immunological memory, enabling a more targeted and efficient response upon repeated encounters with the same pathogen. Although slower to develop than innate responses, adaptive immunity provides long-lasting protection. It can be further divided into humoral and cellular arms. Humoral immunity is mediated by B lymphocytes, which produce antibodies that neutralize pathogens or tag them for clearance by other immune cells. Cellular immunity is orchestrated by T lymphocytes, which can directly kill infected or malignant cells and regulate immune responses through the secretion of cytokines (Abbas et al., 2014, pp. 49–70).

The coordination between innate and adaptive immunity is fundamental for mounting effective responses against a diverse range of pathogens, ensuring both immediate protection and the establishment of long-term immune surveillance.

4.1 Effects of PM on immune system components

Inhaled PM interacts with both epithelial and immune cells within the respiratory tract. The airway epithelium, acting as the initial interface with inhaled particles, is closely associated with a rich network of immune cells including alveolar macrophages, dendritic cells, granulocytes, innate lymphoid cells, and memory T and B lymphocytes. Exposure to PM can induce a pro-inflammatory profile in many of these cellular populations.

Various components of air pollution activate these cells through distinct sensing pathways, notably those involving Toll-Like Receptors (TLRs), ROS, and PAH detection mechanisms such as the aryl hydrocarbon receptor. These upstream signals trigger downstream inflammatory signalling pathways, including NF-κB and MAPK (Muralidharan and Mandrekar, 2013). While TLRs typically recognize PAMPs, pollutants can aberrantly engage these receptors, with responses varying according to both cell type and PM composition (Shoenfelt et al., 2009).

Respiratory tract lining fluid

A crucial protective interface in the lungs is the respiratory tract lining fluid (RTLF), which shields the epithelium and underlying tissue. This fluid contains secretions from epithelial and immune cells as well as plasma-derived components. Key elements include antioxidants like glutathione and ascorbate, antioxidant enzymes (e.g., superoxide dismutase, catalase), metal-binding proteins, and opsonizing agents such as mucins, complement proteins, surfactants, and immunoglobulins. Exposure to PM has been linked to oxidative stress and depletion of these antioxidant defences (van der Vliet et al., 1999).

Epithelial and parenchymal cells

Bronchial epithelial cells play several roles: they create a physical barrier, contribute to mucous production within the RTLF, and participate in mucociliary clearance. Upon detecting harmful particles, they secrete a range of inflammatory mediators, including IL-6, CXCL8, and GM-CSF. These cytokines enhance local immune responses. GM-

CSF, for instance, promotes the development and survival of dendritic cells and granulocytes (Becher et al., 2016), while IL-6 supports inflammatory signalling and suppresses regulatory pathways. Bronchial epithelial cells also secrete key alarmins, such as IL-33, TSLP, IL-25, HMGB1, ATP and S100 proteins, in response to allergens (e.g. house dust mites), pathogens (e.g. viruses and bacteria), pollutants (e.g. cigarette smoke and $PM_{2.5}$) and mechanical and oxidative stress (e.g. ozone) (Ogulur et al., 2025).

Macrophages

Innate immune cells, particularly alveolar macrophages and neutrophils, serve as rapid responders to inhaled agents. Alveolar macrophages (AMs) are major in clearing inhaled particles via phagocytosis. When overloaded with PM, their function becomes impaired. These macrophages also produce cytokines such as TNF-α and IL-1β, which further activate epithelial cells and amplify inflammation, demonstrating a synergistic relationship between macrophages and the epithelium.

Dendritic cells and lymphocytes

Dendritic cells are central in antigen presentation and play a pivotal role in bridging innate and adaptive immunity by detecting environmental cues through receptors like TLRs, processing antigens, and presenting them via MHC molecules to T cells to initiate antigen-specific responses. They also produce co-stimulatory signals and soluble mediators. PM exposure has been shown to enhance the antigen-presenting capacity of these cells, increasing expression of maturation markers such as CD80 and MHC II and stimulating cytokine production (Porter et al., 2007). These changes can differentially modulate CD4+ and CD8+ T cell responses.

Adaptive immunity, represented by T and B lymphocytes, offers antigen-specific responses, ranging from immune tolerance to robust defence against pathogens. However, maladaptive activation can result in chronic inflammation. These responses are often categorized into Th1, Th2, or Th17 phenotypes, reflecting distinct cytokine environments and immunological outcomes.

Granulocytes

Granulocytes, including eosinophils and neutrophils, use pattern recognition receptors (PRRs) to detect foreign material. Their cytoplasmic granules contain enzymes like

proteases and oxidases, which help destroy pathogens but may also damage host tissue. Long-term exposure to $PM_{2.5}$ has been associated with shifts in eosinophil activity, mimicking inflammatory patterns observed in conditions such as asthma (Ramanathan et al., 2017).

Neutrophils are a particularly important granulocyte when considering air pollution pathogenesis. They are the most abundant leukocytic cell in the blood and are rapidly recruited to inflammatory sites. They express myeloperoxidase enzymes, capable of producing oxidants upon neutrophil activation. These oxidants in presence of transition metals within PM can further redox cycling and trigger oxidative damages on biological systems. Human exposure studies have revealed an increase in the production of neutrophil attracting chemokines such as IL-8 and CXCL1 in healthy airways following diesel exhaust exposure (Salvi et al., 2000).

While neutrophilic activation in response to air pollution is well documented, the effects of PM on neutrophil function remain insufficiently explored. Neutrophils are recognized not only for their role in acute inflammation but also for their capacity to modulate the adaptive immune environment through immunoregulatory functions. In this context, the present work aims to investigate how PM exposure influences the recruitment and behaviour of lung neutrophils, and how these alterations may contribute to a microenvironment that supports lung cancer progression.

5. Neutrophils

Neutrophils, also known as polymorphonuclear neutrophils (PMNs), are the most abundant white blood cell in the human circulation. Neutrophils are characterized by a segmental lobular nucleus and cytoplasmic granules filled with degradative enzymes. They are considered as the primary line of defence against extracellular pathogens and acute inflammation (Soehnlein and Lindbom, 2010). Circulating neutrophils are short lived with an average half-life of 19 hours in humans during homeostasis and are therefore constantly replaced by new cells through the process of granulopoiesis (Lahoz-Beneytez et al., 2016). Neutrophils exhibit significant functional and phenotypic heterogeneity, particularly in pathological contexts such as inflammation and cancer, contributing to the development of various diseases.

5.1 Granulopoiesis

Neutrophil development, or granulopoiesis, originates in the bone marrow, beginning with hematopoietic stem cells (HSCs), which give rise to multipotent progenitors (MPPs). Collectively, these two cell types constitute the hematopoietic stem and progenitor cell population (Laurenti and Göttgens, 2018). MPPs then differentiate into either common lymphoid progenitor, which generate lymphocytes and natural killer cells, or common myeloid progenitors, which further mature into granulocyte-monocyte progenitors (GMPs), the precursors of neutrophils (Hidalgo et al., 2019).

Beyond the GMP stage, the neutrophil lineage progresses through defined precursor stages: promyelocytes and myelocytes, now commonly referred to as neutrophil progenitors and precursors. When these cells mature, they undergo characteristic nuclear morphologies: from round nuclei in promyelocytes to kidney-shaped nuclei in metamyelocytes, followed by banded nuclei in immature neutrophils, and finally segmented nuclei in fully differentiated neutrophils (Hidalgo et al., 2019). Under normal physiological conditions, only mature neutrophils are released into circulation. However, in the context of infection, inflammation, or malignancy, increased mobilization from the bone marrow can lead to the presence of immature, non-proliferating neutrophils in the peripheral blood (Zhu et al., 2018).

The retention of neutrophils in the bone marrow is regulated by molecular signals exchanged between neutrophils and the bone marrow microenvironment. One key player is CXCR4, a chemokine receptor found on the surface of neutrophils. When CXCR4 binds to its ligand, stromal cell-derived factor 1 (SDF-1), also known as CXCL12, which is produced by bone marrow stromal cells, a chemotactic gradient is established that helps keep neutrophils within the bone marrow.

For neutrophils to be released into the bloodstream, the bone marrow secretes a different set of signalling molecules, including CXCL1, CXCL2, and G-CSF (Granulocyte Colony-Stimulating Factor) (Summers et al., 2010). G-CSF plays a central role by triggering intracellular signalling pathways essential for the proliferation, differentiation, release, transport, and survival of granulocytes (Panopoulos and Watowich, 2008). In addition, G-CSF downregulates the expression of both CXCL12 and CXCR4, weakening the retention signal (Kim et al., 2006). The chemokines

CXCL1 and CXCL2, which bind to the receptor CXCR2, work together with G-CSF to promote neutrophil mobilization from the bone marrow (Eash et al., 2010) (**Fig. 3**).

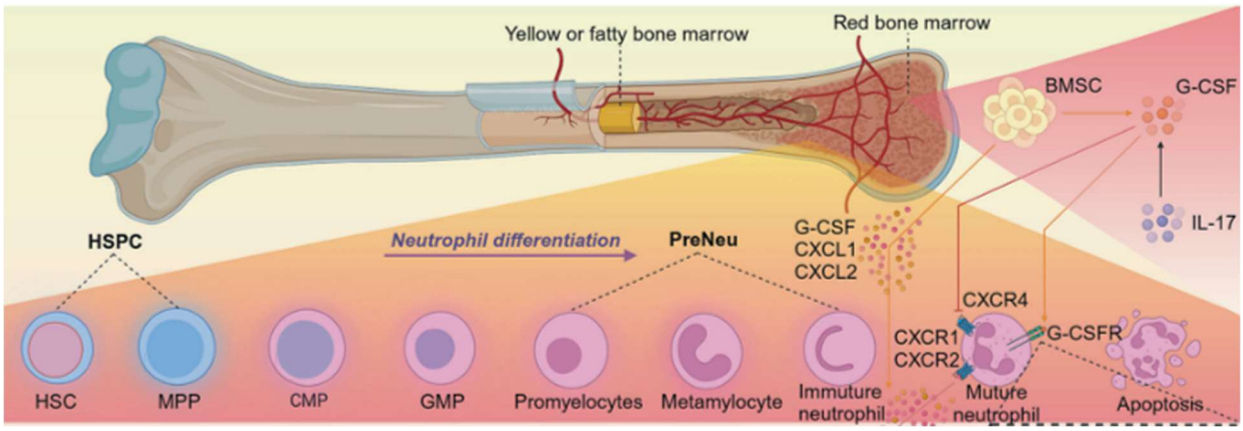

Figure 3. Graphic overview of granulopoiesis within the bone marrow. The formation of neutrophils initiates from hematopoietic stem cells (HSCs), which reside in the bone marrow. These stem cells progressively differentiate, passing through various developmental phases, including the promyelocyte stage. As differentiation continues, the cells mature and are eventually released into the bloodstream as fully developed neutrophils. Hematopoietic stem cell (HSC); Multipotent progenitor cell (MPP); Common myeloid progenitor cell (CMP); Granulocyte-monocyte progenitor cell (GMP); Neutrophil precursors (preNeu); Granulocyte colony stimulating factor (G-CSF); Bone marrow stromal cell (BMSC). *Cropped from the original figure by (Zhang et al., 2024).*

5.2 Release and recruitment

Once released in the bloodstream, neutrophils circulate freely, ready to be recruited to tissues in response to chemoattractant signals. When endothelial cells are exposed to inflammatory stimuli, whether from PAMPs derived from microbes, or damage-associated molecular patterns DAMPs released by injured host cells, they become activated and begin to express adhesion molecules such as P-selectin and E-selectin on their surface (Ley et al., 2007).

The recruitment of neutrophils involves a multi-step process: tethering, rolling, adhesion, crawling, and extravasation. Initially, P-selectin binds to P-selectin glycoprotein ligand 1 (PSGL-1) on the neutrophil surface, capturing the cells and enabling them to roll slowly along the vessel wall in the direction of blood flow (Zarbock et al., 2011). As the P-selectin-PSGL-1 bonds break at the trailing edge of the neutrophil, new bonds form at the leading edge, maintaining contact and enabling progressive movement (Khismatullin and Truskey, 2012).

This rolling behaviour slows the neutrophils down, allowing their chemokine receptors to interact with chemokines displayed on the endothelial surface. These interactions trigger integrin activation (Kolaczkowska and Kubes, 2013). Once activated, integrins such as MAC-1 and LFA-1 undergo conformational changes that enhance their binding affinity for intercellular adhesion molecules (ICAM-1 and ICAM-2) on endothelial cells (Phillipson et al., 2006), leading to firm adhesion.

Following firm attachment, neutrophils begin to crawl along the endothelium, particularly toward intercellular junctions, guided by chemoattractant gradients that orient them toward the site of infection or injury (Petri and Sanz, 2018). To reach the affected tissues, neutrophils must traverse several structural barriers: the endothelial cell layer, the basement membrane, and pericytes (Kolaczkowska and Kubes, 2013) (**Fig. 4**).

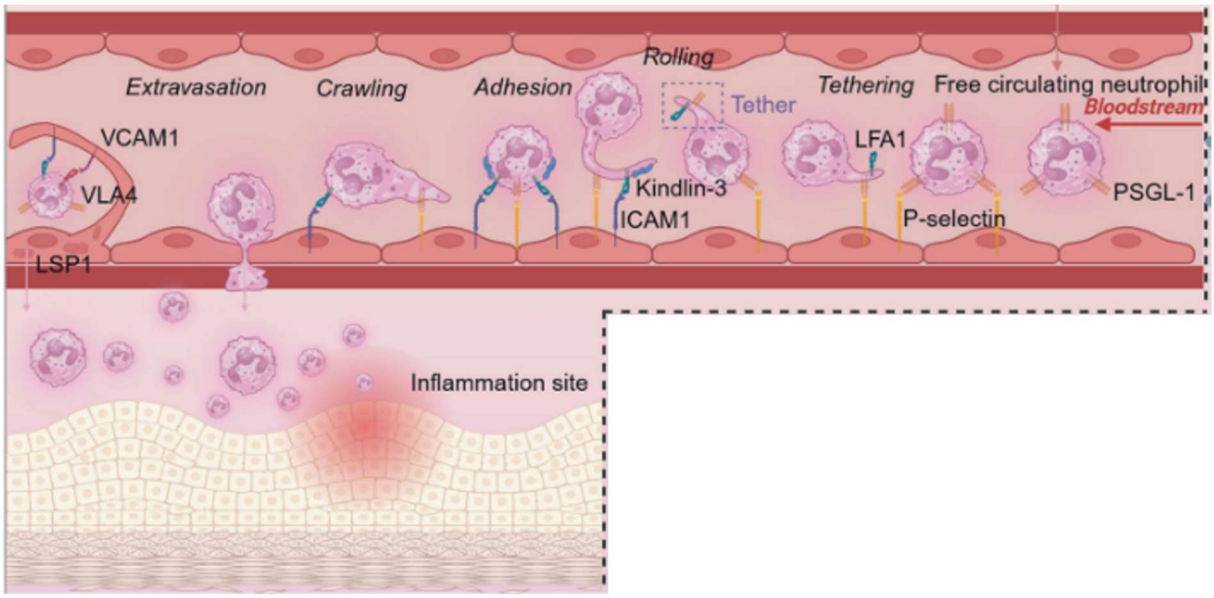

Figure 4. Illustration of the neutrophil recruitment cascade, showing the sequential steps of tethering, rolling, adhesion, crawling, and migration. These processes are regulated by selectins, integrins, and chemokines to direct neutrophil chemotaxis toward inflammatory sites. P-selectin glycoprotein ligand 1 (PSGL1); Leukocyte function antigen 1 (LFA-1); Intercellular adhesion molecule 1 (ICAM1); Vascular adhesion molecule (VCAM1); Lymphocyte-specific protein 1 (LSP1). *Cropped from the original figure by Zhang et al., 2024.*

The primary route for neutrophil migration across the endothelium is paracellular diapedesis, where cells pass between endothelial junctions. However, an alternative route known as transcellular migration, also occurs. In this process, endothelial cells

generate projections that rise along the sides of the neutrophil to envelop the neutrophil within a dome-like structure (Carman and Springer, 2004). Once past the endothelium, neutrophils engage with pericytes through ICAM-1-dependent interactions, extending cellular projections to navigate between pericyte gaps and exit the vascular compartment (Pieper et al., 2013).

5.3 Phagocytosis and roles of granules

Once neutrophils reach the site of infection or inflammation, they detect pathogens that have been marked by opsonins through specific membrane-bound receptors, thereby initiating the process of phagocytosis. The engagement of these receptors triggers a reorganization of the actin cytoskeleton, enabling the neutrophil's plasma membrane to extend pseudopodia that wrap around the target and form a cup-like phagocytic structure (Flannagan et al., 2012). Inside the resulting phagosome, two primary antimicrobial mechanisms are activated: (1) the production of ROS mediated by the enzyme complex NADPH oxidase 2 (NOX2), and (2) the fusion of the phagosome with granules containing pre-synthesized bactericidal proteins. Subsequently, the phagosome is transported toward the cell center, where it merges with intracellular components, allowing the coordinated destruction of the engulfed pathogen.

Neutrophils contain three main types of granules that enable rapid, stage-specific antimicrobial action. Primary (azurophilic) granules are the most abundant type and deliver a range of antimicrobial agents such as myeloperoxidase (MPO), defensins, cathepsin G, lysozyme, and proteinase 3 (Nordenfelt and Tapper, 2011). Secondary (specific) granules, carry proteins such as lactoferrin, lysozyme, NADPH oxidase components and antimicrobial peptides. These proteins support the oxidative burst, the killing of microbes and the modulation of inflammation (McKenna et al., 2021). Tertiary (gelatinase) granules contain gelatinase (MMP-9) and other matrix-degrading enzymes that facilitate neutrophil migration through tissues (Rosales, 2018). These three granule types are released in a regulated, calcium and receptor-dependent sequence: tertiary first, then secondary, and finally primary, to balance effective defence with minimal tissue damage.

5.4 Neutrophils death

5.4.1 Non- lytic cell death

Following their powerful antimicrobial action, neutrophils must be efficiently eliminated to prevent an excessive and potentially harmful inflammatory response in the host body. Under homeostatic conditions, non-lytic cell death pathways, particularly apoptosis, are the predominant mode of neutrophil turnover. This regulated form of cell death promotes the resolution of inflammation by sequestering cytotoxic granules and cytoplasmic content, thereby minimizing collateral tissue damage (Lawrence et al., 2020).

Neutrophil apoptosis can occur through two main routes: one involves the activation of canonical apoptotic signalling pathways, while the other is triggered by pathogens, linking pathogen ingestion and elimination with the swift removal of neutrophils. This pathogen-induced apoptosis is closely coupled to efferocytosis, a specialized phagocytic process that ensures the silent clearance of dying neutrophils by macrophages and other phagocytes (Morioka et al., 2019).

When this clearance mechanism fails, apoptotic neutrophils may undergo secondary necrosis, leading to the release of toxic granules and DAMPs. These molecules amplify the local inflammatory response and contribute to tissue injury, underlining the importance of timely and effective neutrophil clearance in maintaining immune balance.

5.4.2 Lytic cell death

In addition to non-lytic mechanisms, neutrophils can also undergo lytic forms of cell death, particularly in response to certain infections or inflammatory stimuli. This type of death results in the release of cytotoxic granule contents and pro-inflammatory cytokines, which, if not properly regulated, can significantly contribute to local tissue damage (Thieblemont et al., 2018).

One such lytic pathway is pyroptosis, a programmed cell death process that plays a crucial role in limiting pathogen spread and promoting tissue repair following exposure to infectious agents or environmental stressors (Shi et al., 2014). Pyroptosis is characterized by the formation of pyroptotic bodies, which ultimately lead to cell membrane rupture and the extracellular release of key pro-inflammatory cytokines,

notably IL-1β and IL-18. These cytokines not only aid in pathogen clearance but also function to recruit additional immune cells and amplify inflammation at the site of infection (Van Opdenbosch and Lamkanfi, 2019).

Another lytic form of cell death relevant to neutrophils is ferroptosis, which is driven by the iron-dependent accumulation and peroxidation of polyunsaturated phospholipids within the cell membrane. When this oxidative damage reaches a critical threshold, it triggers membrane breakdown and cell death, further contributing to inflammatory processes (Stockwell et al., 2017).

5.4.3 NETosis

NETosis is a distinctive and tightly regulated form of programmed cell death specific to neutrophils, representing a unique antimicrobial strategy involving the release of neutrophil extracellular traps (NETs) (Brinkmann et al., 2004). The process begins when neutrophils recognize microbial elements, such as whole bacteria, bacterial components, or inflammatory mediators, which activate signalling pathways leading to NET formation (Baz et al., 2024). During this process, the nuclear envelope disintegrates, allowing decondensed chromatin to mix with granule proteins, histones, and cytoplasmic contents. This mixture is subsequently expelled into the extracellular space following plasma membrane rupture, forming web-like NET structures capable of immobilizing and neutralizing virulent pathogens (Yipp and Kubes, 2013).

NETosis occurs in two distinct forms: lytic and non-lytic. In lytic NETosis, cell death results from a cascade initiated by ligand-receptor interactions, followed by intracellular signalling and an increase in ROS production, often involving MPO. MPO collaborates with neutrophil elastase (NE) to disrupt chromatin structure, leading to its decondensation. The nucleus expands, and pore formation in the plasma membrane eventually results in cell lysis and NET release (Papayannopoulos et al., 2010).

In contrast, non-lytic NETosis does not compromise neutrophil viability. This process is triggered by an elevation in intracellular calcium levels, which activates protein arginine deiminase 4 (PAD4). PAD4 induces citrullination of histones, reducing their positive charge and thereby weakening their binding affinity for DNA. As a result, chromatin expands without nuclear rupture, enabling NET release without membrane lysis (Leshner et al., 2012). Neutrophils that release NETs via the non-lytic route remain

functional, retaining key immune abilities such as chemotaxis, phagocytosis, and pathogen elimination (Jorch and Kubes, 2017).

NETs play a crucial role in containing pathogens and preventing the spread of infection. However, when NET formation becomes excessive or poorly regulated, often due to impaired clearance, it can contribute to various pathological conditions. These include delayed wound healing, systemic inflammation, defective immune surveillance, thromboembolic complications, and even the promotion of cancer metastasis (Ronchetti et al., 2021; Schoen et al., 2022; James et al., 2024).

5.5 Neutrophils heterogeneity

There are phenotypically and functionally distinct neutrophil subtypes that exist in circulating or in tissue under physiological and pathological conditions.

5.5.1 Neutrophils diversity in health

The bone marrow contains the largest reservoir of neutrophils, comprising neutrophils at various stages of maturation. Its granulocyte reserves are much more abundant that those found in the peripheral circulation. Consequently, non-proliferative immature neutrophils serve as a reservoir of neutrophils that can be rapidly deployed to the bloodstream, whereas mature neutrophils are important for effector functions.

Once released from the bone marrow into the bloodstream, neutrophils circulate for approximately 12 hours before migrating into peripheral tissues. This process follows a circadian rhythm (Casanova-Acebes et al., 2018), accompanied by marked diurnal changes in neutrophil phenotype. In both mice and humans, neutrophils progressively lose CD62L expression while upregulating CD11b and CXCR4 within a six-hour window. Concurrently, their nuclei become increasingly hypersegmented, and the cells acquire features characteristic of aged neutrophils, including enhanced integrin activation and an increased capacity to form NETs. These phenotypic shifts are particularly evident in the early morning in mice, coinciding with the time of their release from the bone marrow (Casanova-Acebes et al., 2013). These observations suggest that neutrophils dynamically adapt their functional properties to align with the organism’s circadian needs, particularly during the active phase when the risk of pathogen exposure is highest (Man et al., 2016).

In healthy tissue, neutrophils, traditionally characterized as short-lived immune cells, exhibit a remarkable degree of plasticity that varies depending on the tissue environment. Upon entry into tissues, they acquire distinct phenotypic and functional profiles shaped by local cues, reflecting an adaptation to the specific physiological context (Casanova-Acebes et al., 2018; Ballesteros et al., 2020). Notably, their lifespan within tissues exceeds that observed in circulation, providing sufficient time for functional and transcriptional reprogramming. In the lungs, for instance, a substantial population of neutrophils becomes marginated within the pulmonary microvasculature through CXCR4-dependent signalling, positioning them to mount rapid responses to microbial challenges (Ballesteros et al., 2020). These findings support the emerging view that neutrophils function as dynamic immune sentinels, actively contributing to tissue-specific immune surveillance and homeostasis.

5.5.2 Neutrophils diversity in disease

Neutrophils exhibit considerable phenotypic and functional flexibility, particularly under inflammatory conditions. In response to such stimuli, they can express various pattern recognition receptors and secrete a diverse range of cytokines. While neutrophils are central to the initial stages of the inflammatory response, their continued activation in the context of chronic inflammation can lead to tissue damage (Soehnlein et al., 2017). Importantly, the capacity of neutrophils to form NETs varies significantly between species and even among mouse strains (Ermert et al., 2009).

In cancer, neutrophils are frequently present in the tumour microenvironment and display different behaviours. They can contribute to anti-tumour immunity by releasing cytotoxic mediators and directly interacting with tumour cells to enhance immunogenic responses (Sun et al., 2024). Conversely, neutrophils may also promote tumour progression by supporting local tumorigenesis, stimulating tumour cell proliferation, facilitating angiogenesis and metastatic dissemination, and establishing immunosuppressive networks in the tumour microenvironment (Zhao et al., 2020; Hedrick and Malanchi, 2022).

The abundance and role of neutrophils vary across cancer types, and the neutrophil-to-lymphocyte ratio (NLR) is commonly used as a prognostic marker for disease progression. Similar to what is observed during acute infections, primary tumours secrete pro-inflammatory factors which drive the expansion and mobilization of

immature neutrophils into the bloodstream and tumour site. These immature neutrophils, often referred to as granulocytic myeloid-derived suppressor cells (G-MDSCs or PMN-MDSCs), are key mediators of immunosuppression. This tumour-induced process resembles "emergency granulopoiesis" observed during infections, highlighting a shared mechanism that fuels neutrophil heterogeneity and contributes to cancer progression (Chiba et al., 2018).

6. PMN-MDSCs

MDSCs are broadly divided into two main subtypes: polymorphonuclear MDSCs (PMN-MDSCs), which arise from bone marrow granulocytic precursors that give rise to neutrophils, and monocytic MDSCs (M-MDSCs), which originate from mononuclear cells that give rise to monocytes, as well as terminally differentiated macrophages and dendritic cells. Myeloid cells are essential for host defence against pathogens and play a key role in tissue repair and remodelling. Under physiological conditions, their differentiation is driven by growth factors such as granulocyte-macrophage colony-stimulating factor (GM-CSF), granulocyte CSF (G-CSF), and macrophage CSF (M-CSF) (Barreda et al., 2004). In cancer and other pathological settings, excessive production of these factors promotes the expansion of MDSCs (Marvel and Gabrilovich, 2015), following developmental pathways similar to those that generate neutrophils and monocytes.

PMN-MDSCs are phenotypically and morphologically similar to neutrophils and are a strongly associated with poor prognosis in cancer patients (Zhou et al., 2018). Under normal immune responses, classical activation of myeloid cells is triggered by strong stimuli such as PAMPs, DAMPs, and ligands of TLRs. These signal trigger the release of neutrophils from the bone marrow and the secretion of proinflammatory cytokines, typically resulting in a rapid response that is resolved upon the elimination of the infectious threat (Kruger et al., 2015).

In contrast, some pathological conditions, such as cancer, chronic inflammation and autoimmune disease, are characterized by a different mode of myeloid cell activation. Here, the stimuli are generally weaker, prolonged, and often consist of growth factors or various inflammatory mediators (Landskron et al., 2014). Neutrophils that arise under these chronic conditions tend to exhibit immature features, enhanced production of ROS and nitric oxide (NO), and elevated levels of enzymes and cytokines associated

with immune suppression, such as Arginase 1 (ARG-1), prostaglandin E2 (PGE2), and anti-inflammatory cytokines (Umansky et al., 2016). These features are absent in classically activated neutrophils, highlighting a distinct, pathologically activated state associated with immune dysregulation and tumour progression. Cells exhibiting this dysfunctional profile are referred to as PMN-MDSCs, which can be identified by their unique functional, biochemical, and phenotypic markers. Notably, the longer the exposure of the myeloid compartment to chronic inflammatory stimuli, the more pronounced this pathological state becomes in both humans and murine models (Veglia et al., 2018).

The accumulation of PMN-MDSCs is driven by two interconnected categories of signalling events. The first promotes the proliferation and expansion of immature myeloid cell populations and is primarily induced by factors derived from tumours or the bone marrow stroma under chronic inflammatory conditions. These factors include GM-CSF, G-CSF, stem cell factor (S-SCF), vascular endothelial growth factor (VEGF), alarmins such as S100A8 and S100A9, and polyunsaturated fatty acids (Umansky and Sevko, 2013). The second category consists of signals that drive the pathological activation of these cells, often mediated by inflammatory cytokines and DAMPs, including interferon-gamma (IFN-γ), interleukins IL-1β, IL-4, IL-6, IL-13, tumour necrosis factor (TNF), and the TLR ligand high mobility group box 1 (HMGB1) (Condamine et al., 2015).

6.1 Phenotypic and molecular feature of PMN-MDSCs

In humans, PMN-MDSCs and neutrophils share a similar phenotype, typically expressing $CD11b^+$, $CD15^+$ and/or $CD66b^+$, $CD33^+$ and $CD14^-$. Despite these phenotypic similarities, they can be distinguished based on their physical properties during Ficoll gradient centrifugation: PMN-MDSCs are found in the low-density fraction, whereas neutrophils settle in the high-density fraction. In healthy individuals, PMN-MDSCs are practically undetectable (Veglia et al., 2018).

A study by Condamine et al. demonstrated that, in patients with non-small cell lung cancer (NSCLC) or head and neck cancer (HNC), PMN-MDSCs exhibit higher expression of the LOX-1 gene compared to neutrophils from the same individual, suggesting LOX-1 as a potential discriminatory marker (Condamine et al., 2016).

In mouse models, PMN-MDSCs are defined by the expression of $CD11b^+$, $Ly6G^+$, $Ly6C^{int}$, a phenotype also shared with classical neutrophils, making their distinction challenging (Bronte et al., 2016). Using single-cell RNA sequencing (scRNA-seq), Alshetaiwi et al. identified CD84 as a novel surface marker associated with MDSCs (Alshetaiwi et al., 2020).

Further insight was provided by Veglia et al., who showed that classical neutrophils and PMN-MDSCs coexist within tumors in both mice and humans. Their transcriptomic analyses identified CD14 as a marker correlated with the immunosuppressive capacity of PMNs in mice, thus serving as a key identifier for distinct PMN subsets. CD14 is highly expressed on monocytes and the majority of tissue macrophages, whereas it is absent from myeloblasts and other granulocytic precursors. Neutrophils, however, can exhibit low levels of CD14 expression. Functionally, CD14 is a glycosylphosphatidylinositol (GPI)-anchored receptor that, in association with TLR4 and MD-2, constitutes a multireceptor complex responsible for recognizing lipopolysaccharide (LPS) at the cell surface (Lloyd and Kubes, 2006). Additionally, researchers found that the gene expression profile of human PMN-MDSCs closely resembles that of tumor-bearing mice, and this signature was strongly associated with poor clinical outcomes in cancer patients. However, unlike mouse PMNs, CD14 was not express in human PMNs (Veglia et al., 2021).

Engblom et al. demonstrated both in human and mouse that neutrophils characterized by high expression of the lectin SiglecF (sialic acid-binding immunoglobulin-like lectin F) exhibit a gene expression profile associated with cancer-promoting processes, displaying a phenotype similar to that of MDSCs (Engblom et al., 2017).

6.2 Immune suppressive activity of PMN-MDSCs

In mice, PMN-MDSCs lack a unique defining marker, making them difficult to distinguish from classical neutrophils based on phenotype alone. However, their defining feature is their potent ability to suppress immune responses. This immunosuppressive function is mediated through multiple mechanisms that allow them to be distinguished functionally from conventional neutrophils (**Fig. 5**).

6.2.1 Immune checkpoint molecules expression

Programmed cell death ligand 1 (PD-L1), an important ligand of the inhibitory receptor programmed cell death protein 1 (PD-1), functions as a key immune checkpoint by regulating the activation of immune cells in response to antigens. By binding to PD-1, PD-L1 suppresses T cell activity, impairing their ability to recognize and destroy tumor cells, which allows cancer cells to escape immune detection (Filippone et al., 2022). Research has shown that PMN-MDSCs enhance the expression of PD-L1 as a strategy to inhibit T cell responses, primarily through its interaction with PD-1 on T cells (Antonios et al., 2017; Kwantwi et al., 2021).

SIRPα is another inhibitory receptor expressed on neutrophils that inhibits the phagocytosis of CD47-expressing cells by delivering a "don't eat me" signal, thereby enabling tumor cells to evade immune attack and promoting tumour immune escape (Behrens et al., 2022).

6.2.2 Depletion of amino acids required for T cell activity

PMN-MDSCs can impair T cell metabolism and function by depleting essential amino acids. One key enzyme involved in this process is ARG1, which breaks down L-arginine into urea and L-ornithine. This reduction in extracellular L-arginine availability has been linked to the downregulation of the CD3ζ chain on T cells and a subsequent decline in their proliferative capacity (Zea et al., 2004). In the context of cancer, studies have shown that PMN-MDSCs secrete ARG1 into the extracellular milieu, thereby accelerating L-arginine depletion and contributing to T cell suppression through similar mechanisms (Rodriguez et al., 2009).

In PMN-MDSCs, the upregulation of inducible nitric oxide synthase (iNOS) leads to the metabolism of L-arginine into nitric oxide (NO) and L-citrulline. Similar to ARG1, iNOS also uses L-arginine as a substrate (García-Ortiz and Serrador, 2018). NO produced by MDSCs, has been implicated in T cell suppression through several molecular mechanisms. Notably, NO can disrupt IL-2 receptor signaling and nitrate components of TCR, thereby impairing T cell function (Xue et al., 2018). Mechanistically, NO rapidly reacts with O_2^- to form reactive nitrogen species (RNS), including peroxynitrite ($ONOO^-$) and nitrogen dioxide ($\bullet NO_2$), which induce tyrosine nitration in various proteins (Moldogazieva et al., 2018). This modification has been shown to alter the structure and function of key immune molecules. In particular, MDSC-derived

peroxynitrite can nitrate tyrosine residues within the TCR–CD8 complex, thereby reducing its affinity for peptide–MHC (pMHC) dimers and limiting antigen recognition by cytotoxic T cells. Such nitrotyrosine modifications represent a major mechanism by which neutrophils and MDSC-like populations exert immunosuppressive activity in inflammatory and tumour contexts (Feng et al., 2018).

6.2.3 Immunosuppressive molecules production

Adenosine is a well-established immunosuppressive molecule involved in the inhibition of T cell responses mediated by MDSCs (Ryzhov et al., 2011). Within hypoxic tumor environments, large quantities of ATP are released into extracellular space and rapidly transformed into adenosine. This degradation involves a two-step enzymatic process: CD39 first hydrolyzes ATP into ADP and AMP, followed by CD73, which converts AMP into adenosine (Allard et al., 2017). The resulting adenosine accumulates and engages specific receptors, most notably A2A and A2B, which are strongly linked to immunosuppressive effects, as well as A1 and A3 receptors. In the tumor microenvironment, adenosine-generating components such as CD39, CD73, A2AR, and A2BR are typically expressed by not only tumor cells, but also stromal and immune cells. This configuration forms a positive feedback loop, maintaining high adenosine levels that promote both the suppressive functions of MDSCs and the inhibition of anti-tumor immune cells, including T cells, dendritic cells, and natural killer cells (Vijayan et al., 2017). In addition, some activated MDSCs from patients with non-small cell lung cancer (NSCLC) have been found to co-express CD39 and CD73, a phenotype associated with tumor progression and resistance to chemotherapy (J. Li et al., 2017).

Another key mechanism underlying PMN-MDSC immunosuppressive activity is the production of prostaglandin E2 (PGE2), derived from arachidonic acid (He et al., 2018). PGE2 exerts potent anti-inflammatory and immunosuppressive effects, notably by inhibiting T cell function. Its synthesis is regulated by two critical enzymes: cyclooxygenase-2 (COX-2), encoded by the Ptgs2 gene, and prostaglandin E synthase (PTGES), encoded by Ptges.

6.2.4 Crosstalk between PMN-MDSCs and Tregs

Regulatory T cells (Tregs) originate either in the thymus or in peripheral tissues following the recognition of self-antigens. Their primary role is to suppress the activation of autoreactive lymphocytes that could otherwise cause damage to the host.

The majority of Tregs are CD4+ T cells characterized by high expression of CD25, which corresponds to the alpha chain of the IL-2 receptor. The transcription factor FoxP3 is essential for both the development and the suppressive functions of these cells. In addition, the cytokine transforming growth factor-beta (TGF-β) contributes to the induction and maintenance of regulatory T cell populations (Abbas et al., 2014, pp. 97–101).

MDSCs can incite inhibitory cells such as Tregs to facilitate immunosuppression. MDSCs can induce Tregs proliferations through either a direct cell-cell interaction or secretion of soluble factors like IL-10 and TGF-β (Siret et al., 2019).

6.2.5 Neutrophil extracellular traps (NETs) production

NETs may contribute to immune evasion by shielding tumor cells from cytotoxic T lymphocytes, which could undermine the efficacy of anti-PD-1 immunotherapy (Teijeira et al., 2020). Strategies targeting NETs formation, such as the use of PAD4 or DNase I inhibitors, have demonstrated potential in enhancing $CD8^+$ T cell infiltration, inhibiting tumor progression, and sensitizing colorectal tumors to anti-PD-1 treatment (Zhang et al., 2021). Additionally, Kaltenmeier et al. highlights the role of NETs in driving T cell dysfunction by inducing both metabolic and functional exhaustion, further facilitating tumor development (Kaltenmeier et al., 2021). In an experimental mouse model of ozone-mediated PMN recruitment in the lung, blocking neutrophils or degrading NETs significantly reduced the metastasis of breast cancer and melanoma to the lung. These results demonstrate a direct correlation between NET production and metastasis (Rocks et al., 2019).

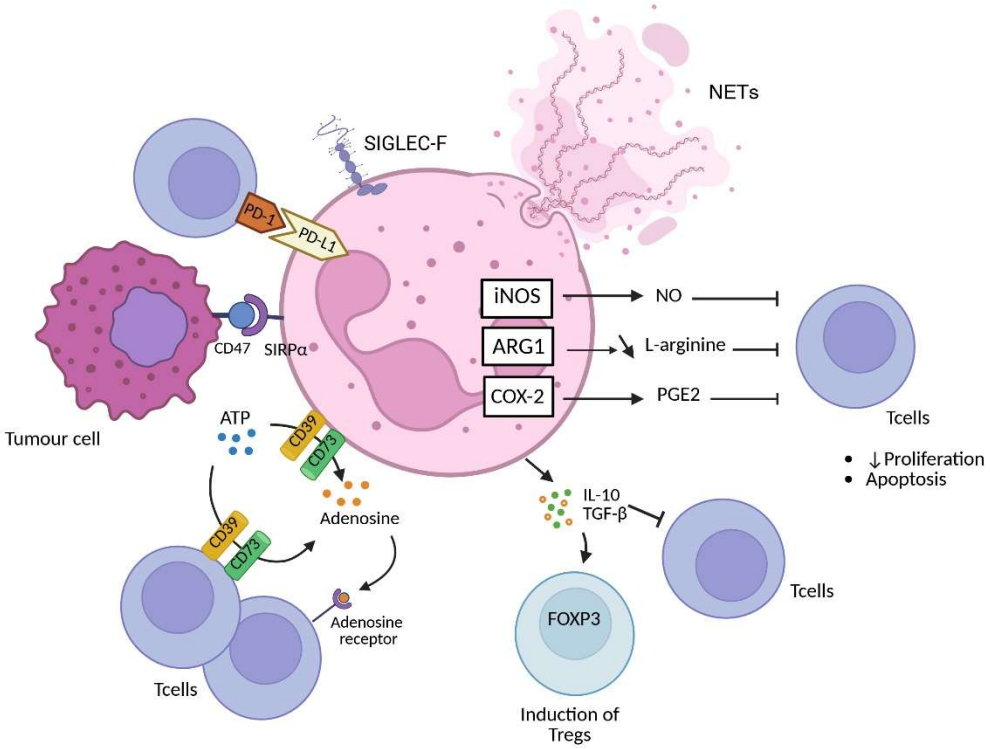

Figure 5. Immunosuppressive mechanisms of PMN-MDSCs. PMN-MDSCs inhibit T cell responses via multiple pathways: nitric oxide (NO) production by iNOS, depletion of L-arginine via ARG1, adenosine generation through CD39/CD73, SIRPα/CD47 and PD-L1/PD-1 signaling. They also secrete IL-10, TGF-β, and PGE2, contributing to T cell suppression and Treg induction. SiglecF expression is associated with their suppressive phenotype, and NETs formation may further support immune evasion. Inducible nitric oxide synthase (iNOS); Arginase-1 (ARG1); Cyclooxygenase 2 (COX-2), Prostaglandin E2 (PGE2). Programmed cell death ligand 1 (PD-L1); programmed cell death protein 1 (PD-1). *Figure created with BioRender.com*

7. T cell mediated immunity

7.1 Generalities

The control and elimination of malignant cells by the immune system, a process known as immune surveillance, is a pillar of anti-tumor immunity. Nevertheless, the occurrence of tumors in immunocompetent individuals highlights the ability of malignant cells to evade or overwhelm immune responses. The primary mechanism through which tumors are eradicated involves cytotoxic T lymphocytes (CTLs) that specifically recognize tumor antigens.

Tumor antigens are presented on class I major histocompatibility complex (MHC) molecules, allowing CD8+ T cells to identify and destroy antigen-expressing tumor cells. The activation of CTLs typically begins when antigen-presenting cells (APCs), such as dendritic cells, capture tumor-derived antigens and present them via a process known as cross-presentation. This mechanism enables dendritic cells to simultaneously activate both CD8+ cytotoxic T cells and CD4+ helper T cells, as the latter recognize antigens presented on class II MHC molecules. Effective T cell priming requires not only antigen recognition, but also co-stimulatory signals provided by APCs (Abbas et al., 2014, pp. 97–101).

Following activation, naïve CD8+ T cells differentiate into effector CTLs capable of targeting tumor cells independently of further co-stimulation. However, optimal differentiation into potent cytotoxic and memory T cells often necessitates help from CD4+ T cells, which provide crucial cytokines and costimulatory signals. T cell activation relies on the coordinated engagement of several receptors: the T cell receptor (TCR) recognizes the MHC-peptide complex, while the CD4 or CD8 coreceptors bind to MHC class II or class I molecules, respectively, at distinct sites. Adhesion molecules reinforce the interaction between T cells and APCs, and receptors for co-stimulatory molecules, such as CD28, are essential to initiate robust signaling cascades. The TCR complex itself is composed of the antigen-recognizing TCR (formed by α and β chains) and associated signaling molecules, notably the CD3 proteins and the ζ (zeta) chain (Abbas et al., 2014, pp. 97–101).

Depending on the origin of antigens, the presentation pathway differs: antigens from the extracellular environment are processed and displayed via class II MHC molecules to CD4+ T cells, whereas cytosolic or nuclear antigens are presented on class I MHC molecules to CD8+ T cells. The complete activation of T cells demands not only TCR engagement but also costimulation, predominantly mediated by the interaction of CD28 on T cells with B7-1 (CD80) or B7-2 (CD86) on APCs. These co-stimulatory signals are critical, particularly for the activation of naïve T cells. Furthermore, to regulate and terminate immune responses, activated T cells upregulate inhibitory receptors such as CTLA-4 and PD-1. Both molecules dampen T cell activity by binding to the same ligands as CD28, thus competing with activating signals. The capacity of tumors to exploit these inhibitory pathways underlies the therapeutic success of immune checkpoint inhibitors, notably antibodies targeting CTLA-4 and PD-1, which

can restore and amplify anti-tumor immune responses in cancer patients (Abbas et al., 2014, pp. 171–179) (**Fig. 6**).

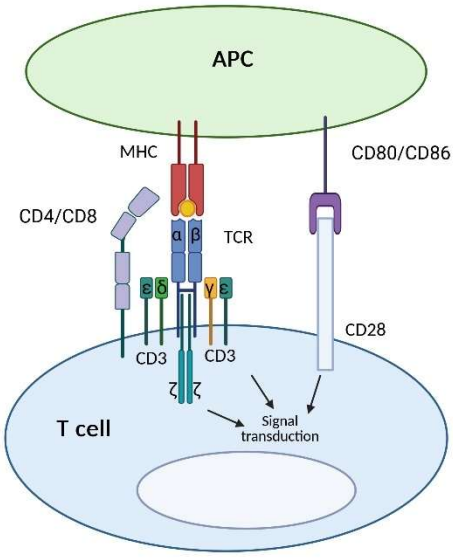

Figure 6. Antigen recognition and signal transduction during T cell activation. The T cell receptor (TCR), composed of α and β chains, associates noncovalently with CD3 and ζ proteins through interactions in their transmembrane domains. Upon antigen recognition, these molecules transmit intracellular signals. CD4 or CD8 co-receptors stabilize the interaction by binding to MHC class II or I molecules, respectively. Antigen-presenting cell (APC); Major histocompatibility (MHC). *Figure created with BioRender.com*

Regulatory T cells (Tregs) employ multiple mechanisms to suppress immune responses. One strategy involves the secretion of inhibitory cytokines, such as interleukin-10 (IL-10) and transforming growth factor-beta (TGF-β), which can dampen the activation of lymphocytes, dendritic cells, and macrophages. Tregs also express high levels of the inhibitory receptor CTLA-4, which can interfere with the function of APCs by removing or blocking B7 molecules, thereby preventing these APCs from delivering the necessary costimulatory signals through CD28 to activate T cells. Furthermore, due to their elevated expression of the IL-2 receptor, Tregs are able to sequester IL-2, a critical growth factor for T cells, limiting its availability to other lymphocytes and thus restraining their expansion and activation (Abbas et al., 2014, pp. 171–179).

7.2 T cell exhaustion

The activation of T cells naturally leads to the upregulation of inhibitory receptors (IRs) on their surface, establishing a negative feedback mechanism aimed at balancing activation signals and preventing excessive proliferation and inflammatory responses. In contexts of persistent antigen stimulation, T cells progressively lose functionality in a process termed "exhaustion," which acts as a regulatory program to limit effector functions under chronic stimulation conditions (McLane et al., 2019).

CD8+ T cell exhaustion can arise in various settings of sustained antigen exposure, notably during chronic infections and cancer (Guo et al., 2018; Fenwick et al., 2019). Although exhaustion may help to protect against autoimmunity, it also impairs effective tumor control, facilitating tumor progression. Despite the expression of early activation markers such as CD69, exhausted CD8+ T cells are incapable of efficiently killing tumor cells and fail to produce interferon-gamma (IFN-γ) upon restimulation.

Functionally, exhausted T cells exhibit a broad range of defects, including diminished cytolytic activity (e.g., impaired granzyme production), reduced cytokine secretion, decreased proliferative capacity, metabolic reprogramming, and sustained expression of multiple inhibitory receptors, ultimately contributing to the failure of tumor eradication (Baessler and Vignali, 2024).

Among the key inhibitory receptors involved are CTLA-4, PD-1, LAG-3 and TIM-3. These molecules, initially induced following TCR engagement, serve to modulate T cell activation by counterbalancing costimulatory signals and regulating both proliferation and effector functions. In the tumor microenvironment, CD8+ tumor-infiltrating lymphocytes (TILs) commonly display high co-expression levels of these inhibitory receptors, reflecting their chronic activation status (Jiang et al., 2015) (**Fig. 7**).

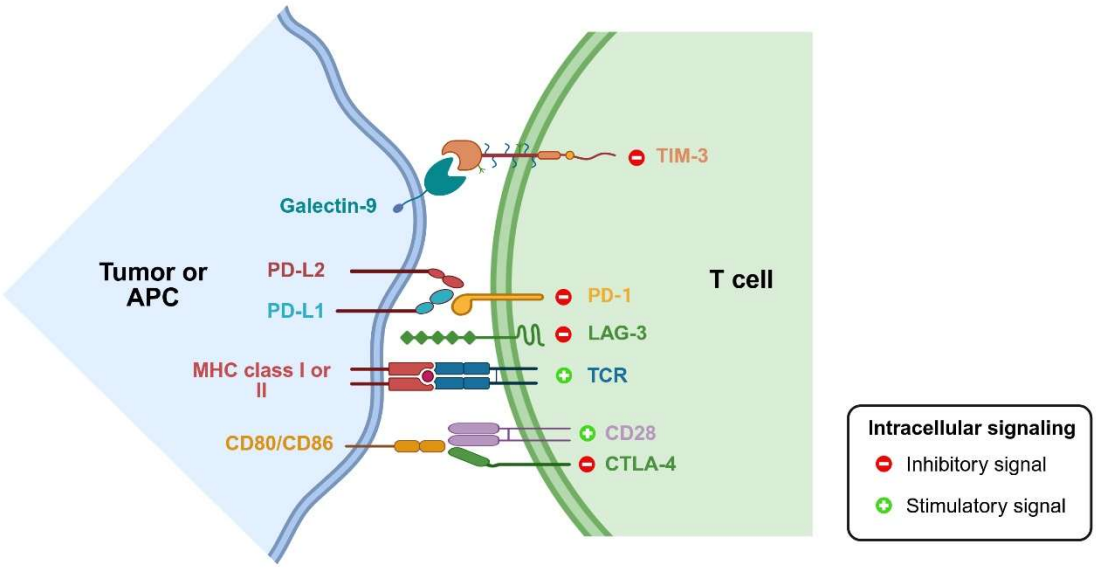

Figure 7. Stimulatory and inhibitory receptor-ligand interactions regulating T cell activation. T cells are activated upon TCR recognition of peptide-MHC complexes on dendritic or tumor cells. Binding of inhibitory ligands (PD-L1, Galectin-9) to inhibitory receptors (e.g., PD-1, LAG-3, TIM-3, CTLA-4) on T cells can induce anergy or apoptosis. In contrast, engagement of costimulatory ligands (e.g., CD80/CD86) with costimulatory receptors (e.g., CD28) promotes T cell proliferation and differentiation into effector T cells. *Figure created with BioRender.com*

OBJECTIVE

OBJECTIVE

The immune system plays a central role in detecting and eliminating cancer cells, from early transformation stages to metastatic dissemination. Nevertheless, solid tumours such as lung cancer can adopt immune evasion strategies that compromise this surveillance. Given the strong influence of PM on pulmonary inflammation and immunity, its potential role in facilitating tumour escape remains insufficiently understood. By focusing on how PM exposure reshapes lung immune dynamics, this thesis highlights a critical yet underexplored mechanism by which PM may contribute to lung tumour progression.

Although neutrophil activation in response to air pollution is well established, the specific impact of PM on neutrophil function remains poorly characterized. Beyond their role in acute inflammation, neutrophils are emerging as key modulators of adaptive immunity through their immunoregulatory properties. This work will therefore examine how PM exposure shapes the recruitment and function of lung neutrophils, and how these changes may promote a pro-tumorigenic microenvironment.

We hypothesize that DEP promote inflammatory alterations in the lung microenvironment that favour tumour expansion. To test this, we analysed the heterogeneity and immunosuppressive properties of PMNs recruited to the lungs of mice exposed to acute and chronic DEP. Using flow cytometry and functional assays, we characterized their molecular, phenotypic, and functional profiles. In parallel, we examined how chronic DEP exposure influences T cell phenotypes and contributes to lung tumour progression, with a specific focus on the expression of exhaustion markers and the accumulation of Tregs, using a genetically engineered mouse model of lung adenocarcinoma.

EXPERIMENTAL SECTION

EXPERIMENTAL SECTION

1. Materials and Methods

Mice

Animal procedures were conducted in accordance with the Federation of European Laboratory Animal Science Associations (FELASA) and all experiments had previously been approved by the Animal Ethical Committee of the University of Liege (protocol references: # 2136). C57BL/6 mice (male, 6–8-week-old) were purchased from Janviers-Labs (France). $Kras^{LSL\text{-}G12D/+}$-$Trp53^{lox/lox}$ (KP) mice were obtained from Dr Pierre Close's laboratory at University of Liège (male and female mice aged 12-16 weeks were used). All mice were housed and bred in institutional specific pathogen-free facilities at the GIGA Institute (Liège, Belgium), maintained in a 12-hour light-dark cycle and had access to normal diet chow and water ad libitum.

Intratracheal instillations of DEP into mouse lungs

Diesel Exhaust Particles (DEP) were provided by a Standard Reference Material (SRM) produced and certified by the National Institute of Standards and Technology (NIST) (Sigma Aldrich; NIST1650b; 1333-86-4). DEP (4mg/ml) were resuspended in sterile PBS with 0,05% Tween-20 (Sigma-Aldrich) using sonication. Mice were briefly anesthetized using 2,5% isoflurane/O_2 mixture followed by intratracheal administration of 100µg or 200µg DEP in a volume of 50µl Phosphate-Buffered Saline Tween-20 solution (PBST) at the indicated time points.

Acute exposure model

C57BL/6 mice were intratracheally (i.t.) administered 200 µg of DEP or PBST on days 0 and 4, followed by euthanasia on day 5.

Chronic exposure model

In this model, Cre recombination was never induced and $Kras^{LSL\text{-}G12D/+}$-$Trp53^{lox/lox}$ (KP) mice did not develop spontaneous lung tumours. Non-recombined KP mice received two i.t. doses of 200 µg DEP or PBST on days 0 and 4, followed by weekly administration of 100 µg DEP or PBST. Mice were euthanized 90 days after the first i.t. administration.

Transgenic mouse model of lung adenocarcinoma

In this model, $Kras^{LSL\text{-}G12D/+}$-$Trp53^{lox/lox}$ mice initially followed the same protocol of DEP instillation as the chronic exposure model. In addition, Cre-mediated recombination was initiated at day 5 by intratracheal administration of an AAV-Cre vector (AAV6.2ff-Spb-Cre; 5,8 x 10^{12} virus particles per 100 µl) to induce spontaneous tumorigenesis. Mice were euthanized 90 days after the AAV-Cre administration, and tumour burden was assessed by histological analysis using hematoxylin and eosin (H&E) staining.

Lung cell isolation

Mice were perfused with ice-cold PBS via the right ventricle after sacrifice. The lungs were then excised, finely minced with scalpel blades, and subjected to enzymatic digestion in HBSS medium containing collagenase D (1 mg/ml, Roche) and deoxyribonuclease I (50 µg/ml, Roche) at 37°C for 1 hour with intermittent shaking. Red blood cells were removed by resuspending cells in 1 ml of 1x RBC lysis buffer (Thermo Fisher Scientific) incubated for 5 minutes at room temperature, then washed with PBS containing 2% FBS and 2.5 mM EDTA. Lung cells were subsequently filtered through a 70 µM cell strainer (Corning). Resulting in a single-cell suspensions that was kept at 4°C for all steps if not stated otherwise.

Spleen cell isolation

Spleens were crashed manually with the embole of a syringer. Red blood cells were removed by resuspending cells 2x in 1ml of 1x RBC lysis buffer (Thermo Fisher Scientific) incubated for 5 minutes at room temperature, then washed with PBS containing 2% FBS and 2.5 mM EDTA. Spleen cells were subsequently filtered through a 70 µM cell stainer (Corning), resulting in a single-cell suspensions that was kept at 4°C for all follow up steps if not stated otherwise.

T cell isolation from lymphoid tissues

Lymphocytes were isolated by mechanically disrupting lymph nodes from naïve C57BL/6 mice using a flat-bottomed syringe, followed by collection in PBS-EDTA. Pan T cells were then isolated using the Pan T Cell Isolation Kit (Miltenyi Biotec) in accordance with the manufacturer's instructions, and separation was performed using LS columns on a QuadroMACS separator (Miltenyi Biotec).

Flow cytometry staining

Cells were first incubated for 15 min with Fc Block (anti-mouse CD16/32, clone 93, BioLegend), diluted in FACS buffer (PBS with 0,5% BSA). Surface marker antibodies were resuspended in FACS buffer (PBS with 0,5% BSA) and cells were incubated for 30 min with the corresponding fluorochrome-conjugated antibodies (listed in the key resources table). Cells were washed with PBS and stained with fix viability staining Zombie Aqua, Violet, or NIR (BioLegend) resuspended in PBS and incubated for 20 min. Cells were than washed with PBS and resuspended on FACS buffer or follow intracellular staining of target proteins.

For the detection of intracellular cytoplasmic proteins (GZMA, GZMB, and IFNγ), cells were first subjected to a restimulation and accumulation step prior to surface and intracellular staining. Cells were cultured in a stimulation/accumulation medium composed of RPMI 1640 (Lonza) supplemented with 10% FBS (Gibco), 50 U/mL penicillin-streptomycin (Gibco), 1% MEM non-essential amino acids (Gibco), 0.05 mM 2-mercaptoethanol (Gibco), brefeldin A (5 µg/ml), and monensin (2µM) (to inhibit cytokine secretion and allow intracellular accumulation). Anti-mouse CD3 (5 µg/mL; eBioscence) and anti-mouse CD28 (1 µg/mL; eBioscience) antibodies were added for T cell stimulation. The cells were incubated for 4 hours at 37 °C in a 5% CO_2 atmosphere. Following restimulation, cells were stained with surface antibodies and viability dye, then fixed and permeabilized using the Cyto-Fast™ Fix/Perm buffer set (BioLegend), according to the manufacturer's instructions. Intracellular staining was performed in permeabilization buffer by incubating cells with the appropriate antibodies for 30 minutes at room temperature.

For intranuclear protein staining, cells were first incubated with surface antibodies and viability dye. Following this, fixation and permeabilization were performed using the Foxp3/Transcription Factor Staining Buffer Set (eBioscience), according to the manufacturer’s instructions. Intranuclear antibodies were diluted in the kit’s permeabilization buffer and incubated with the cells for 1 hour at room temperature

Flow cytometry acquisition was performed on BD LSR Fortessa using FACSDiva software, and the data was processed with Flow Jo software (V10). Gating strategies to identify the different cell populations are provided in Figure 8-10.

Isolation of CD14^{neg} and CD14^{pos} PMNs

Mouse neutrophils (PMNs) were isolated from lung single-cell suspensions prepared as previously described. The cell suspension was incubated with Anti-Ly-6G Microbeads (Miltenyi Biotec) and passed through MACS LS columns (Miltenyi Biotec) on a QuadroMACS separator (Miltenyi Biotec) to capture neutrophils, following the manufacturer's protocol. Neutrophils were eluted by gently plunging the LS columns and subsequently stained with anti-Ly6G, anti-CD14 and the viability marker SYTOX™ blue (ThermoFisher Scientific). They were then sorted using a BD FACS Aria (BD Biosciences) as CD14 negative or positive neutrophils. The isolated PMNs were then used for further analysis.

Cytospin of neutrophils

After FACS sorting of CD14^{neg} and CD14^{pos} PMNs, cytospins were prepared using a StatSpin CytoFuge 2 (IRIS compagny). In detail, 2.5x10^4 cells were centrifuged (4400 rpm, 2 min) onto Superfrost microscope slides (Epredia) and dried overnight at room temperature. Cells were then fixed in Methanol and stained with hematoxylin and eosin (H&E). Image documentation was performed using the NanoZoomer 2.0-HT slide scanner system (Hamamatsu) and the NanoZoomer Digital Pathology software.

T cell suppression assay

CD14^{neg} and CD14^{pos} PMNs were FACS sorted as described above.

T cells were isolated as previously described, then washed in PBS and labelled with CellTrace Violet (Invitrogen) following the manufacturer’s instructions. To activate the T cells in culture, a 96-well tissue culture plate was pre-coated with anti-mouse CD3 antibody (5 µg/ml; eBioscience) overnight at 4°C, then washed with PBS. PMNs and T cells were co-cultured at a 1:1 ratio or alone as controls in 200 µl RPMI medium (Lonza) per well, supplemented with 10% FBS (Gibco), 50 U/ml penicillin-streptomycin (Gibco), 1% MEM nonessential amino acids (Gibco), 1 mM sodium pyruvate (Gibco), and 0.05 mM 2-mercaptoethanol (Gibco). Anti-mouse CD28 (1 µg/ml; eBioscience) was also added to the culture to provide co-stimulatory signalling on T cells. The cells were incubated at 37°C in a 5% CO_2 environment for 72 hours, after which T cells were collected from the supernatant, stained for surface markers (anti CD3 and CD8) and viability. Finally, proliferation of CD8$^+$ T cells was assessed using a BD LSR Fortessa flow cytometer.

Treg induction assay

$CD14^{neg}$ and $CD14^{pos}$ PMNs were FACS sorted as described above. Lymphocytes were isolated by mechanically disrupting lymph nodes from naïve C57BL/6 mice using a flat-bottomed syringe, followed by collection in PBS-EDTA. Naïve CD4+ T cells were then isolated using the MojoSort Mouse CD4 Naive T Cell Isolation Kit (BioLegend) in accordance with the manufacturer's instructions, and separation was performed using LS columns on a QuadroMACS separator (Miltenyi Biotec).

To activate the T cells in coculture, a 96-well tissue culture plate was pre-coated with anti-mouse CD3 antibody (5 µg/ml; eBioscience) overnight at 4°C, then washed with PBS. PMNs and naïve CD4+ T cells were co-cultured at a ratio of 1 PMN for 5 naïve T cells in 200 µl RPMI medium (Lonza) per well, supplemented with 10% FBS (Gibco), 50 U/ml penicillin-streptomycin (Gibco), 1% MEM nonessential amino acids (Gibco), 1 mM sodium pyruvate (Gibco), and 0.05 mM 2-mercaptoethanol (Gibco). Anti-mouse CD28 (1 µg/ml; eBioscience) was also added to the culture. The cells were incubated at 37°C in a 5% CO_2 environment for 5 days, after which expression of the Treg-associated markers CD25 and Foxp3 was analyzed using a BD LSR Fortessa flow cytometer.

Quantitative real time polymerase chain reaction (qRT-PCR)

Total RNA was extracted from sorted $CD14^{neg}$ and $CD14^{pos}$ PMNs using the ReliaPrep RNA Cell Miniprep System kit (Promega) according to the manufacturer's instructions. cDNA was produced using FastGene Scriptase II cDNA 5x ReadyMix (Nippon Genetics EUROPE) and the reverse transcription reaction was then subjected to PCR amplification using FastStart Universal SYBR Green Master (Roche). PCR signals were recorded on a QuantStudio 3 Real-Time PCR System (ThermoFisher) and analysed using the ThermoFisher Design and Analysis Software 2.6.0. Primer sets included murine iNOS-Fwd (5'-GTTCTCAGCCCAACAATACAAGA-3'), murine iNOS-Rv (5'-GTGGACGGGTCGATGTCAC -3'), murine CD274-Fwd (5'-GCTCCAAAGGACTTGTACGTG-3'), murine CD274-Rv (5'-TGATCTGAAGGGCAGCATTTC-3'), murine PTGS2-Fwd (5'-TGAGCAACTATTCCAAACCAGC-3'), murine PTGS2-Rv (5'-GCACGTAGTCTTCGATCACTATC-3'), murine ARG1-Fwd (5'-CTCCAAGCCAAAGTCCTTAGAG-3'), murine ARG1-Rv (5'-AGGAGCTGTCATTAGGGACAT-3'), murine IL10-Fwd (5'-

GCTCTTACTGACTGGCATGAG-3'), murine IL10-Rv (5'-CGCAGCTCTAGGAGCATGTG-3'), murine TGFβ-Fwd (5'-CGTCACTGGAGTTGTACGGCAG-3'), murine TGFβ-Rv (5'-CGTTTGGGGCTGATCCCGTTG-3').

Identification of NETs *in vivo* and *in vitro*

In our *in vivo* experiments, 4 µm sections of paraffin-embedded mouse lungs were prepared and mounted on glass slides. Following dewaxing, antigen retrieval was conducted using EDTA buffer (Dako), and the sections were permeabilized with 0.5% Triton X-100 for 2 minutes. The specimens were then blocked with Animal-Free Blocking Solution (Cell Signaling). The sections were incubated with primary antibodies: anti-citrullinated-histone H3 (1:100; Abcam ab5103) and anti-myeloperoxidase (MPO) (1:60; R&D Systems AF3667). Detection was performed using Alexa Fluor 555 donkey anti-rabbit (1:200; ThermoFisher A-31572) and Alexa Fluor 488 donkey anti-goat (1:200; ThermoFisher A-11055) secondary antibodies for 1 hour at room temperature. Hoechst staining was used to detect DNA.

In our *in vitro* experiments, sorted $CD14^{neg}$ and $CD14^{pos}$ PMNs ($2x10^5$) were plated and allowed to adhere to Poly-D-lysine-coated slides (Sigma-Aldrich) in DMEM without FBS at 37°C in a 5% CO_2 environment for 16 hours. The slides were fixed in 4% paraformaldehyde (PFA), then permeabilized, blocked, and incubated with the previously described primary and secondary antibodies at the same concentrations. Visualization was performed using an Olympus Slideview VS200. Fluorescence microscopy images were analysed with Image J software to count the number of NETs per one hundred neutrophils. To quantify NET-DNA in bronchoalveolar lavage fluid (BALF), a PicoGreen assay kit (Invitrogen) was employed.

Collection of bronchoalveolar lavage fluid (BALF)

After sacrifice, a bronchoalveolar lavage was performed by injecting 3x 1ml of PBS-EDTA 0,05mM into lungs. Collected bronchoalveolar lavage fluid (BALF) was centrifuged 10 min at 110 rcf and supernatants were stored at -80°C for further analyses.

Immunohistochemistry

Tumour-bearing lungs of KP mice were perfused post-mortem by PBS injection through the right ventricle of the heart. The tissues were then fixed overnight in 10%

formalin and subsequently transferred to 70% ethanol for storage until further processing. For histological analysis, the tissues were paraffin-embedded, sectioned, and stained with hematoxylin and eosin (H&E).

An original image analysis algorithm was implemented to automatically perform image processing and measurements using the Image Processing Toolbox of MATLAB 9.13 (R2022b) software (MathWorks, Inc.). This method allowed the determination of tumour size distribution through the following steps:

1. Image acquisition: Histological section images were acquired in full-colour red, green, and blue (RGB) space. In these images, tumours appeared as dark red regions clearly contrasted against a light red background. Image processing was then carried out using only the red channel.

2. Image binarization: To determine tumour size, the red channel images were binarized using an automatic thresholding technique (8). In the resulting binary images, all pixels corresponding to the objects of interest (i.e., dark red tumours) were assigned a value of 1, while background pixels were assigned a value of 0. Binary images also contained non-tumour structures, such as epithelial cells surrounding the alveoli and these were removed using morphological filtering. The resulting binary images were then systematically compared with the original images and manually corrected when necessary.

3. Tumour labelling and measurement: Each tumour in the binary images was labelled, and the number of pixels in each tumour was recorded. These pixel counts were then multiplied by the calibrated size of a single pixel to calculate tumour areas.

4. Size distribution analysis: A histogram of tumour sizes was generated for each mouse, and the mean histogram was calculated for each experimental condition.

Ki67 staining was performed in, paraffin-embedded tissue sections that were first deparaffinized and rehydrated. Antigen retrieval was conducted using Target Retrieval Solution (Citrate pH 6, Dako) under heat-induced conditions. To inhibit endogenous peroxidase activity, sections were incubated in 3% hydrogen peroxide (H_2O_2) in distilled water for 20 minutes at room temperature. Subsequently, sections were blocked with an Animal-Free Blocking Solution (Cell Signaling) for 1 hour at room temperature. The sections were then incubated with the primary antibody, Ki67 (1:100,

Abcam ab1667), for 1 hour at room temperature. Detection was carried out using the EnVision System-HRP, followed by incubation with the DAB substrate. Sections were counterstained with hematoxylin-eosin, and images were captured using a NanoZoomer 2.0-HT slide scanner system (Hamamatsu) with NanoZoomer Digital Pathology software. Cellular proliferation was assessed by quantifying the density of Ki67 staining, defined as the area occupied by Ki67-positive regions divided by the total area of the whole image. Ki67 regions were binarized from the red channel of the original RGB images, using the same method described above. From the resulting binary images, the total number of pixels corresponding to Ki67 staining was calculated and normalized to the total image area.

Statistical analysis

All statistical analyses were performed using GraphPad Prism software (8.0.1). Results were expressed as means ± SEM. An unpaired t test was used to compare two groups with normally distributed data. When the assumption of normality was not met, the non-parametric Mann–Whitney test was used instead. For comparisons of means between more than two experimental groups, one-way analysis of variance (ANOVA) was used as appropriate. Pvalue > 0,05 was considered not significant (ns); Pvalue < 0,05 was considered significant. P values are provided within each figure legend, together with the statistical test performed for each experiment.

Reagent or resource

REAGENT or RESOURCE	SOURCE	IDENTIFIER
Antibodies		
PerCP/Cyanine5.5 anti-mouse Ly-6G Antibody (Clone 1A8)	Biolegend	127615; RRID : AB_1877272
PE anti-mouse CD64 (FcγRI) Antibody (Clone X54-5/7.1)	Biolegend	139303; RRID : AB_10613467
PE/Dazzle™ 594 anti-mouse CD8a Antibody (Clone 53-6.7)	Biolegend	100761; RRID : AB_2564026
PE-Cy™7 anti-Mouse CD11c (Clone HL3)	BD Biosciences	558079; RRID : AB_647251
APC anti-mouse CD170 (Siglec-F) Antibody (Clone S17007L)	Biolegend	155507; RRID : AB_2750236
Brilliant Violet 650™ anti-mouse Ly-6C Antibody (Clone HK1.4)	Biolegend	128049; RRID : AB_2800630
Brilliant Violet 785™ anti-mouse/human CD11b Antibody (Clone M1/70)	Biolegend	101243; RRID : AB_2561373
BUV395 anti-Mouse CD45 (Clone 30-F11)	BD Biosciences	564279; RRID : AB_2651134
Spark UV™ 387 anti-mouse CD45 Antibody (Clone 30-F11)	Biolegend	103187; RRID : AB_3083254
BUV737 Rat Anti-Mouse CD4 (Clone RM4-5)	BD Biosciences	612843; RRID : AB_2870165
PE anti-mouse/human CD11b Antibody (Clone M1/70)	Biolegend	101207; RRID : AB_312790
PE/Cyanine7 anti-mouse CD45 Antibody (Clone 30-F11)	Biolegend	103113; RRID : AB_312978
APC anti-mouse CD14 Antibody (Clone Sa14-2)	Biolegend	123311; RRID : AB_940574
Brilliant Violet 421™ anti-mouse Ly-6G Antibody (Clone 1A8)	Biolegend	127627; RRID : AB_10897944
Brilliant Violet 785™ anti-mouse Ly-6C Antibody (Clone HK1.4)	Biolegend	128041; RRID : AB_2565852
PE-CF594 anti-mouse Siglec-F (Clone E50-2440)	BD Biosciences	562757; RRID : AB_2687994
Brilliant Violet 711™ anti-mouse CD64 (FcγRI) Antibody (Clone X54-5/7.1)	Biolegend	139311; RRID : AB_2563846
PE anti-mouse CD3ε Antibody (Clone KT3.1.1)	Biolegend	155607; RRID : AB_2750433
FITC anti-mouse CD3ε Antibody (Clone 145-2C11)	Biolegend	100306; RRID : AB_312670

APC anti-mouse CD4 Antibody (Clone RM4-5)	Biolegend	100515; RRID : AB_312718
FITC anti-mouse CD8a Antibody (Clone 53-6.7)	Biolegend	100705; RRID : AB_312744
CD3 monoclonal antibody (Clone 17A2)	eBioscience	16-0032-82; RRID : AB_468851
PerCP/Cyanine5.5 anti-mouse/human CD11b Antibody (Clone M1/70)	Biolegend	101227; RRID : AB_893233
APC/Fire™ 750 anti-mouse Ly-6G Antibody (Clone 1A8)	Biolegend	127651; RRID : AB_2616732
Brilliant Violet 711™ anti-mouse CD274 (B7-H1, PD-L1) Antibody (Clone 10F.9G2)	Biolegend	124319; RRID : AB_2563619
PE/Dazzle™ 594 anti-mouse CD172a (SIRPα) Antibody (Clone P84)	Biolegend	144015; RRID : AB_2565279
PE anti-mouse CD73 Antibody (Clone TY/11.8)	Biolegend	127205; RRID : AB_1089065
Brilliant Violet 421™ anti-mouse CD170 (Siglec-F) Antibody (Clone S17007L)	Biolegend	155509; RRID : AB_2810421
Alexa Fluor® 700 anti-mouse CD45 Antibody (Clone 30-F11)	Biolegend	103127; RRID : AB_4937140
PE anti-mouse CD3 Antibody (Clone 17 A2)	Biolegend	100205; RRID : AB_312662
APC/Fire™ 750 anti-mouse CD4 Antibody (Clone RM4-5)	Biolegend	100567; RRID : AB_2629698
PerCP/Cyanine5.5 anti-mouse CD8a Antibody (Clone 53-6.7)	Biolegend	100733; RRID : AB_2075239
Brilliant Violet 785™ anti-mouse CD69 Antibody (Clone H1.2F3)	Biolegend	104543; RRID : AB_2629640
PE-Cyanine7 anti-mouse CD279 (PD-1) monoclonal Antibody (Clone J43)	eBioscience	25-9985-80; RRID : AB_10853805
APC anti-mouse CD39 Antibody (Clone Duha59)	Biolegend	143809; RRID : AB_2750319
Brilliant Violet 711™ anti-mouse CD25 Antibody (Clone PC61)	Biolegend	102049; RRID : AB_2564130
eFluor™ 450 anti-mouse FOXP3 monoclonal Antibody (Clone FJK-16s)	eBioscience	48-5773-82; RRID : AB_1518812
PE-Cyanine7 anti-mouse Arginase 1 monoclonal Antibody (Clone A1exF5)	eBioscience	25-3697-82 ; RRID : AB_2734841
FITC Mouse anti-Ki67 Set	BD Biosciences	556026; RRID : AB_396302
APC anti-mouse NK-1.1 Antibody (Clone S17016D)	Biolegend	156505; RRID : AB_2876525

eFluor™ 450 anti-mouse CD4 monoclonal Antibody (Clone RM4-5)	eBioscience	48-0042-82; RRID : AB_1272194
Brilliant Violet 711™ anti-mouse CD223 (LAG-3) Antibody (Clone C9B7W)	Biolegend	125243; RRID : AB_2876450
PE anti-mouse Granzyme A Antibody (Clone 3G8.5)	Biolegend	149703; RRID : AB_2565309
FITC anti-human/mouse Granzyme B Antibody (Clone GB11)	Biolegend	515403; RRID : AB_2114575
PE/Cyanine7 anti-mouse IFN-γ Antibody (Clone XMG1.2)	Biolegend	505825; RRID : AB_1595591
Purified anti-mouse CD16/32 Antibody (Clone 93)	Biolegend	101301; RRID : AB_312800
Anti-Histone H3 (citrulline R2 + R8 + R17) antibody	Abcam	Ab5103
Anti-Human/Mouse Myeloperoxidase/MPO antibody	R&D Systems	AF3667
Anti-Ki67 antibody	Abcam	Ab16667
Donkey anti-Rabbit IgG (H+L) Highly Cross-Adsorbed Secondary Antibody, Alexa Fluor™ 555	ThermoFisher Scientific	A-31572
Donkey anti-Goat IgG (H+L) Cross-Adsorbed Secondary Antibody, Alexa Fluor™ 488	ThermoFisher Scientific	A-11055
Anti-Ly-6G MicroBeads UltraPure, mouse	Miltenyi Biotec	130-120-337
Chemicals		
Zombie Aqua™ Fixable Viability Kit	Biolegend	423101
Zombie NIR™ Fixable Viability Kit	Biolegend	423105
Zombie Violet™ Fixable Viability Kit	Biolegend	423113
CellTrace™ Violet Cell Proliferation Kit	ThermoFisher Scientific	C34557
SYTOX™ Blue Dead Cell Stain	ThermoFisher Scientific	S34857
Hoechst 33342, trihydrochloride, trihydrate	ThermoFisher Scientific	H3570
Pan T cells Isolation Kit II, mouse	Miltenyi Biotec	130-095-130
MojoSort Mouse CD4 Naive T Cell Isolation Kit	Biolegend	480039

Gating strategies

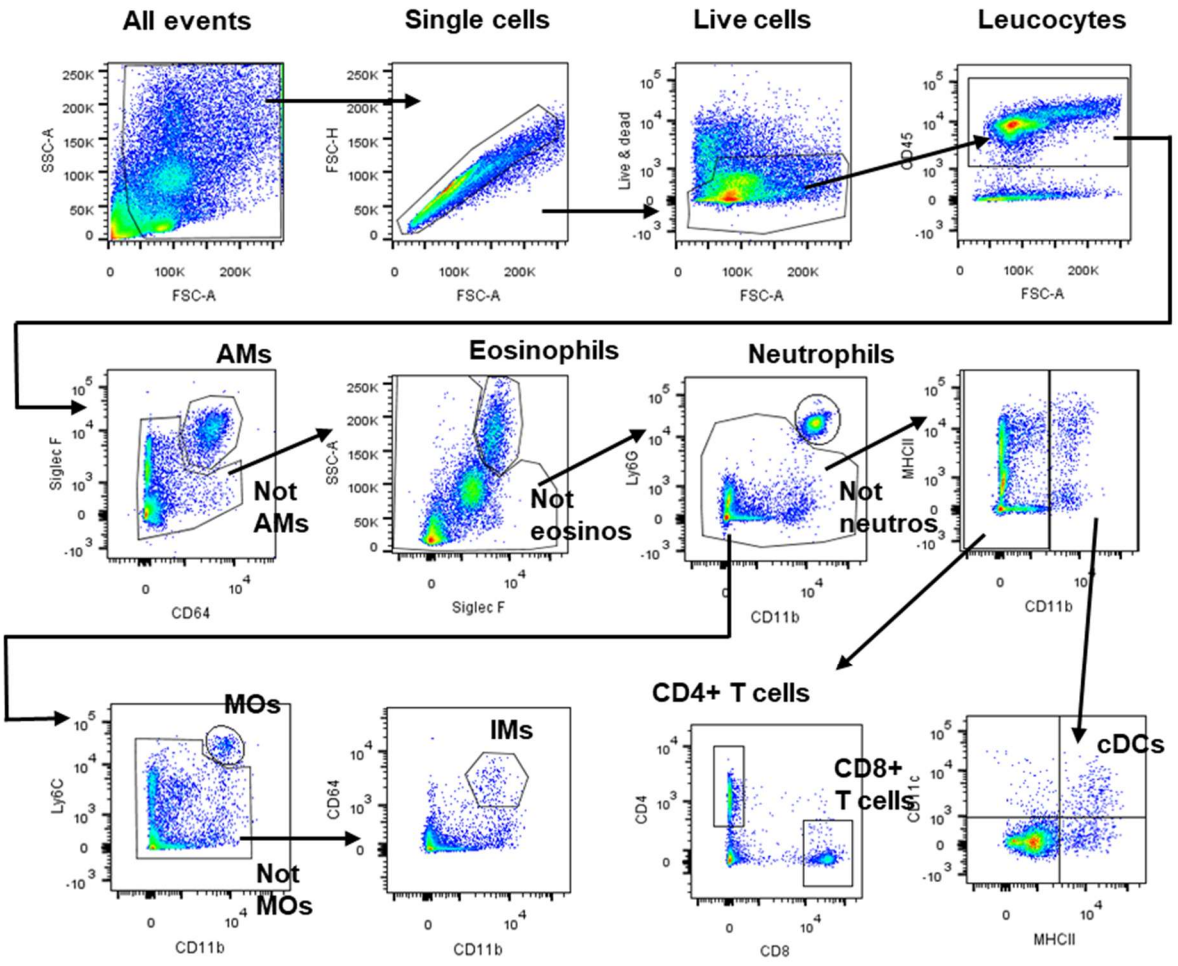

Figure 8. Flow cytometry gating strategy used to identify immune cells. Example of flow gating strategy to determine frequency of alveolar macrophages (AMs), eosinophils, neutrophils, monocytes (MOs), interstitial macrophages (IMs), CD4+ T cells, CD8+ T cells and dendritic cells (cDCs). All samples were first gated to exclude debris and doublets, followed by live cell discrimination.

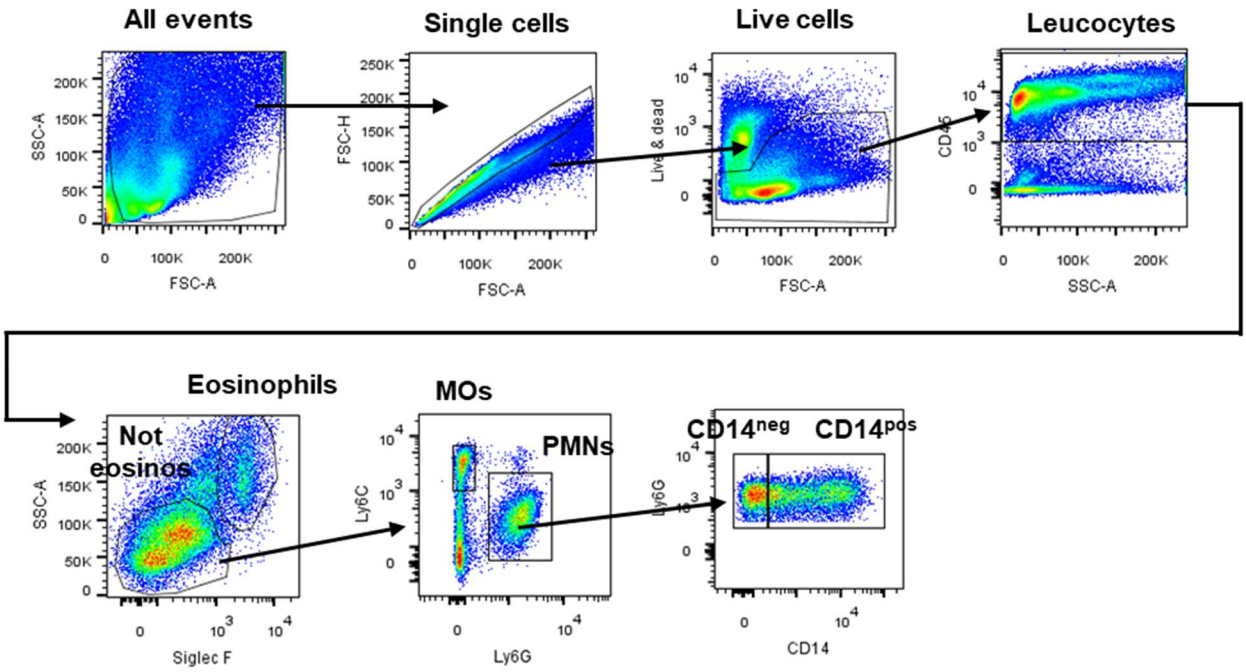

Figure 9. Flow cytometry gating strategy used to identify different subsets of PMNs. Example of flow gating strategy to determine frequency of $CD14^{neg}$ and $CD14^{pos}$ PMNs populations. All samples were first gated to exclude debris and doublets, followed by live cell discrimination.

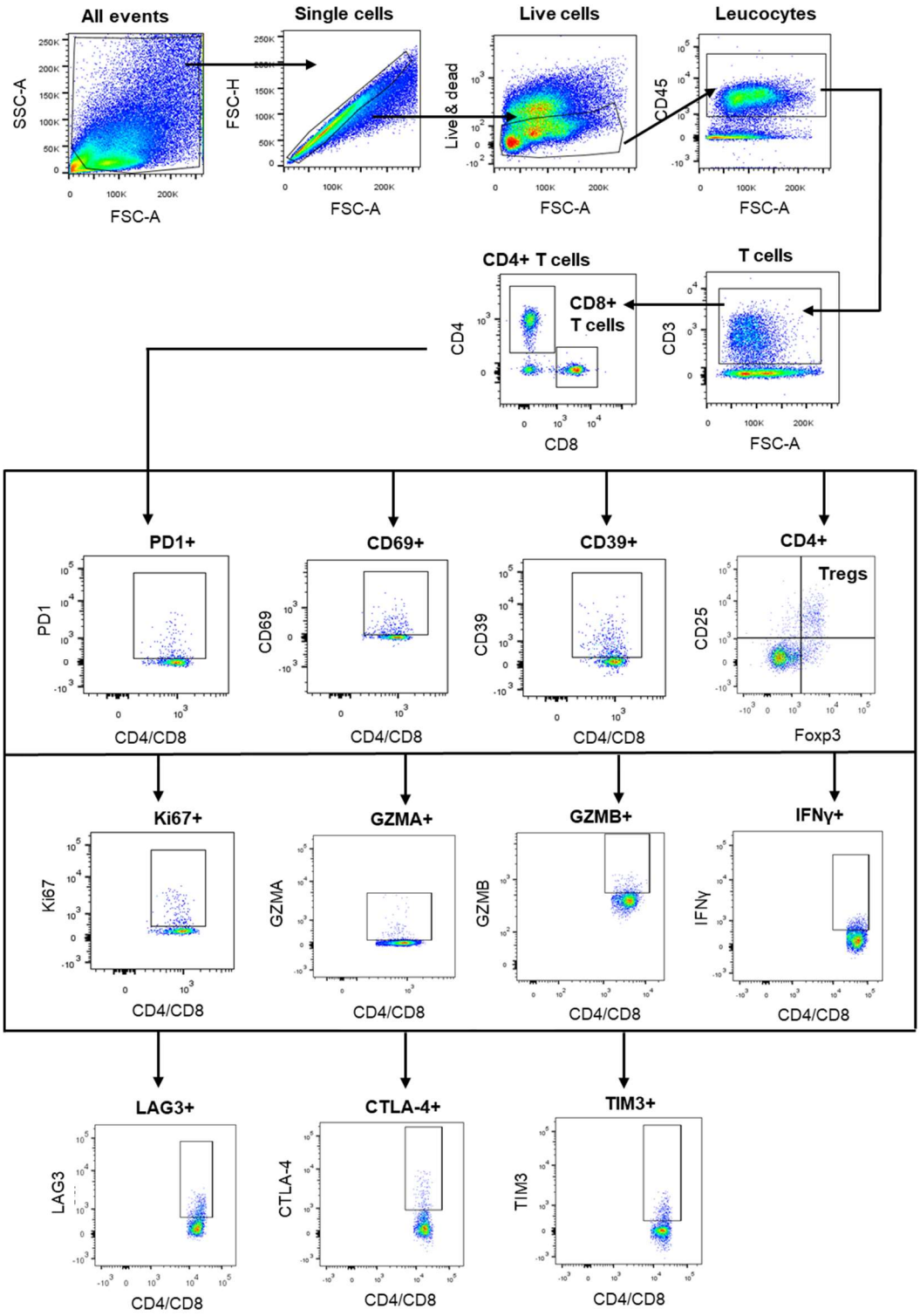

Figure 10. Flow cytometry gating strategy used to identify exhaustion markers on T cells. Example of flow gating strategy to determine frequency of T cells positive for PD1, CD69, CD39, Ki67, GZMA, GZMB, IFNg, LAG3, CTLA-4, TIM3 and Tregs. All samples were first gated to exclude debris and doublets, followed by live cell discrimination.

2. Results

2.1 Acute exposure to DEP induces PMN CD14^{pos} recruitment and NET formation in the lungs

To assess lung inflammation caused by acute DEP exposure in C57BL/6 mice, we quantified lung immune cell populations by flow cytometry. We administered two intratracheal (i.t.) doses of DEP (200 µg per mouse) or PBST on days 0 and 4 (Fig. 11A). After sacrifice on day 5, counts of different leukocytes' subpopulations in lung tissue were measured. Acute DEP exposure led to a significant infiltration of polymorphonuclear neutrophils (PMNs) and a reduction in alveolar macrophages (AMs) while monocytes (MOs), interstitial macrophages (IMs), eosinophils, conventional dendritic cells (cDCs), CD4+ and CD8+ lymphocytes remained unchanged (Fig. 11B).

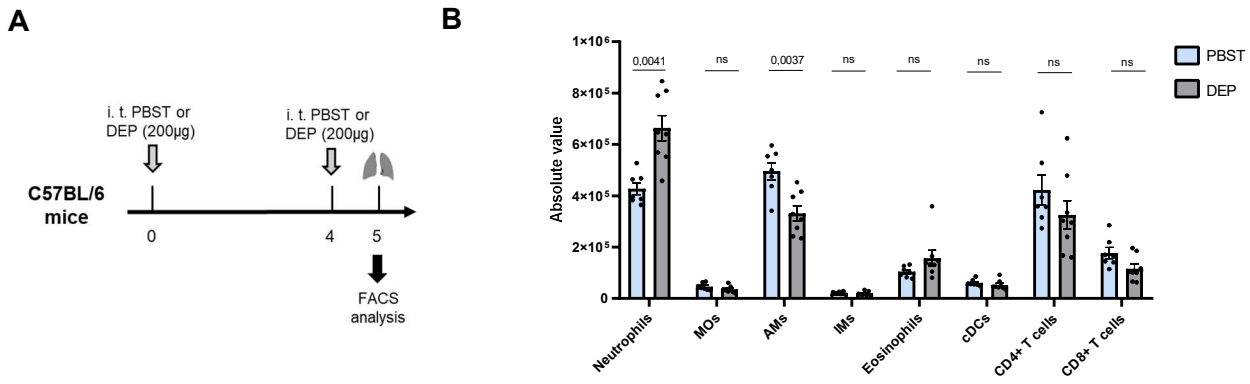

Figure 11. (**A**) Experimental exposure protocol. (**B**) Number of indicated immune cell populations detected by flow cytometry in the lungs after intratracheal instillations of PBST or DEP (200µg) according to the exposure protocol in (A) (n = 7 to 8 mice per group, one experiment).

We measured the proportion of PMN expressing CD14 at the cell membrane, as CD14 has been identified as a marker carried by PMN with immunosuppressive activity in mice, known as polymorphonuclear myeloid-derived suppressor cells (PMN-MDSCs) (Veglia et al., 2021). Interestingly, we observed that DEP exposure led to the emergence of a CD14^{pos} PMNs subpopulation, while we observed no changes in the total count of monocytes (Ly6C^{high}Ly6G^{-}) (Fig. 12A-D). Of note, in the spleen, while the total number of PMNs was higher in the DEP-exposed group, CD14^{pos} was not detectable among PMNs. Indeed, the increased PMN cell counts in the spleen was attributed solely to the infiltration of CD14^{neg} PMNs. Importantly, monocyte counts

remained unchanged between the two groups (Fig. 12E-G). These findings indicate that DEP treatment induces the emergence of CD14^{pos} PMNs restricted to the local lung environment.

Lung

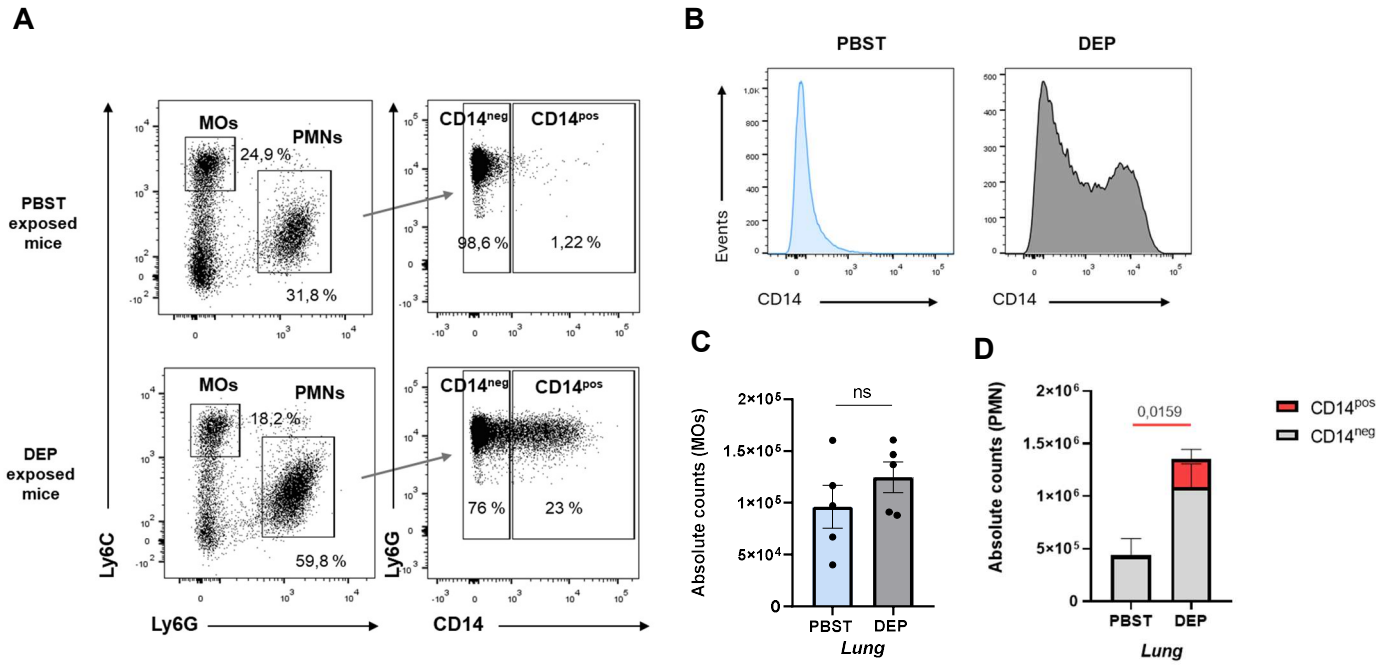

Spleen

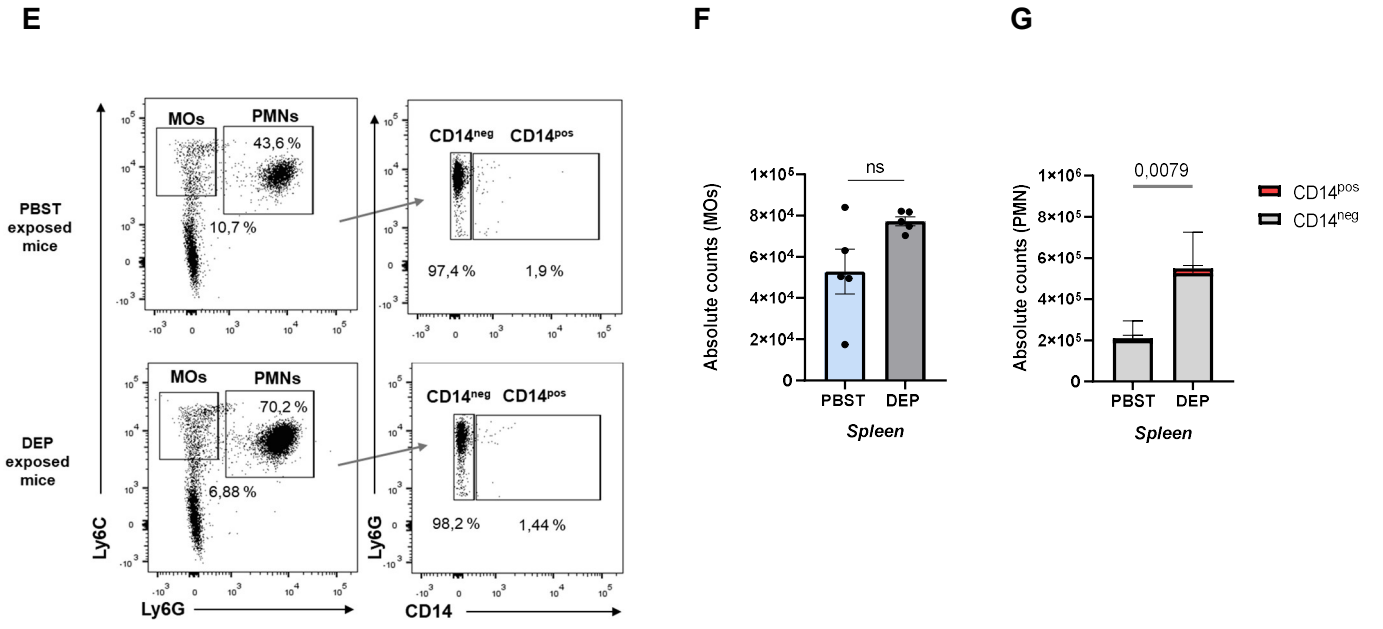

Figure 12. (**A**) Gating strategy used for the identification of MOs, PMNs and their subsets in lungs of PBST or DEP exposed mice according to the exposure protocol in Fig. 11A. Representative flow cytometry histogram of (**B**) CD14 expression in PMNs and absolute counts of (**C**) MOs, (**D**) PMNs $CD14^{neg}$ and $CD14^{pos}$ recruited in the lungs of PBST or DEP exposed mice (n = 4 to 6 mice per group, three independent experiments were performed). (**E**) Gating strategy used for the identification of MOs, PMNs and their subsets in spleen of PBST or DEP exposed mice according to the exposure protocol in Fig. 11A. Absolute counts of (**F**) MOs, (**G**) PMNs $CD14^{neg}$ and $CD14^{pos}$ recruited in the spleen of PBST or DEP exposed mice (n = 5 mice per group, one experiment). Data are presented as mean +/- SEM. Statistical significance was assessed using Mann-Whitney test.

Considering the established link between NET formation and tumour progression (Rocks et al., 2019; Zhang et al., 2024), we investigated whether PMNs increase NET formation after DEP acute exposure. We identified NETs in lung histological samples by the co-localization of citrullinated-histone (Cit-H3), myeloperoxidase (MPO), and DNA -key components of neutrophil granules that are released during NET formation. NET formation was observed in lung tissue of mice exposed to DEP administration but was absent in control mice (Fig. 13A). Furthermore, mice exposed to DEP showed significantly higher levels of dsDNA in their BALF as compared to the control group (Fig. 13B). These results demonstrate that acute DEP exposure triggers the recruitment of PMNs into the lung, promotes the appearance of a $CD14^{pos}$ subpopulation, and leads to NET formation.

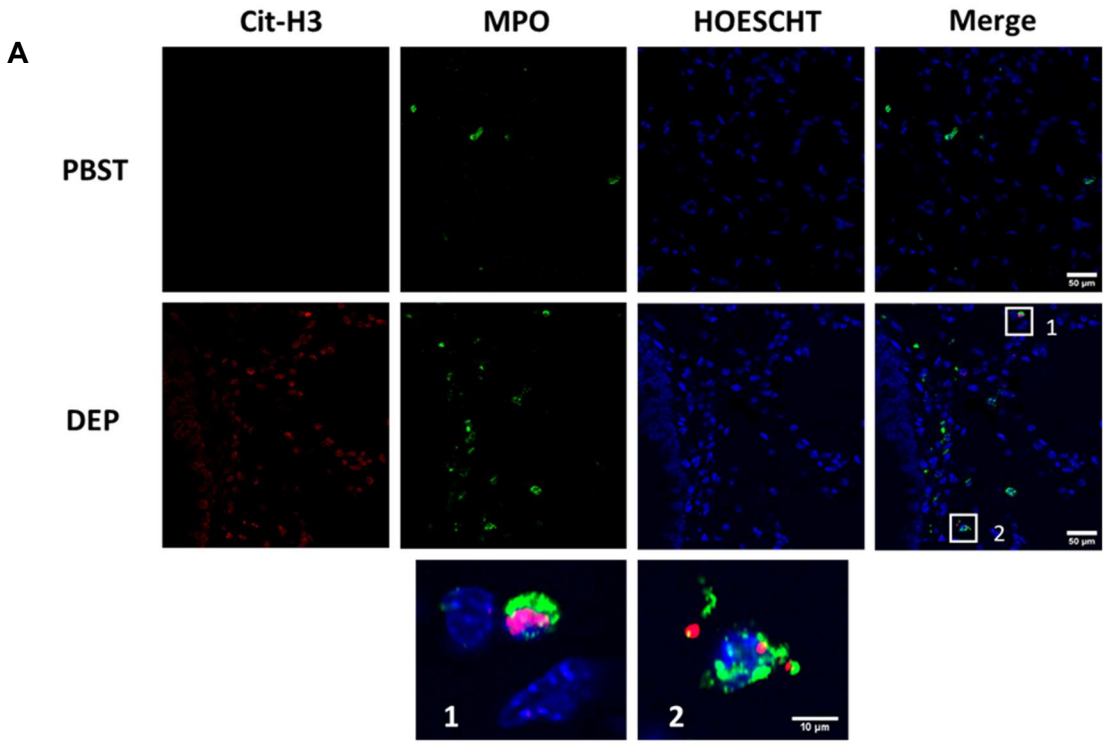

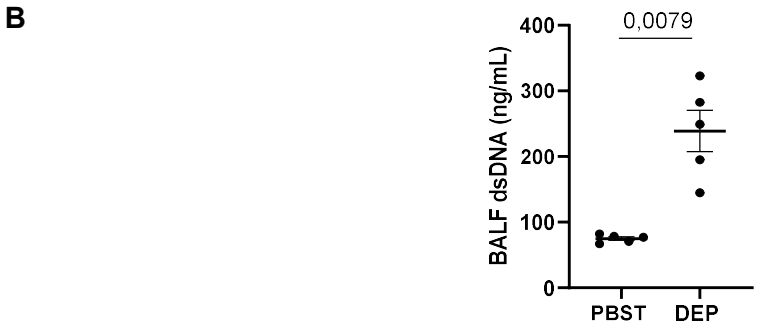

Figure 13. (**A**) Representative immunofluorescence images obtained by performing confocal microscopy of lung sections from mice 24h after intratracheal DEP treatment compared to PBST as described previously. Staining shows Cit-H3 (red), MPO (green) and Hoechst (blue). The higher magnification views in the inserts (1-2) show NETs formation, demonstrated by the co-localization of Cit-H3 (red), MPO (green) and DNA (blue). (**B**) BALF levels of dsDNA were measured using a PicoGreen assay kit (n= 5 mice per group, one experiment). Data are presented as mean +/- SEM. Statistical significance was assessed using Mann-Whitney test.

2.2 DEP-recruited CD14^{pos} PMNs exhibit an immunosuppressive phenotype

To elucidate the functional immunosuppressive characteristics of PMNs recruited to the lungs in acute DEP-exposed mice (Fig. 14A), we isolated PMNs based on CD14 expression (Fig. 14B). No distinct morphological differences were observed between two CD14^{neg} and CD14^{pos} PMN populations (Fig. 14C).

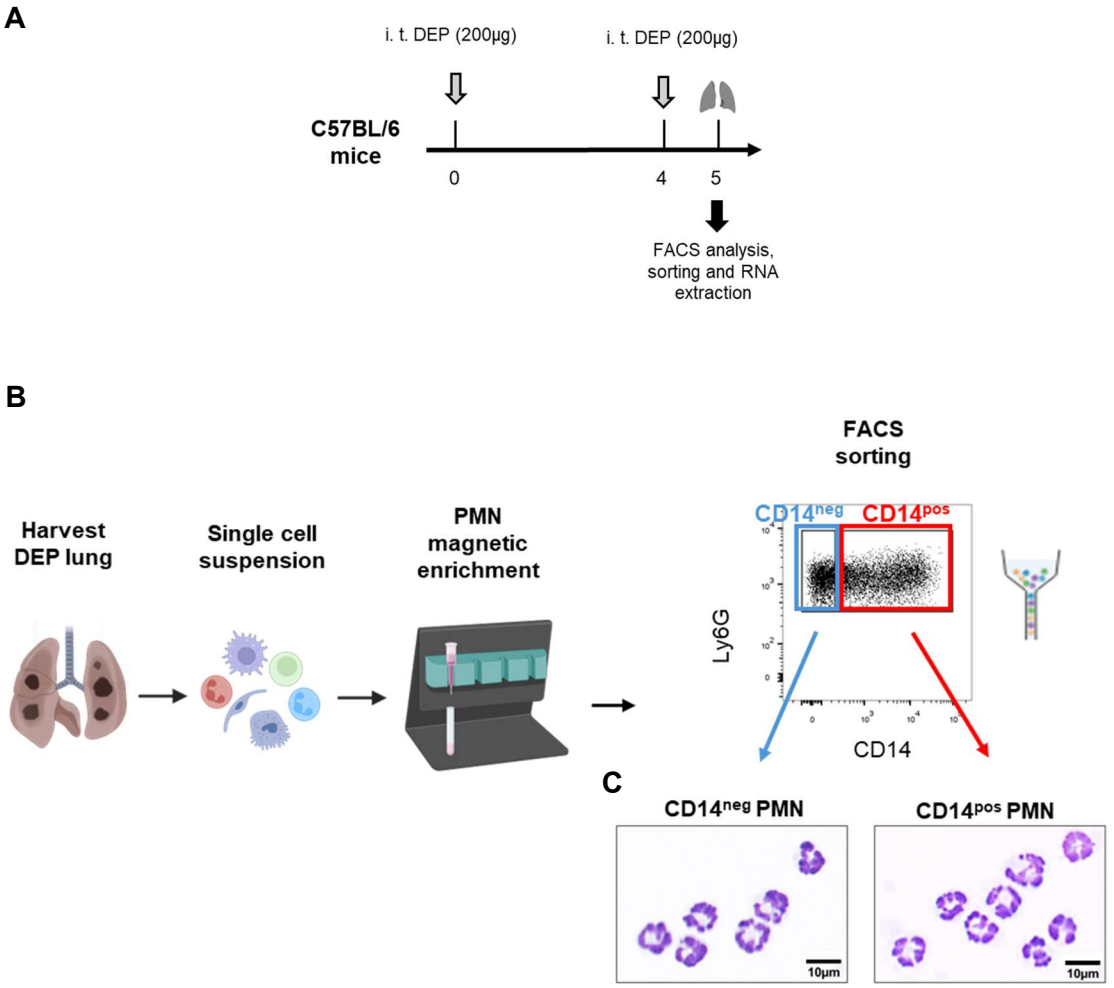

Figure 14. (**A**) Experimental exposure protocol (**B**) Scheme representing PMN isolation from DEP exposed lungs using magnetic column separation of Ly6G+ cells, followed by FACS cell sorting of CD14^{neg} and CD14^{pos}. (**C**) Representative cytospin images from CD14^{neg} and CD14^{pos} PMN sorted populations stained with H&E. Scale bar, 10µm.

However, immunocytochemistry analysis revealed increased NET formation in CD14^{pos} PMNs compared to their CD14^{neg} counterparts (Fig. 15A, 15B).

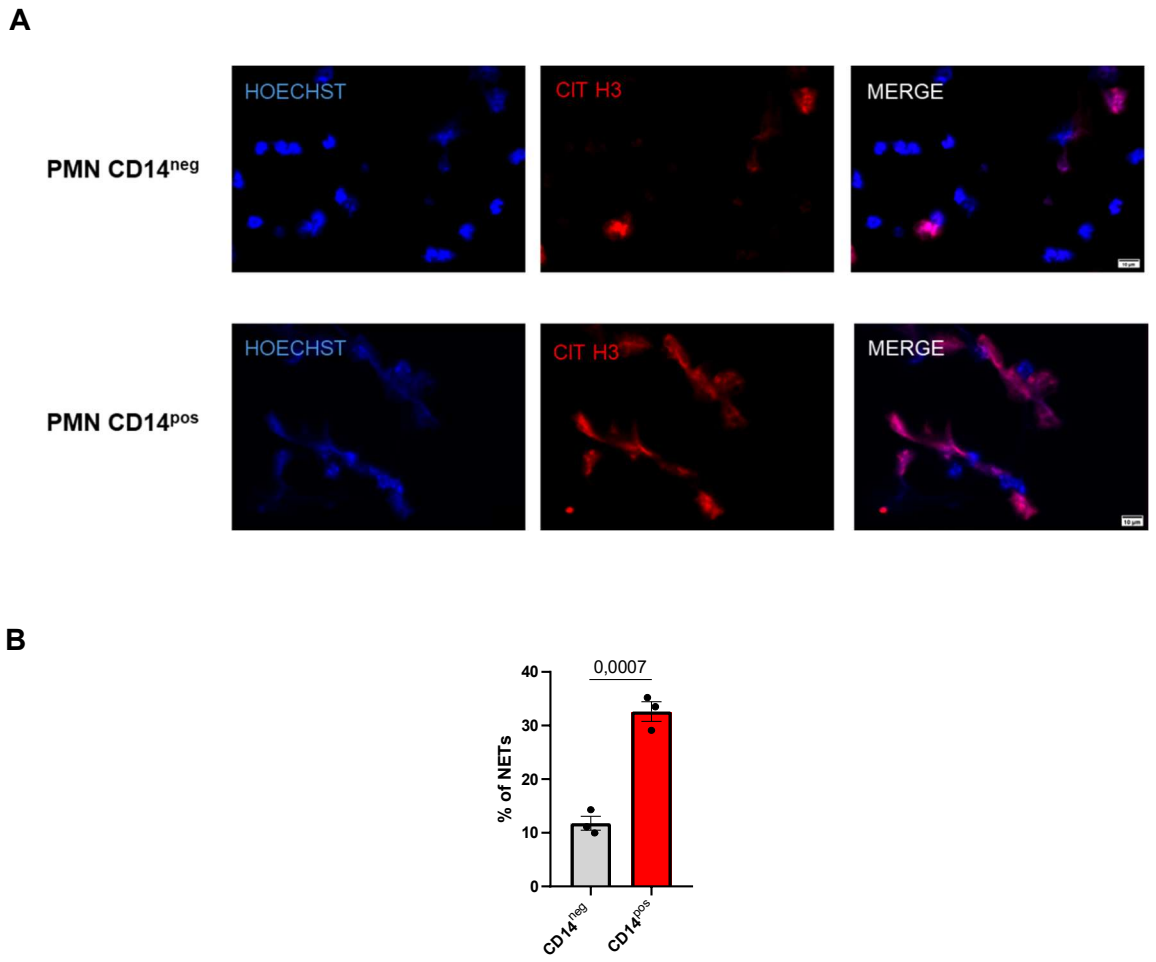

Figure 15. (**A**) Representative images of ex vivo cultured CD14^{neg} and CD14^{pos} PMNs stained with anti-citrunillated histone 3 antibody (CIT H3; red) and Hoechst (blue). NETs are identified by the colocalization of CIT H3 and Hoechst. Scale bar = 10µm. (**B**) Percentage of NETs measured on fluorescence microscopy image of ex vivo cultured CD14^{neg} and CD14^{pos} PMNs (n=5 pooled mice per experiment, one experiment, 3 technical replicates). Data are presented as mean +/- SEM. Statistical significance was assessed using Mann-Whitney test.

Next, we quantified in both PMN populations the expression of key genes associated with the immunosuppressive activity of MDSCs such as Arg1, Nos2, Cd274, Ptgs2, Il10 and Tgfβ (Li et al., 2021). RT-qPCR analysis demonstrated a significant upregulation of all assessed genes in $CD14^{pos}$ PMNs compared to $CD14^{neg}$ PMNs in DEP-exposed mice, with Nos2 and Ptgs2 showing only a non-significant trend toward increased expression (Fig. 16A). In addition, $CD14^{pos}$ PMNs also exhibited elevated protein levels of SIGLEC-F and PD-L1 and ARG1 compared to $CD14^{neg}$ PMNs (Fig. 16B).

A

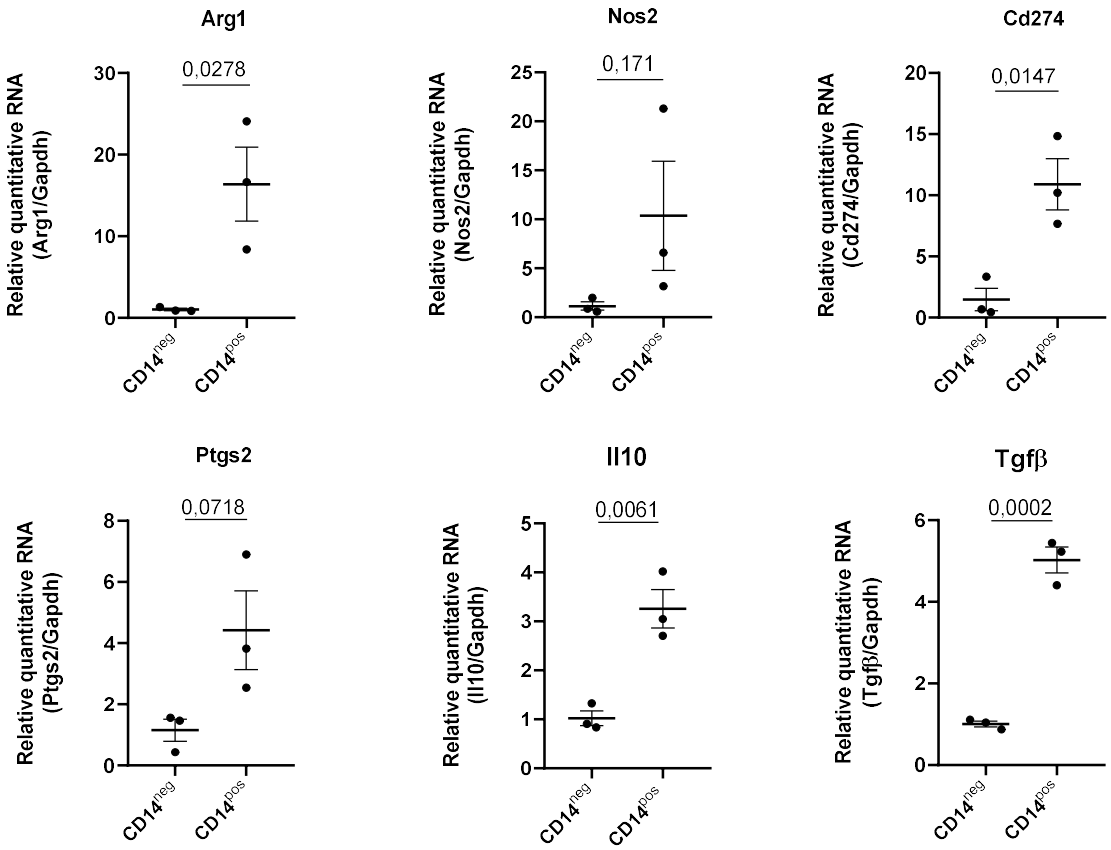

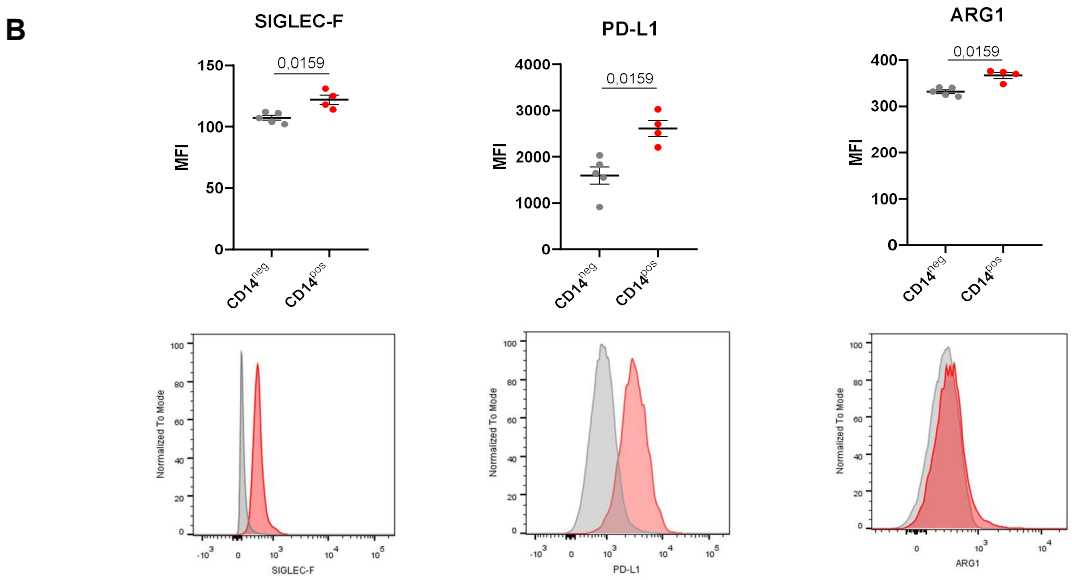

Figure 16. (**A**) Expression of indicated genes by qPCR in CD14^{neg} and CD14^{pos} PMNs from lungs of DEP exposed mice (n = 5 pooled mice by experiment, three independent experiments). Data were analysed using an unpaired t-test. (**B**) Mean fluorescence intensity (MFI) quantification and representative flow cytometry plots of selected markers in CD14^{neg} and CD14^{pos} PMNs from lungs of DEP exposed mice (n = 4 to 5 mice per experiment, one experiment). Data are presented as mean +/- SEM. Statistical significance was assessed using Mann-Whitney test.

To functionally confirm the suppressive activity of DEP-recruited $CD14^{pos}$ PMNs, we conducted a T cell suppression assay. Both $CD14^{neg}$ and $CD14^{pos}$ PMNs isolated from DEP exposed lungs were cultured in presence of activated T cells (Fig. 17A). The $CD14^{neg}$ PMNs exhibited no detectable suppressive activity when co-cultured with activated T cells, whereas co-culture with $CD14^{pos}$ PMNs significantly reduced T cell proliferation (Fig. 17B, 17C). These results demonstrate that $CD14^{pos}$ PMNs exhibit a MDSC-like phenotype and are functionally able to suppress T cell proliferation, potentially contributing to the establishment of an immunosuppressive microenvironment in the lungs of DEP-exposed mice.

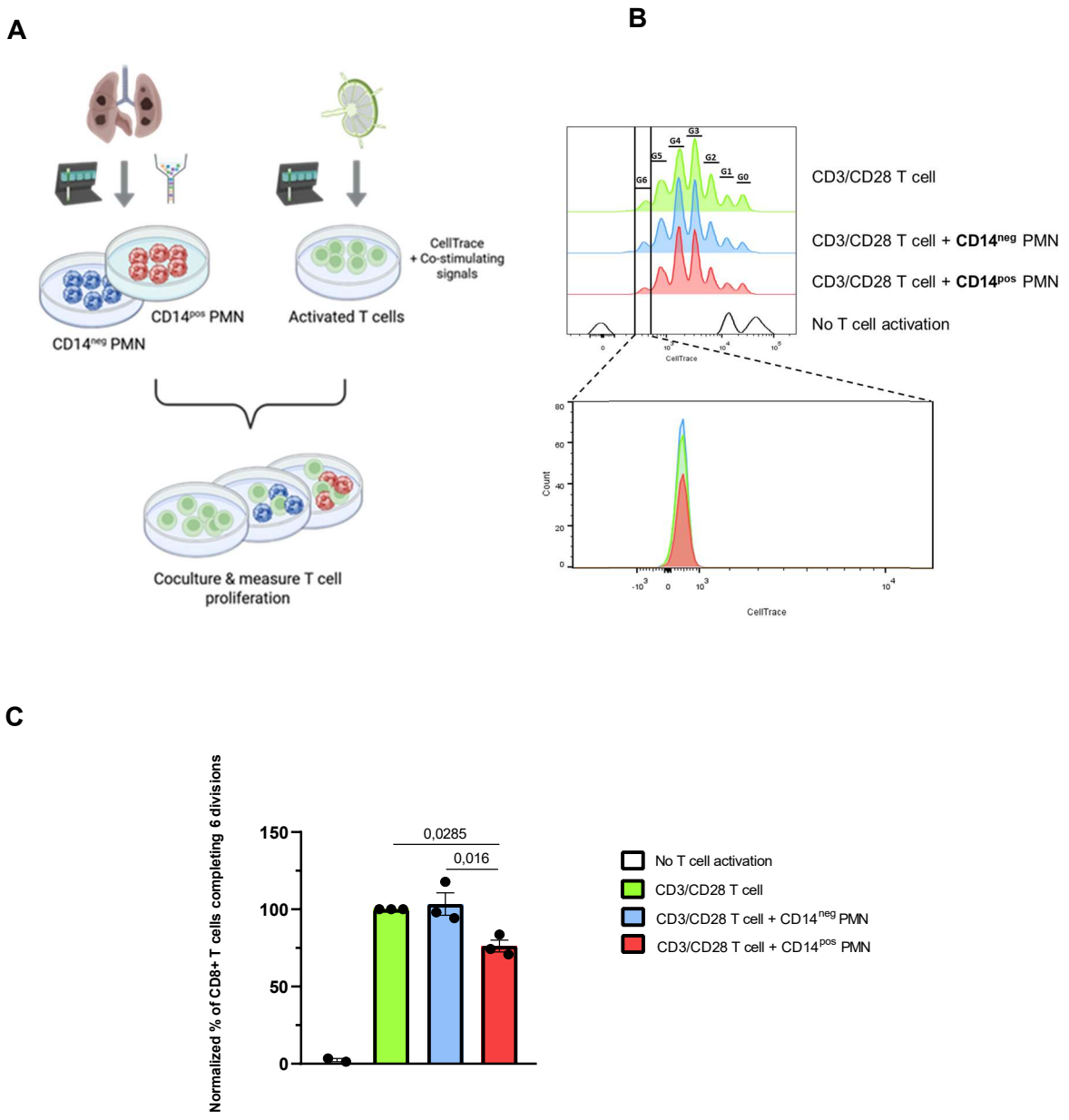

Figure 17. (**A**) Scheme representing PMN-induced T cell suppression assay. T cells were isolated from lymph nodes of untreated C57BL6 mice by negative magnetic column separation, stained with Cell Trace dye and co-cultured in the presence of co-stimulatory molecules CD3/CD28 for 72 hours with $CD14^{neg}$ and $CD14^{pos}$ PMN isolated from DEP exposed mice lungs. (**B**) Representative overlay histogram showing Violet Cell Trace signals in control group with only T cells without stimulation (white), only T cells activated by anti CD3/CD28 (green), activated T cells in presence of $CD14^{neg}$ PMN (blue) and activated T cells in presence of $CD14^{pos}$ PMN (red). Zoomed-in view of T cells that have undergone six divisions (below). (**C**) Quantitative bar chart showing the normalized percentage of CD8+ T cells completing 6 divisions. Each data point represents one experiment with at least 5 pooled mice per experiment. Data coming from the T cell suppression assay was analysed using a one-way

ANOVA followed by Tukey's post hoc test for multiple comparisons. Data are presented as mean +/- SEM.

2.3 Chronic exposure to DEP induces an immunosuppressive microenvironment in the lung

We next investigated whether chronic DEP exposure, which may better reflect real-world environmental conditions, also promotes the emergence of CD14^{pos} PMNs with immunosuppressive properties in the lung (Fig. 18A). Consistent with our observations in the acute exposure model, DEP-exposed lungs showed a significant increase in numbers of PMNs compared to controls, along with a higher proportion of CD14^{pos} PMNs (Fig. 18B, 18D), while monocytes remained unchanged (Fig. 18B, 18C). Furthermore, CD14^{pos} PMNs exhibited significantly higher expression of Siglec-F and PD-L1, as well as regulatory markers, such as CD73, which is involved in adenosine production (O'Brien et al., 2023), and SIRPα, which is involved in the inhibition of phagocytosis of CD47-expressing target cells (Behrens et al., 2022) compared to CD14^{neg} PMNs (Fig. 19). In the spleen, on the other hand, no significant differences in MO and PMN recruitment were observed and CD14^{pos} PMNs were not detected in either group (Fig. 18E-G).

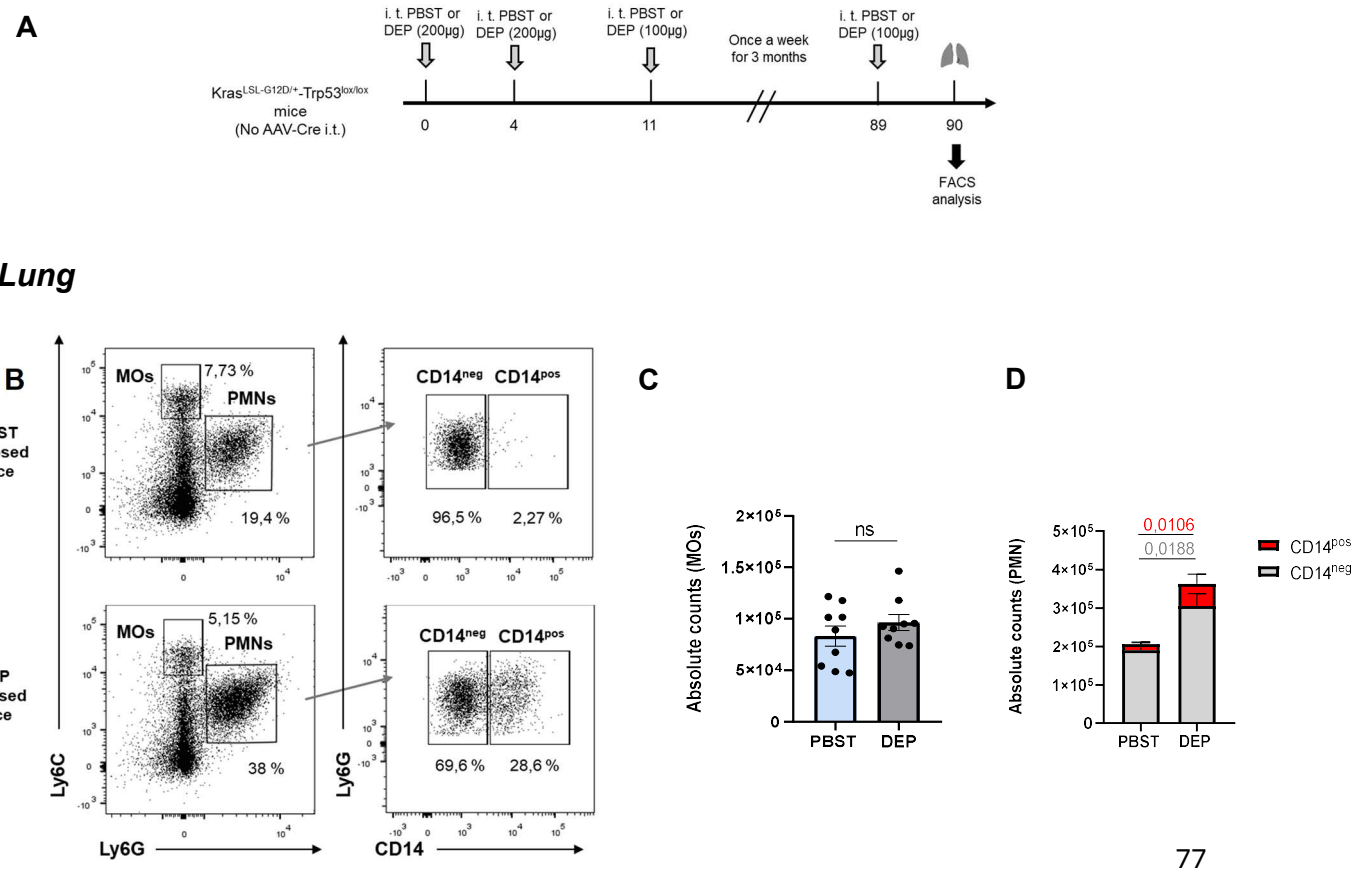

Spleen

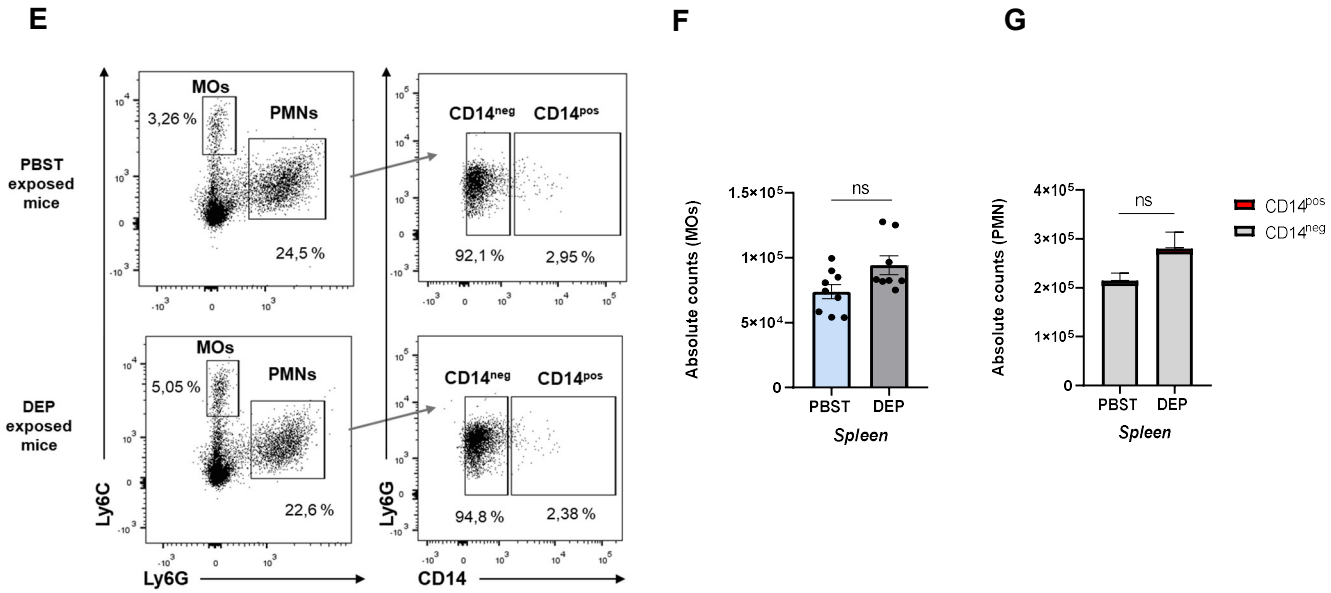

Figure 18. (**A**) Experimental exposure protocol. (**B**) Gating strategy used for the identification of MOs, PMNs and their subsets in lungs of PBST or DEP exposed mice. Absolute counts of (**C**) MOs, (**D**) $CD14^{neg}$ and $CD14^{pos}$ (**E**) Gating strategy used for the identification of MOs, PMNs and their subsets in spleen of PBST or DEP exposed mice. Absolute counts of (**F**) MOs, (**G**) PMNs $CD14^{neg}$ and $CD14^{pos}$ recruited in the spleen of PBST or DEP exposed mice. Bar graphs represent the mean +/- SEM of one representative experiment (n = 8-9 mice per group). For comparisons between two groups, Mann-Whitney test was used. ns, not statistically different.

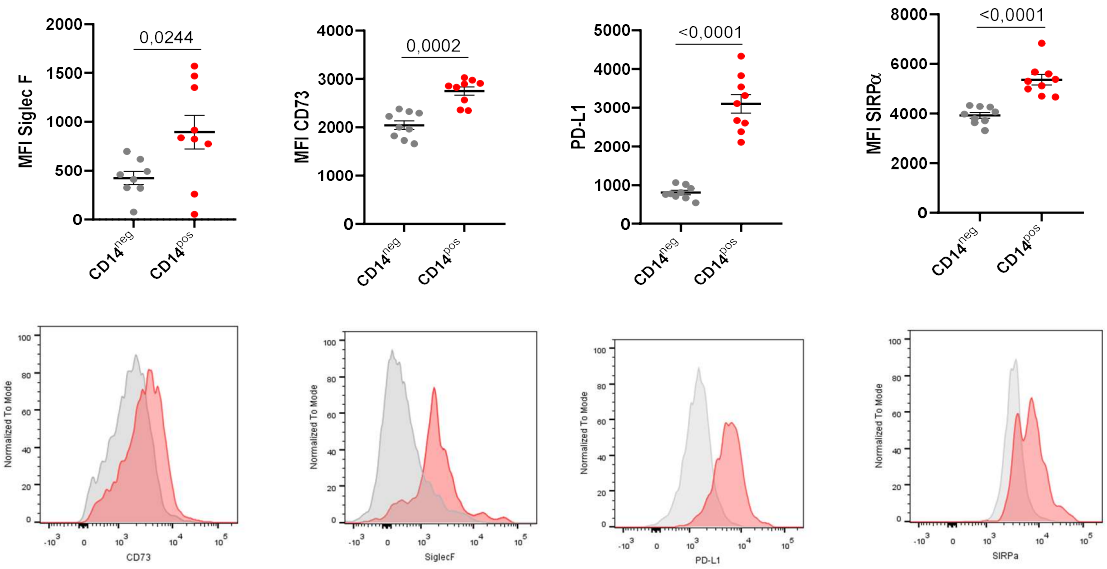

Figure 19. Mean fluorescence intensity (MFI) quantification of selected markers and representative flow cytometry plots of $CD14^{neg}$ and $CD14^{pos}$ PMNs from lungs of DEP exposed mice (n = 8 to 9 mice per group, one experiment). For comparisons between two groups, Mann-Whitney test was used.

Although total T cell numbers again remained unchanged in the lung following DEP chronic exposure (Fig. 20B, 20F), we observed alterations in the composition and activation state of T cell populations. Specifically, there was an increased proportion of Tregs (Fig. 20D), along with an upregulation of activation and exhaustion markers such as CD69, PD-1 and LAG-3 (only in CD4 T cells), as well as CD39, which contributes along with CD73 to adenosine production in the lung microenvironment, thereby promoting immunosuppression (Fig. 20C, 20G). These results demonstrate that chronic DEP exposure induces the emergence of MDSCs-like PMNs with a regulatory phenotype that may promote immunosuppression in the context of cancer, given the pivotal roles of PD-L1, CD73 and SIRPα in suppressing anti-tumour immune responses (Glodde et al., 2017; Huang et al., 2024; Zheng et al., 2021). Furthermore, we observed that this regulatory and immunosuppressive signature extended to T cell populations, which showed increased expression of regulatory and activation/exhausted markers, changes that may impair effective T cell responses.

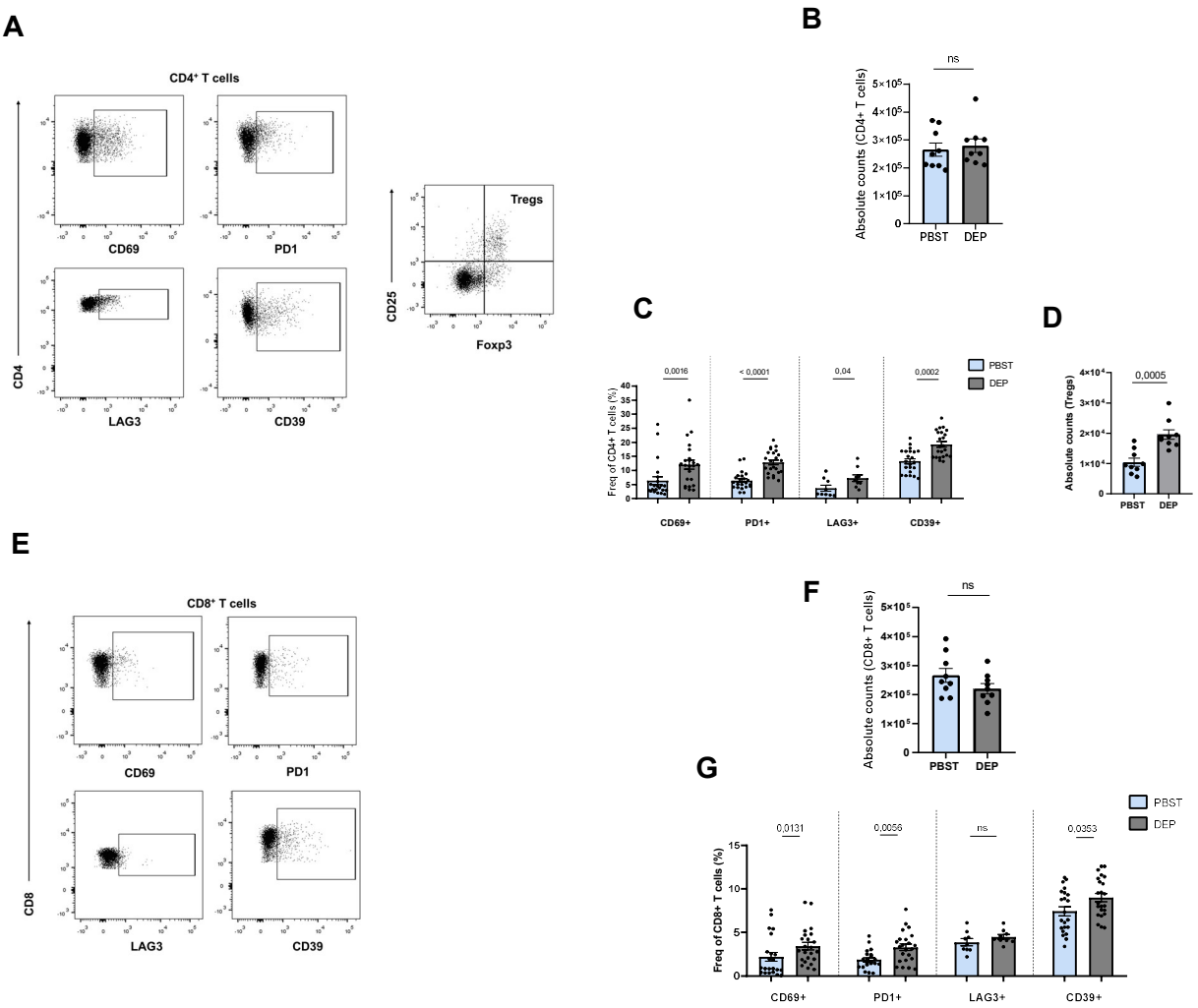

Figure 20. Representative flow cytometry plots of (**A**) CD4+ T cells and (**E**) CD8+ T cells, absolute counts of (**B**) CD4+ T cells, (**D**) Tregs and (**F**) CD8+ T cells, frequency (%) of indicated markers present in (**C**) CD4+ T cells and (**G**) CD8+ T cells from PBST and DEP exposed mice. Bar graphs represent the mean +/- SEM of up to three pooled experiments (n = 8-9 mice per group). Statistical significance was assessed using Mann-Whitney test. ns, not statistically different.

2.4 Chronic exposure to DEP favours tumour progression in a genetically engineered mouse model of lung adenocarcinoma

Given the regulatory and immunosuppressive signatures observed in PMN-MDSCs and T cells following chronic DEP exposure, we next investigated whether this immunosuppressive environment could influence lung tumour progression. To test this, we used a genetically engineered mice model that develops lung tumours upon KRAS oncogenic activation combined with p53 loss (KP model). Tumour burden in the lungs of KP mice was assessed 90 days after AAV-Cre administration (Fig. 21A). Strikingly, we observed larger tumour nodules in DEP-exposed mice (Fig. 21B, 21C).

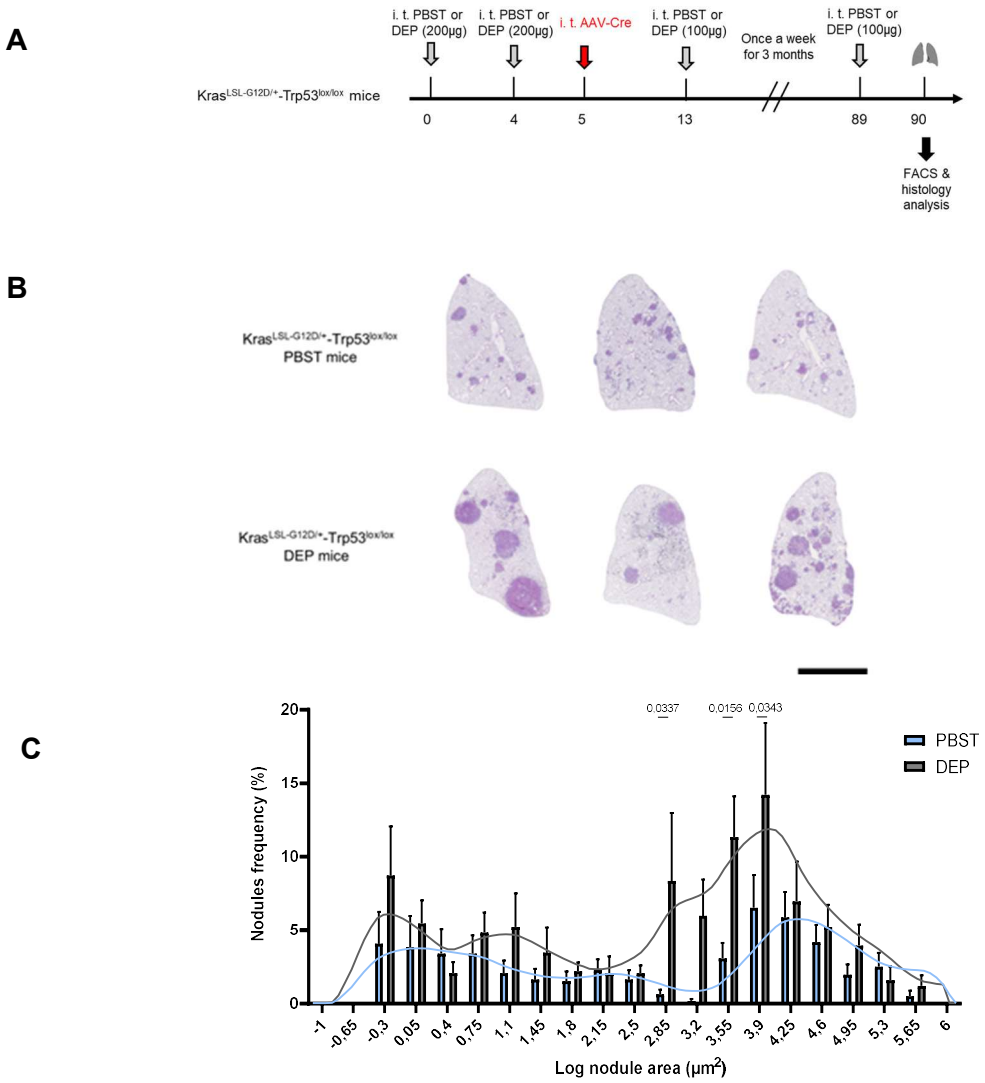

Figure 21. (**A**) Experimental exposure protocol. (**B**) Representative images of HE-stained lungs and (**C**) nodules sizes distribution in PBST and DEP treated KP mice. Scale bar = 5 mm. Statistical analysis was performed using two-way ANOVA, followed by Sidak's multiple comparisons test to assess pairwise differences between groups.

Additionally, the density of Ki67^{+} cells within tumour nodules was higher in DEP-exposed KP mice, indicating increased tumour cell proliferation in the DEP-altered lung microenvironment (Fig. 22A, 22B).

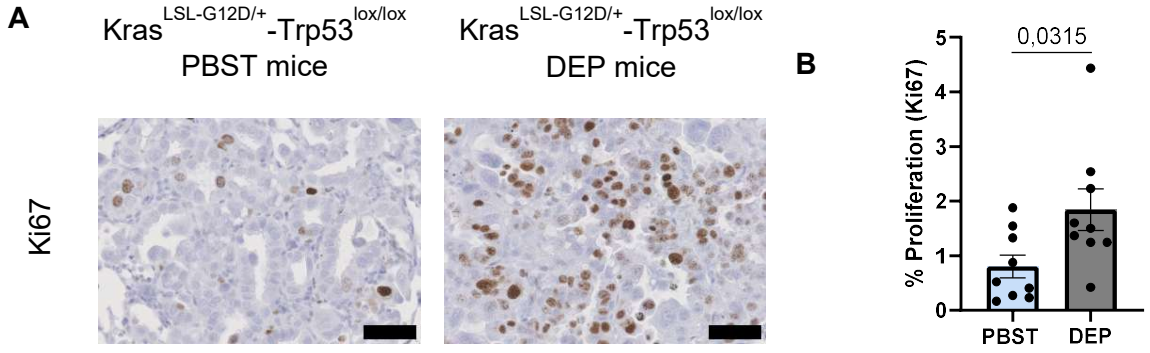

Figure 22. (**A**) Representative images of Ki67 immunohistochemistry in lung sections from PBST and DEP-exposed KP mice. Scale bar = 50µm (**B**) Quantification of cellular proliferation (Ki67) within nodules (n = 3 to 6 mice per group, two pooled experiments). For comparisons between two groups, Mann-Whitney test was used.

While we observed no changes in the total counts of MOs upon chronic DEP exposure in our KP model (Fig. 23B), we observed that CD14^{pos} PMNs were also present in the lungs of PBST-exposed mice, but their numbers were markedly increased in DEP-exposed mice (Fig. 23A, 23C). In the spleen, however, no significant differences in MOs and PMN recruitment were observed, and the proportion of CD14^{pos} PMNs did not differ between the groups (Fig. 23D-23F).

Lung

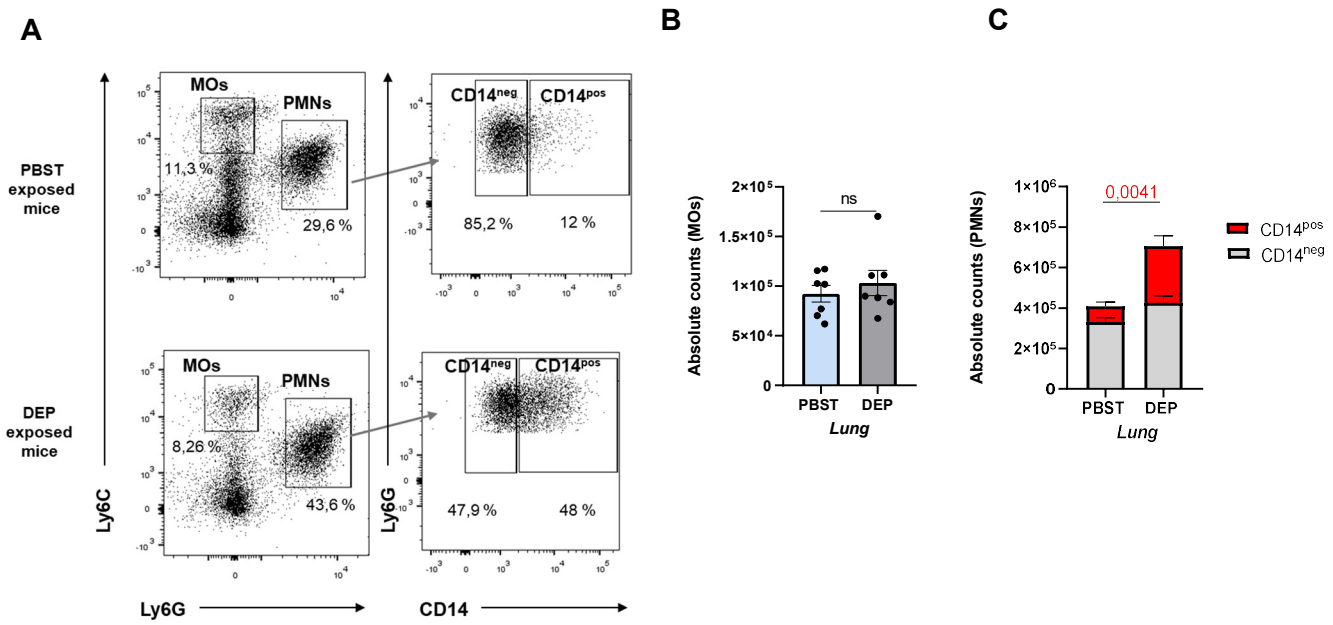

Spleen

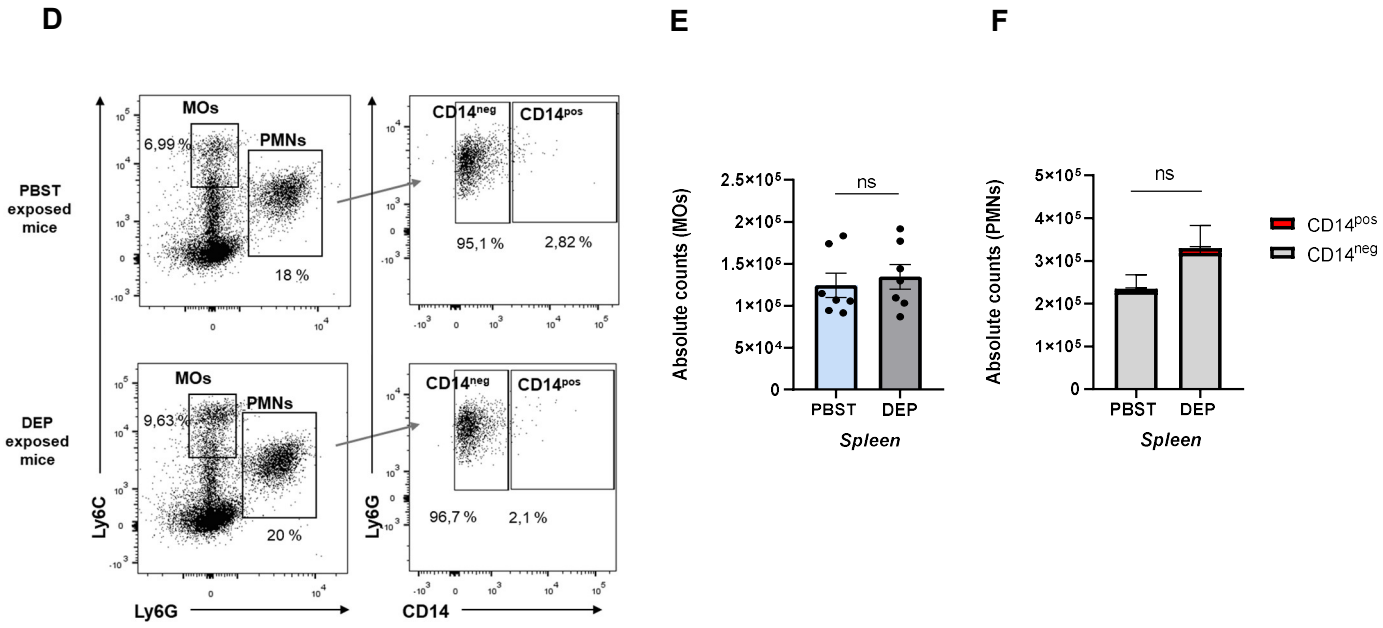

Figure 23. Gating strategy used for the identification of MOs, PMNs and their subsets in (**A**) lungs and in (**D**) the spleen of PBST or DEP exposed KP mice according to the exposure protocol in Fig. 21A. Absolute counts of MOs, PMNs CD14^{neg} and CD14^{pos} recruited in (**B, C**) lungs and in (**E, F**) the spleen of PBST or DEP exposed KP mice (n = 7 mice per group, one experiment). Data are presented as mean +/- SEM. Statistical significance was assessed using Mann-Whitney. ns, not statistically different.

Consistent with our observations in the chronic model of DEP exposure, CD14^{pos} PMN subset exhibited significantly higher expression of CD73, Siglec F, PD-L1 and SIRPα as compared to CD14^{neg} (Fig. 24).

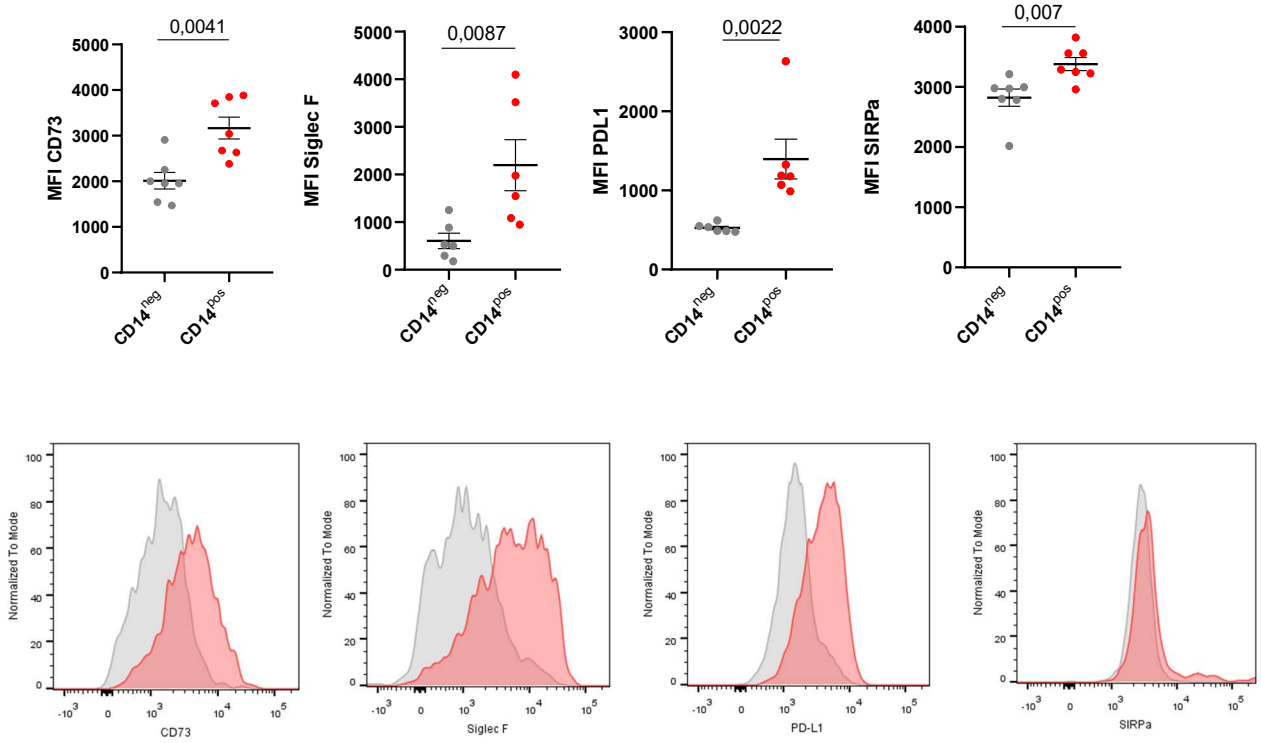

Figure 24. Mean fluorescence intensity (MFI) quantification of selected markers and representative flow cytometry plots of CD14^{neg} and CD14^{pos} PMNs from lungs of DEP exposed KP mice (n = 6 to 7 mice per group, one experiment). Data are presented as mean +/- SEM. For comparisons between two groups, Mann-Whitney test was used.

Although total CD4+ and CD8+ T cell numbers were unchanged in the lung following DEP chronic exposure (Fig. 25B, 25F), we observed alterations in the composition and activation state of T cell populations. Specifically, there was an increase in Treg numbers (Fig. 25D), along with an upregulation of activation and exhaustion markers such as CD69, PD-1, TIM-3, and CD39, indicative of T cell activation/exhaustion and immunosuppressive reprogramming (Fig. 25A, 25C, 25E, 25G). Of note, similar to what we observed in the chronic model, expression of these markers on CD8^{+} T cells (Fig. 25G) was less compared to CD4^{+} T cells (Fig. 25C). Collectively, these findings suggest that chronic DEP exposure establishes and maintains an immunosuppressive lung microenvironment that supports cancer progression.

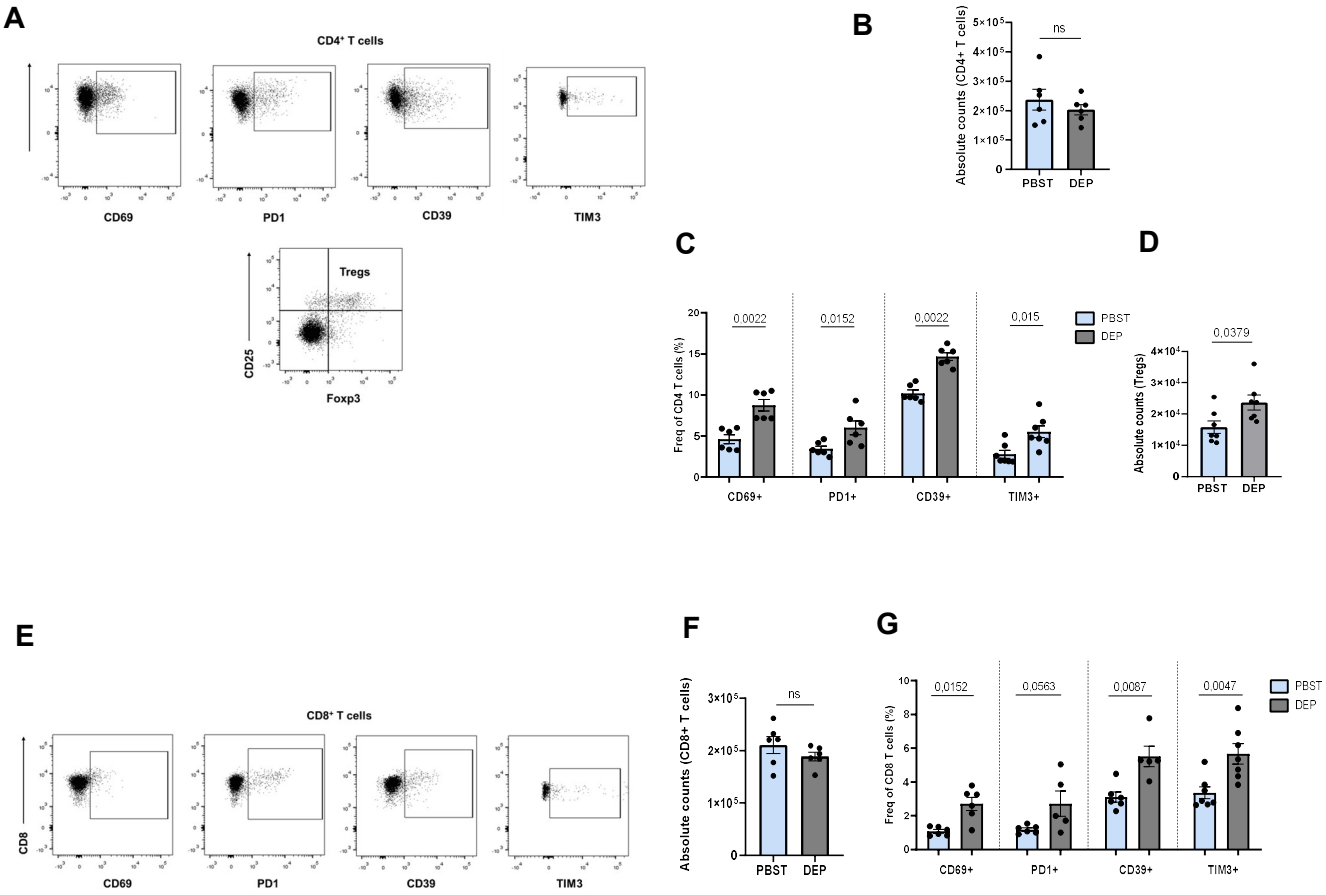

Figure 25. Representative flow cytometry plots of (**A**) CD4+ T cells and (**E**) CD8+ T cells, absolute counts of (**B**) CD4+ T cells, (**F**) CD8+ T cells and (**D**) Tregs. Frequency (%) of indicated markers in (**C**) CD4+ T cells and (**G**) CD8+ T cells, present from PBST or DEP-exposed KP mice according to the exposure protocol in Fig. 21A (n= 6 mice per group, one experiment). Data are presented as mean +/- SEM. Statistical significance was assessed using Mann-Whitney test. ns, not statistically different.

2.5 DEP recruited CD14^{pos} PMNs do not promote Treg induction ex vivo

To determine whether DEP-recruited CD14^{pos} PMNs can induce Tregs, we performed an *ex vivo* co-culture assay using MACS-sorted naïve CD4^{+} T cells from spleen and lymph nodes. CD14^{neg} and CD14^{pos} PMNs were FACS-sorted from the lungs of mice following an acute DEP exposure protocol (Fig. 26A, 26B). After T cell activation and five days of co-culture, expression of the Treg-associated markers CD25 and Foxp3 were analyzed. No significant difference in the induction of CD25^{+}Foxp3^{+} T cells was observed between the conditions (Fig. 26C). These results suggest that CD14^{pos} PMNs recruited in response to acute DEP exposure are not sufficient to promote Treg differentiation *ex vivo*.

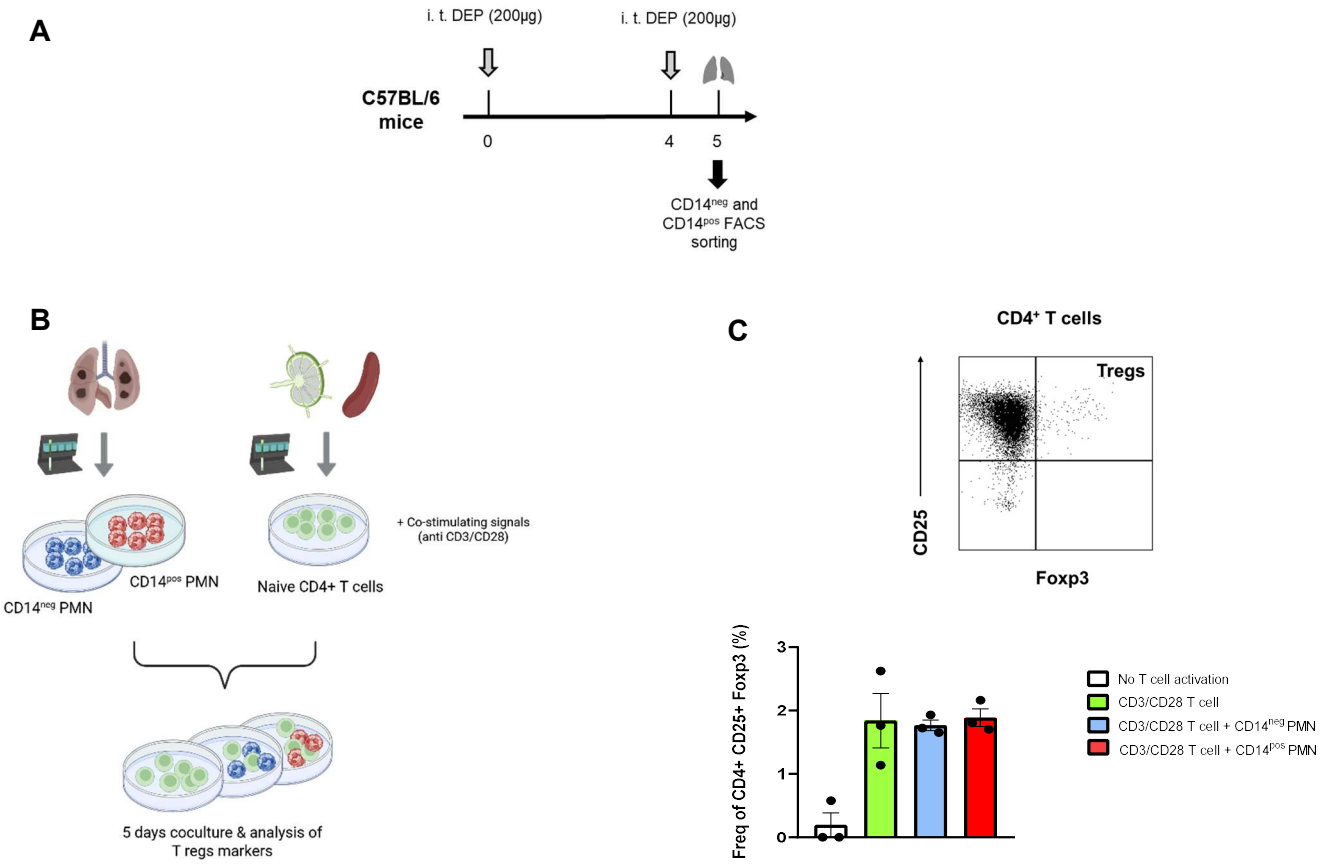

Figure 26. (**A**) Experimental exposure protocol. (**B**) Scheme of PMN-induced CD4+ T cell orientation assay. Lymph nodes and spleen naïve CD4+ T cells from normal mice were magnetically sorted, stimulated and then cocultured for 5 days with CD14^{neg} and CD14^{pos} PMN isolated from DEP exposed mice lungs according to the exposure protocol in (A). (**C**) Representative flow plots and frequency (%) of Tregs population present following the protocol described in (B) (one experiment, 3 technical replicates).

2.6 Chronic exposure to DEP does not impair T cell proliferative capacity, cytolytic function, or expression of IFNγ, CTLA-4 and TIM-3

Functionally, exhausted T cells exhibit diminished cytolytic activity, including reduced production of granzymes (GZMA, GZMB), decreased proliferative capacity, and impaired IFN-γ production upon restimulation. To assess their exhausted state, we evaluated the secretion of GZMA, GZMB, and IFN-γ, as well as Ki67 expression, in T cells following chronic exposure to DEP. No significant differences in the secretion of GZMA, GZMB, or IFN-γ, nor in proliferative capacity, were observed between PBST-treated and DEP-exposed mice (Fig. 27).

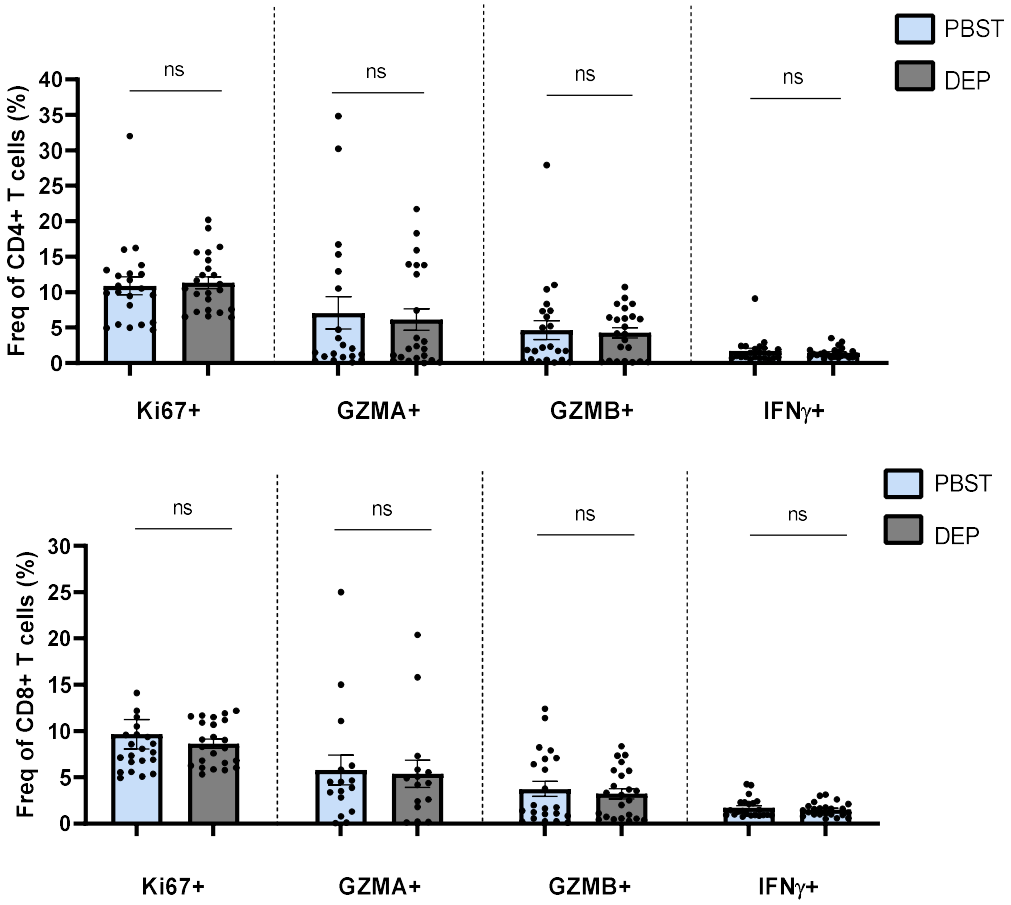

Figure 27. Frequency (%) of Ki67+, GZMA+, GZMB+ and IFNɣ+ CD4+ and CD8+ T cells recruited in the lungs of PBST or DEP exposed mice following the exposure protocol in Fig. 18A. Bar graphs represent the mean +/- SEM of three pooled experiments (n = 8-9 mice per group). For comparisons between two groups, unpaired t test was used. ns, not statistically different.

In addition to PD1 and LAG3 (Fig. 25B), other important inhibitory receptors such as CTLA-4 and TIM-3 were also examined following chronic DEP exposure. No significant differences in the expression of these receptors were observed between PBST-treated and DEP-exposed mice (Fig. 28). Gating strategy used to identify these markers is illustrated in Figure 10.

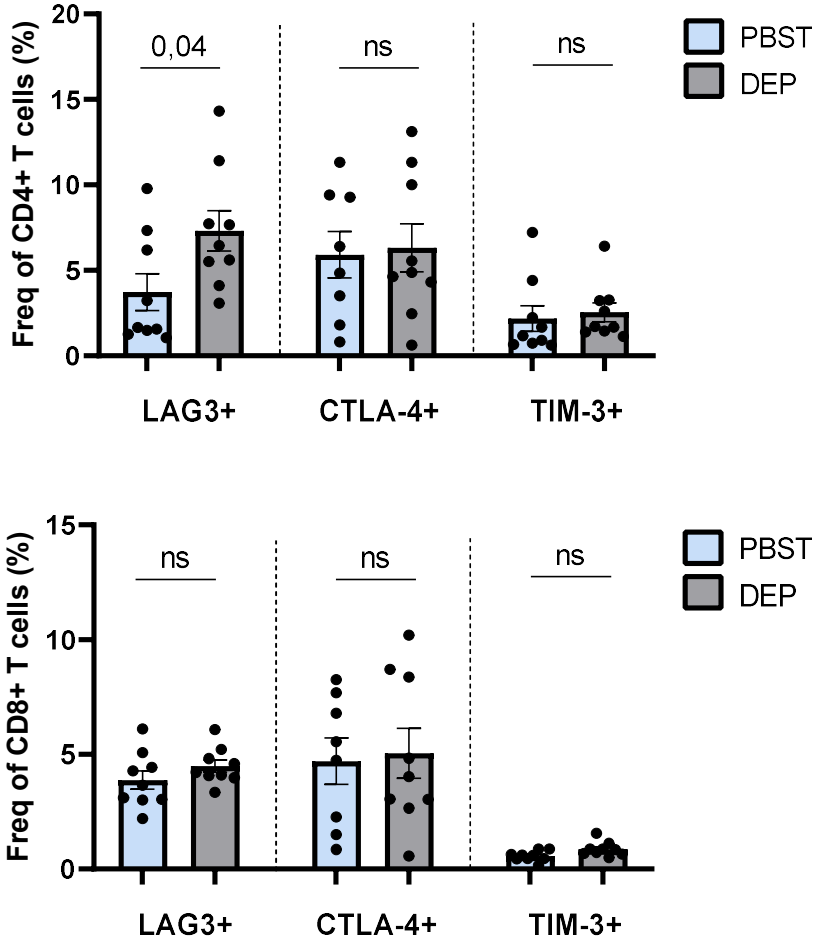

Figure 28. Frequency (%) of LAG3+, CTLA-4+ and TIM-3+ $CD4^+$ and $CD8^+$ T cells recruited in the lungs of PBST or DEP exposed mice following the exposure protocol in Fig. 18A. Bar graphs represent the mean +/- SEM of one experiment (n=8-9 mice per group). For comparisons between two groups, unpaired t test was used. ns, not statistically different.

2.7 Chronic exposure to DEP of a transgenic mouse model of lung adenocarcinoma does not impair T cell proliferative capacity, cytolytic function or expression of IFNγ, LAG3 and CTLA-4.

To assess the exhausted state of T cells in a transgenic mouse model of lung adenocarcinoma chronically exposed to DEP, the expression of Ki-67, the secretion of GZMA and GZMB, as well as the expression of IFN-γ, LAG-3, and CTLA-4 were evaluated. No significant differences were observed between PBST-treated and DEP-exposed mice in terms of GZMA, GZMB, or IFN-γ secretion, nor in proliferative capacity (Ki-67 expression) and expression of the immune checkpoint molecules LAG-3 and CTLA-4 (Fig. 29).

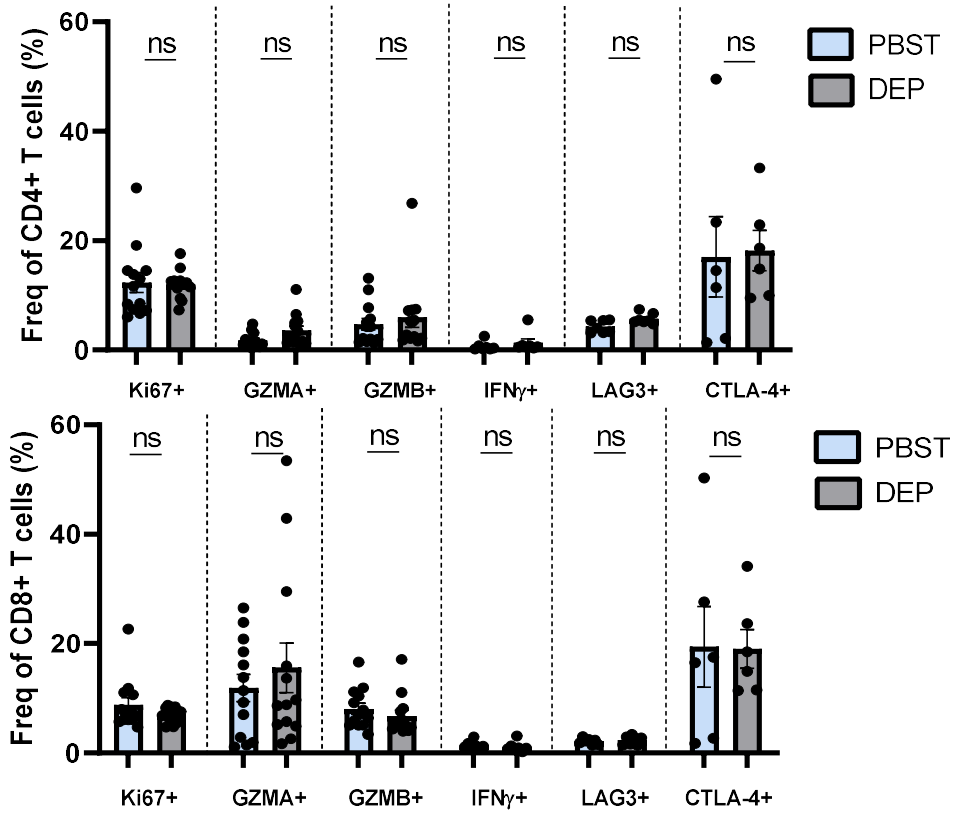

Figure 29. Frequency (%) of Ki67+, GZMA+, GZMB+, IFNɣ+, LAG3+ and CTLA-4+ CD4+ and CD8+ T cells recruited in the lungs of PBST or DEP exposed mice following the exposure protocol in Fig. 21A. Bar graphs represent the mean +/- SEM of one to two pooled experiments (n = 6-7 mice per group). For comparisons between two groups, unpaired t test was used. ns, not statistically different.

DISCUSSION

DISCUSSION

Air pollution represents a complex mixture of gaseous pollutants and particulate matter of diverse origins and compositions, making it difficult to directly correlate experimental findings to the entirety of the atmospheric mixture. The intrinsic complexity of diesel exhaust resulting from the complex interaction of its gaseous and particulate components further complicates standardized sample preparation.

In this work, we investigated the mechanisms by which exposure to DEP, a significant component of fine particulate matter and a major contributor to urban atmospheric pollution, may promote lung cancer progression. Previous studies have suggested that engine exhaust contributes to the development of lung tumours by inducing oxidative stress and inflammation leading to genotoxic effects (Santibáñez-Andrade et al., 2023). However, **the impact of DEP exposure on anti-tumour immune mechanisms remains elusive to date, and a comprehensive understanding of its effects on anti-tumour immunity is lacking.** Ideally, studies should rely on exhaust collected from vehicles under real driving conditions to best approximate real-world exposure. However, reproducing such conditions is technically demanding and often impractical. In addition, the heterogeneous physicochemical properties of particulate matter are difficult to mimic accurately in the laboratory. For this reason, integrating standardized PM samples into controlled toxicological studies is an appropriate strategy to improve our understanding of how PM contributes to adverse health effects.

Consistent with previous reports, our study supports the notion that exposure to DEP induces neutrophilic inflammation in the lungs, a phenomenon that has been directly linked to the promotion of lung metastasis (Li et al., 2018). Interestingly, our group previously reported similar mechanisms in ozone exposure models, where neutrophilic infiltration facilitated metastatic spread by priming neutrophils to release NETs and promoting early metastatic colonization (Rocks et al., 2019). Our results provide critical insights into the immunosuppressive signature of PMNs, particularly $CD14^{pos}$ PMNs, following acute and chronic DEP exposure. $CD14^{pos}$ PMNs in the lungs formed NETs as confirmed by the co-localization of citrullinated histone (Cit-H3) and extracellular DNA. NETs can contribute to tumour progression in multiple ways. Firstly, NETs are

known to entrap circulating tumor cells and facilitate lung tissue invasion (Cools-Lartigue et al., 2014; Rocks et al., 2019). In addition, NETs have been shown to modulate the immune lung microenvironment by interacting with adaptive immune cells, for example by shielding tumor cells from cytotoxicity mediated by $CD8^+$ T cells and natural killer (NK) lymphocytes (Teijeira et al., 2020). Furthermore, NETs can directly interact with infiltrating T cells by the expression of PD-L1 which engages PD-1 receptors on T cells. Such interaction promotes the upregulation of multiple inhibitory receptors, leading to diminished mitochondrial function and a shift toward a metabolically exhausted state, thereby facilitating tumor growth (Kaltenmeier et al., 2021). Finally, inhibition of NETosis using PAD4 or DNase I inhibitors has shown promising results in reducing tumor burden (Rocks et al., 2019) enhancing $CD8^+$ T cell infiltration and improving responsiveness to anti-PD-1 immunotherapy in colorectal cancer (Zhang et al., 2021).

Besides undergoing NETosis, DEP- recruited $CD14^{pos}$ PMNs expressed key MDSC-associated genes, including Arg1, Nos2, Ptgs2 and Cd274 (Li et al., 2021). In addition, compared to their $CD14^{neg}$ counterparts, $CD14^{pos}$ PMNs exhibited increased expression of immunoregulatory and immunosuppressive cytokine such as IL-10 and TGF-β, along with Siglec-F expression, a marker associated with neutrophils displaying MDSC-like features (Engblom et al., 2017). $CD14^{pos}$ PMNs demonstrated a functional ability to suppress T cell proliferation, which aligns with prior studies showing that these cells can promote immune suppression in cancer models, facilitating immune evasion and reducing anti-tumour responses (Veglia et al., 2021).

Characterization of $CD14^{pos}$ PMNs recruited following chronic DEP exposure revealed additional immunomodulatory surface markers, notably CD73 and SIRPα. It has been reported that increased CD73 expression on PMN-MDSCs in patients with head and neck squamous cell carcinoma (HNSCC) was associated with advanced clinical stage and lymph node metastasis (Zheng et al., 2021). Moreover, recent insights have highlighted the critical role of SIRPα, in shaping the immunosuppressive tumor microenvironment. In a colorectal cancer model, SIRPα-deficient (Sirpα−/−) mice exhibited significantly enhanced resistance to tumor progression, associated with a reprogramming of myeloid cell populations toward pro-inflammatory and anti-tumour phenotypes (Huang et al., 2024). In line with these findings, our study shows that $CD14^{pos}$ neutrophils induced by chronic DEP exposure express high levels of SIRPα

and CD73, suggesting a role in suppressing anti-tumour immunity and shaping a tumour-permissive microenvironment. Patients chronically exposed to high levels of PM may develop a tumour microenvironment enriched in immunosuppressive marks. As such, they could particularly benefit from immunotherapy targeting the CD47-SIRPα axis and CD73 molecules expressed on immunosuppressive neutrophils.

Our results show partial overlap with those of Qi et al., who identified a population of PD-L1^{hi} inhibitory neutrophils in septic mice capable of suppressing CD4+ and CD8+ T cell responses and promoting Treg differentiation through direct contact (Qi et al., 2021). In our model, CD14^{pos} PMNs recruited following acute DEP exposure also exhibited immunosuppressive potential, as shown by their ability to significantly inhibit CD8+ T cell proliferation in co-culture assays. This observation is consistent with our results reporting PD-L1 expression on CD14^{pos} neutrophils, suggesting that this subset may share phenotypic features with the inhibitory neutrophils described in sepsis. However, in contrast to the sepsis model, our ex vivo co-culture of CD14^{pos} PMNs with naïve CD4+ T cells did not result in an increased induction of CD25+Foxp3+ regulatory T cells after five days of activation. These results indicate that although DEP-induced CD14^{pos} PMNs can impair effector T cell proliferation, they may not be sufficient to actively promote Treg differentiation ex vivo. The discrepancy with the sepsis model may reflect differences in the intensity, duration, or nature of the inflammatory environment, or in the expression of additional immunoregulatory molecules.

Notably, we only observed CD14^{pos} PMN subset in the lung and not in the spleen, which indicates that expression of CD14 is an effect of local factors in the microenvironment. This heterogeneity is likely driven by the expansion and mobilization of immature neutrophils in response to tumour or stroma derived factors under inflammatory conditions. Subsequently, local inflammatory cytokines promote the pathological activation of these neutrophils within the tissue microenvironment (Veglia et al., 2018). These observations were later confirmed experimentally showing that CD14^{pos} PMN did not differentiate from dedicated precursors in bone marrow but are activated in situ in response to different tumour derived factors, hypoxia, GM-CSF and S100A8/A9 protein (Veglia et al., 2021). The coexistence of two PMN subsets in DEP-exposed lungs, along with the presence of CD14^{pos} PMNs in both cancer and non-cancer inflammatory conditions suggests that CD14 expression on tumour-infiltrating neutrophils reflects a broader inflammation-associated phenotype.

T cell exhaustion is a state of T cell dysfunction commonly observed in chronic infections and cancer, characterized by the overexpression of inhibitory receptors, reduced cytolytic activity and IFN-γ production, and diminished proliferative capacity, ultimately leading to a failure to eliminate cancer cells (Baessler and Vignali, 2024). In the current study, chronic DEP exposure led to the upregulation of inhibitory receptors commonly associated with an exhausted T cell phenotype in chronic settings, such as PD-1, LAG-3 and TIM-3 suggesting that chronic exposure to pollutants may drive T cell dysfunction (Roussel et al., 2021; Ciraolo et al., 2022). Furthermore, other markers involved in immunosuppression, such as CD39, was also upregulated on T cells, along with CD73 in $CD14^{pos}$ PMNs. CD39 and CD73 function together to convert extracellular ATP to adenosine, a molecule that inhibits T cell function and promotes T reg activity (Xia et al., 2023). These findings highlight the potential for therapeutic strategies targeting T cell exhaustion, notably through immune checkpoint blockade using anti-PD1, LAG-3 or TIM-3 antibodies. Additionally, growing preclinical evidence supports the therapeutic value of CD39 inhibition as a means to restore T cell function and enhance anti-tumour immunity (Guo et al., 2022).

Despite the upregulation of these inhibitory receptors, we did not observe a significant effect on T cell proliferation, granzyme expression, or IFN-γ production. This suggests that while phenotypic markers of exhaustion are present, the functional impairment of T cells may be partial or context-dependent and warrants further investigation to determine whether these cells are truly dysfunctional or in a transitional activation state. Notably, the detection of granzymes and IFN-γ may require more sensitive approaches, such as ELISA performed on T cell-conditioned media, to confirm potential subtle functional alterations.

Compared to the extensive research on $CD8^+$ T cell dysfunction, the understanding of $CD4^+$ T cell exhaustion in the context of anti-tumour immunity remains limited. Nonetheless, studies in chronic infection models and tumour microenvironment have demonstrated that $CD4^+$ T cells can also enter a dysfunctional state, sharing features with exhausted $CD8^+$ T cells. This includes high expression of inhibitory receptors, diminished proliferative capacity, and reduced cytokine production (Crawford et al., 2014; Fu et al., 2020). Along with these observations, our study shows that $CD4^+$ T cells from DEP-exposed mice exhibit increased expression of PD-1, CD39, and LAG-3 in the chronic exposure model, with TIM-3 expression further elevated in our KP

model. Additionally, we observed a rise in regulatory T cells (Tregs), which are known to suppress the activation and expansion of effector T lymphocytes, thereby contributing to an immunosuppressive environment potentially conducive to tumor progression (C. Li et al., 2020).

Interestingly, studies using immunodeficient mouse models have underscored the critical contribution of the innate immune system to PM-driven tumour promotion. In SCID mice, which lack adaptive immune responses but retain intact innate immunity, $PM_{2.5}$ exposure significantly increased lung tumour burden following intravenous injection of A549 cells (Yang and Xiao, 2018) and promoted tumour growth and metastasis of PDX cells transplanted subcutaneously (Pan et al., 2022). These results suggest that innate immunity alone is sufficient to support PM-enhanced tumour progression.

Among innate immune cells, neutrophils have emerged as central players in this process. Li et al. (2018) demonstrated that blockade of BLT1, which reduced neutrophilic inflammation, was associated with decreased lung metastasis (Li et al., 2018). Similarly, depletion of neutrophils with anti-GSR/Gr1 antibodies abolished the ability of PM to enhance B16F10 lung metastasis. Supporting this notion, in NOD-$Prkdc^{scid}$ $Il2rg^{-/-}$ mice, which display profound immune defects but retain abundant neutrophils, PM exposure still enhanced lung metastasis of B16F10 cells, coinciding with marked neutrophil accumulation in the lungs (Liu et al., 2022).

Moreover, Hill et al. showed that in an EGFR-driven lung adenocarcinoma model (ET mice) crossed with $Rag2^{-/-}$;$Il2rg^{-/-}$ mice, which lack T, B, and NK cells and display an altered myeloid compartment, PM exposure did not increase neoplastic burden. This study indicates that while neutrophils are key contributors, macrophages also play an important role in lung cancer promotion (Hill et al., 2023).

To further assess the cytotoxic potential of T cells in the context of chronic DEP exposure, immune cell killing assays could be employed (Lanigan et al., 2020). In this approach, $CD8^+$ T cells isolated from the lungs of DEP-exposed mice would be co-cultured with tumour cells to evaluate their ability to mediate cancer cell cytotoxicity. Additionally, a tri-culture system involving $CD8^+$ T cells, tumour cells, and either $CD14^{pos}$ or $CD14^{neg}$ PMNs could be implemented to determine whether $CD14^{pos}$ neutrophils suppress the cytotoxic activity of T cells. This experimental design would

provide valuable functional insights into the immunoregulatory role of $CD14^{pos}$ PMNs within the tumour microenvironment.

An immunosuppressive milieu was also observed in KP mice chronically exposed to DEP, characterized by an increased accumulation of $CD14^{pos}$ PMNs, an elevated expression of inhibitory receptors such as PD-1, CD39, and TIM-3, and an expansion of the Tregs population. Subsequently, we observed a significant increase in tumour burden, with larger tumour masses and a higher density of proliferative Ki67-positive cells, indicative of enhanced tumour growth. Our findings, together with those of Hill et al., provide compelling evidence that airborne pollutants play a crucial role in lung cancer progression by shaping the tumour microenvironment rather than directly inducing mutations (Hill et al., 2023). As reported in their study, $PM_{2.5}$ exposure promotes EGFR- and KRAS-driven lung adenocarcinoma through an inflammatory response characterized by sustained influx of interstitial macrophages which upregulate PD-L1 and produce IL-1β. This pro-inflammatory environment facilitates the expansion of pre-existing oncogenic clones and reprograms EGFR -mutant alveolar type II (AT2) epithelial cells into a progenitor cell state, fostering tumour initiation and progression (Hill et al., 2023). Our study extends these findings by showing that chronic DEP exposure promotes an immunosuppressive tumour milieu in KP mice, characterized by the appearance of immunosuppressive PMNs and the emergence of a dysfunctional T cell state. Of note, Hill et al. conducted a study using intratracheal administration of PM at doses of 5 µg or 50 µg, delivered three times per week for three weeks, with at least 48 hours between each exposure, following oncogene induction. Tumour burden was assessed ten weeks post-induction. The PM used in their study (SRM2786) was obtained from the National Institute of Standards and Technology and represents fine particles collected from a modern urban environment. Their results revealed a dose-dependent increase in the number of pre-invasive neoplastic lesions. Interestingly, PM exposure administered prior to CMV-Cre mediated oncogene induction also led to an increased number of early neoplasias, indicating that PM exposure, whether occurring before or after oncogenic activation, is sufficient to promote carcinogenesis. Furthermore, they demonstrated that PM promotes early tumorigenesis through two distinct mechanisms: by expanding the pool of EGFR-mutant cells with tumorigenic potential, and by enhancing the proliferation of these cells within early lesions. Notably, no increase in mutational burden was observed in

tumours from PM-exposed mice, suggesting that PM acts as a tumour promoter rather than a mutagen. Finally, their study showed that an intact immune system is required for PM-enhanced, EGFR-driven lung tumorigenesis, highlighting a key role for immune-tumour interactions in pollution-mediated cancer progression.

In our work, we could have used $Kras^{LSLG12D/+}$ mice instead of $Kras^{LSL\text{-}G12D/+}$-$Trp53^{lox/lox}$. However, in these models, $Kras^{LSLG12D/+}$ display only adenomas and not (or rarely) adenocarcinomas (Sutherland et al., 2014), as the additional genetic alteration (p53 loss), is required for progression to malignant adenocarcinoma (Budczies et al., 2024). However, in our model, tumour burden assessed at 12 weeks revealed well-developed nodules, which limited our ability to evaluate the effect of DEP on the formation of early lesions. Investigating earlier stages of tumorigenesis would require the use of computed tomography (CT) scans and shortening the experimental timeline to capture the emergence of preinvasive or hyperplastic lesions before significant tumour progression occurs. A caveat of our study is that these mouse models develop cancer even in the absence of particulate matter exposure and likely do not fully recapitulate the complex mutational landscape observed in the healthy tissues of adult humans. Nevertheless, they offer a controlled experimental framework to investigate tumour progression. The use of KRAS-driven lung adenocarcinoma models presents important limitations when evaluating immunotherapy efficacy in the context of PM exposure. These tumours typically evolve in an immunologically “cold” environment, characterized by a low neoantigen load and weak T cell response. Consequently, KRAS-driven tumours in mice are largely resistant to checkpoint blockade in preclinical settings, which restricts their value for assessing how PM-induced immune alterations might influence therapeutic responses to agents such as anti PD-1, anti-LAG-3, or anti TIM-3 (Ischenko et al., 2021). Moreover, these models fail to capture the high mutational burden and antigenicity, features observed, for instance, in tobacco-associated human lung cancers, where immunotherapy demonstrates greater clinical relevance (X. Wang et al., 2021).

Along with our findings, where $CD14^{pos}SiglecF^{hi}$ PMN emerged in response to chronic DEP exposure in our KP mice model and exhibited features of immunosuppression, the study by Gungabeesoon et al., highlights the functional heterogeneity of neutrophils in a similar tumour context (Gungabeesoon et al., 2023). Using an orthotopic lung adenocarcinoma mouse model, in which tumour cells harbouring the

oncogenic $KRAS^{G12D}$ mutation and lacking p53, are injected intravenously, the authors investigated the effect of immunostimulatory treatment with a CD40 agonist antibody. This therapy significantly reduced tumour burden and was associated with robust neutrophil infiltration into the tumour. By performing single-cell RNA sequencing, they identified three main neutrophil clusters, with treatment leading to an expansion of the $SiglecF^{low}$ population. This subset expressed a transcriptional profile enriched in interferon-stimulated genes (ISGs) and markers associated with cytotoxic activity, suggesting a potential contribution to anti-tumour responses. In contrast, $SiglecF^{hi}$ neutrophils displayed a pro-tumoral gene signature, consistent with the suppressive phenotype observed in our DEP-exposed model. Interestingly, despite these functional differences, Gungabeesoon et al. reported that CD14 expression was increased in the $SiglecF^{low}$ cluster, whereas in our model, $CD14^{pos}$ neutrophils predominantly belonged to the $SiglecF^{hi}$ subset, which was associated with immunosuppression (Gungabeesoon et al., 2023). This apparent divergence suggests that CD14 expression may not always predict a suppressive phenotype, but rather reflects context-dependent transcriptional programming, potentially shaped by environmental signals, cytokine milieu, or treatment-induced reprogramming. In line with our findings, Engblom et al. (2017) identified two neutrophil subsets distinguished by their SiglecF expression levels. They reported that the ratio of $SiglecF^{high}$ to $SiglecF^{low}$ neutrophils positively correlated with KP tumour burden, and that $SiglecF^{high}$ neutrophils exhibited a transcriptional profile enriched for tumour-promoting functions. Functionally, when $SiglecF^{high}$ neutrophils were co-injected intradermally with KP tumour cells into C57BL/6 mice, they accelerated tumour growth compared to their $SiglecF^{low}$ counterparts. Furthermore, neutrophil depletion using anti-Gr1 antibodies significantly suppressed KP lung tumour progression (Engblom et al., 2017). Together, these results highlight the therapeutic potential of selectively targeting them in the context of pollution-enhanced lung cancer.

To better understand the contribution of $CD14^{pos}$ neutrophils to T cell dysfunction, we first confirmed through co-culture experiments that these cells significantly alter CD8+ T cell proliferation. Moreover, existing knowledge show that the PD-1/PD-L1 axis is a central pathway driving T cell exhaustion and functional impairment within the tumour microenvironment (Jiang et al., 2019). In our model, chronic DEP exposure led to upregulation of PD-L1 on $CD14^{pos}$ PMNs and increased PD-1 expression on T cells,

supporting a possible interaction through this inhibitory checkpoint. While $CD14^{pos}$ PMNs did not promote Treg differentiation in our ex vivo co-culture assay, we observed increased expression of immunoregulatory and immunosuppressive cytokines such as IL-10 and TGF-β, suggesting that these neutrophils may still contribute to a suppressive environment through soluble factors rather than direct Treg induction.

The presence of immunosuppressive neutrophil populations in tumours has emerged as a major barrier to effective anti-tumour immunity and to the success of immunotherapies. Two complementary strategies have been proposed to overcome this challenge: one targeting the development and recruitment of neutrophils, the other aiming to neutralize their immunosuppressive activity. Regarding the first approach, blockade of G-CSF, a cytokine crucial for neutrophil production and release from the bone marrow, has shown efficacy in depleting neutrophils using neutralizing antibodies (Casbon et al., 2015). Similarly, the inhibition of the CXCR2 signaling axis, essential for neutrophil trafficking, has been explored in preclinical and early clinical studies. For instance, targeting CXCR2 with small-molecule inhibitors such as SX-682 reduced the recruitment of suppressive PMN-MDSCs and delayed tumour progression in mouse models of prostate cancer (Wang et al., 2016).

The COX2/PGE2 pathway is another regulatory axis known to support both the expansion and suppressive function of PMN-MDSCs. Pharmacological inhibition of COX2 (e.g., with celecoxib or aspirin) not only reduces MDSC-mediated suppression but also enhances the efficacy of immune checkpoint blockade (Zelenay et al., 2015). Moreover, the c-MET receptor tyrosine kinase, expressed in neutrophils mobilized in response to cancer immunotherapy, has been shown to drive their suppressive functions. Inhibitors such as cabozantinib or capmatinib not only target tumour cell proliferation but also reshape the immune microenvironment by reducing PMN-MDSC infiltration and restoring T cell activity (Glodde et al., 2017; Lu et al., 2017). Furthermore, targeting the CD47-SIRPα axis represents a promising therapeutic strategy, as it may enhance antibody-dependent cellular cytotoxicity (ADCC) mediated by neutrophils and thereby amplify their anticancer effects. Notably, the SIRPα inhibitor BI 765063 (NCT03990233) and the anti-SIRPα antibody CC-95251 (NCT03783403) are currently being evaluated in phase I clinical trials for patients with advanced solid tumors (Behrens et al., 2022; Zhang et al., 2024).

Several chemotherapeutic agents have also been identified for their capacity to deplete MDSCs. Gemcitabine and capecitabine, beyond their cytotoxic effects, induce apoptosis in PMN-MDSCs and reduce immunosuppressive mediators such as TGF-β (Mariathasan et al., 2018; Vincent et al., 2010). In addition, RGX-104, an agonist of Liver X Receptor (LXR), has shown promising effects in early clinical trials by depleting circulating PMN-MDSCs and boosting cytotoxic T cell levels (Tavazoie et al., 2018).

As for direct functional reprogramming, L-arginine supplementation has been shown to restore anti-tumour immunity by countering arginine depletion, a key mechanism used by PMN-MDSCs to suppress T cells. Indeed, treated mice exhibited fewer intratumoral MDSCs and a higher frequency of CD4+ and CD8+ T cells, accompanied by increased pro-inflammatory cytokine production (Cao et al., 2016). Lastly, inhibition of histone deacetylases (HDACs) with agents like entinostat has been shown to reduce the expression of key suppressive enzymes (Arg1, iNOS, COX2) in PMN-MDSCs and to synergize with PD-1 blockade in lung carcinoma models (Orillion et al., 2017).

Taken together, our findings reveal that exposure to DEP significantly alters the pulmonary immune landscape by promoting both inflammation and immunosuppression. In particular, we identify a population of DEP-induced $CD14^{pos}$ PMNs with features of PMN-MDSCs, capable of dampening T cell responses and contributing to a tumour-promoting microenvironment. This immunosuppressive activity, coupled with evidence of T cell dysfunction, suggests that sustained exposure to environmental pollutants such as DEP may impair anti-tumour immunity and facilitate lung cancer progression.

These insights underscore the dual role of neutrophils in modulating adaptive immunity, either enhancing immune activation or suppressing it depending on their phenotype and context. The enrichment of immunosuppressive neutrophil subsets in DEP-exposed lungs highlights their potential as therapeutic targets. However, strategies aimed at targeting PMN-MDSCs must be approached with caution. Given the heterogeneity and plasticity of neutrophils in the tumour microenvironment, indiscriminate depletion could compromise host defence or remove neutrophil subsets with anti-tumour functions. Importantly, recent research has shown that most neutrophil states identified in human lung tumours can also be observed in murine models (Zilionis et al., 2019), reinforcing the translational relevance of our findings. This

supports the validity of our mouse-based insights and their potential applicability to human disease contexts.

Therefore, selectively targeting pollutant-induced immunosuppressive neutrophils represents a promising strategy to counteract immune dysregulation and enhance the effectiveness of cancer immunotherapy. Our results reinforce the need for further studies to define safe and effective strategies for reprogramming neutrophil functions, and more broadly, call attention to air pollution as a modifiable environmental factor with profound implications for cancer immunity and public health.

REFERENCES

REFERENCES

Abbas, A.K., Lichtman, A.H., Pillai, S., 2014. Basic immunology: functions and disorders of the immune system, Fourth edition. ed. Elsevier/Saunders, Philadelphia, PA.

Allard, B., Longhi, M.S., Robson, S.C., Stagg, J., 2017. The ectonucleotidases CD39 and CD73: Novel checkpoint inhibitor targets. Immunol Rev 276, 121–144. https://doi.org/10.1111/imr.12528

Alshetaiwi, H., Pervolarakis, N., McIntyre, L.L., Ma, D., Nguyen, Q., Rath, J.A., Nee, K., Hernandez, G., Evans, K., Torosian, L., Silva, A., Walsh, C., Kessenbrock, K., 2020. Defining the emergence of myeloid-derived suppressor cells in breast cancer using single-cell transcriptomics. Sci. Immunol. 5, eaay6017. https://doi.org/10.1126/sciimmunol.aay6017

Antiñolo, M., Willis, M.D., Zhou, S., Abbatt, J.P.D., 2015. Connecting the oxidation of soot to its redox cycling abilities. Nat Commun 6, 6812. https://doi.org/10.1038/ncomms7812

Antonios, J.P., Soto, H., Everson, R.G., Moughon, D., Orpilla, J.R., Shin, N.P., Sedighim, S., Treger, J., Odesa, S., Tucker, A., Yong, W.H., Li, G., Cloughesy, T.F., Liau, L.M., Prins, R.M., 2017. Immunosuppressive tumor-infiltrating myeloid cells mediate adaptive immune resistance via a PD-1/PD-L1 mechanism in glioblastoma. Neuro Oncol 19, 796–807. https://doi.org/10.1093/neuonc/now287

Baessler, A., Vignali, D.A.A., 2024. T Cell Exhaustion. Annu Rev Immunol 42, 179–206. https://doi.org/10.1146/annurev-immunol-090222-110914

Ballesteros, I., Rubio-Ponce, A., Genua, M., Lusito, E., Kwok, I., Fernández-Calvo, G., Khoyratty, T.E., van Grinsven, E., González-Hernández, S., Nicolás-Ávila, J.Á., Vicanolo, T., Maccataio, A., Benguría, A., Li, J.L., Adrover, J.M., Aroca-Crevillen, A., Quintana, J.A., Martín-Salamanca, S., Mayo, F., Ascher, S., Barbiera, G., Soehnlein, O., Gunzer, M., Ginhoux, F., Sánchez-Cabo, F., Nistal-Villán, E., Schulz, C., Dopazo, A., Reinhardt, C., Udalova, I.A., Ng, L.G., Ostuni, R., Hidalgo, A., 2020. Co-option of Neutrophil Fates by Tissue Environments. Cell 183, 1282-1297.e18. https://doi.org/10.1016/j.cell.2020.10.003

Barreda, D.R., Hanington, P.C., Belosevic, M., 2004. Regulation of myeloid development and function by colony stimulating factors. Dev Comp Immunol 28, 509–554. https://doi.org/10.1016/j.dci.2003.09.010

Baz, A.A., Hao, H., Lan, S., Li, Z., Liu, S., Chen, S., Chu, Y., 2024. Neutrophil extracellular traps in bacterial infections and evasion strategies. Front Immunol 15, 1357967. https://doi.org/10.3389/fimmu.2024.1357967

Becher, B., Tugues, S., Greter, M., 2016. GM-CSF: From Growth Factor to Central Mediator of Tissue Inflammation. Immunity 45, 963–973. https://doi.org/10.1016/j.immuni.2016.10.026

Behrens, L.M., van den Berg, T.K., van Egmond, M., 2022. Targeting the CD47-SIRPα Innate Immune Checkpoint to Potentiate Antibody Therapy in Cancer by Neutrophils. Cancers (Basel) 14, 3366. https://doi.org/10.3390/cancers14143366

Bolton, J.L., Dunlap, T., 2017. Formation and Biological Targets of Quinones: Cytotoxic versus Cytoprotective Effects. Chem Res Toxicol 30, 13–37. https://doi.org/10.1021/acs.chemrestox.6b00256

Bongaerts, E., Lecante, L.L., Bové, H., Roeffaers, M.B.J., Ameloot, M., Fowler, P.A., Nawrot, T.S., 2022. Maternal exposure to ambient black carbon particles and their presence in maternal and fetal circulation and organs: an analysis of two independent population-based observational studies. Lancet Planet Health 6, e804–e811. https://doi.org/10.1016/S2542-5196(22)00200-5

Boogaard, H., Patton, A.P., Atkinson, R.W., Brook, J.R., Chang, H.H., Crouse, D.L., Fussell, J.C., Hoek, G., Hoffmann, B., Kappeler, R., Kutlar Joss, M., Ondras, M., Sagiv, S.K., Samoli, E., Shaikh, R., Smargiassi, A., Szpiro, A.A., Van Vliet, E.D.S., Vienneau, D., Weuve, J., Lurmann, F.W., Forastiere, F., 2022. Long-term exposure to traffic-related air pollution and selected health outcomes: A systematic review and meta-analysis. Environ Int 164, 107262. https://doi.org/10.1016/j.envint.2022.107262

Bowatte, G., Lodge, C., Lowe, A.J., Erbas, B., Perret, J., Abramson, M.J., Matheson, M., Dharmage, S.C., 2015. The influence of childhood traffic-related air pollution exposure on asthma, allergy and sensitization: a systematic review and a meta-analysis of birth cohort studies. Allergy 70, 245–256. https://doi.org/10.1111/all.12561

Brinkmann, V., Reichard, U., Goosmann, C., Fauler, B., Uhlemann, Y., Weiss, D.S., Weinrauch, Y., Zychlinsky, A., 2004. Neutrophil extracellular traps kill bacteria. Science 303, 1532–1535. https://doi.org/10.1126/science.1092385

Budczies, J., Romanovsky, E., Kirchner, M., Neumann, O., Blasi, M., Schnorbach, J., Shah, R., Bozorgmehr, F., Savai, R., Stiewe, T., Peters, S., Schirmacher, P., Thomas, M., Kazdal, D., Christopoulos, P., Stenzinger, A., 2024. KRAS and TP53 co-mutation predicts benefit of immune checkpoint blockade in lung adenocarcinoma. Br J Cancer 131, 524–533. https://doi.org/10.1038/s41416-024-02746-z

Calderón-Garcidueñas, L., Torres-Jardón, R., Greenough, G.P., Kulesza, R., González-Maciel, A., Reynoso-Robles, R., García-Alonso, G., Chávez-Franco, D.A., García-Rojas, E., Brito-Aguilar, R., Silva-Pereyra, H.G., Ayala, A., Stommel, E.W., Mukherjee, P.S., 2023. Sleep matters: Neurodegeneration spectrum heterogeneity, combustion and friction ultrafine particles, industrial nanoparticle pollution, and sleep disorders-Denial is not an option. Front Neurol 14, 1117695. https://doi.org/10.3389/fneur.2023.1117695

Cao, Y., Feng, Y., Zhang, Y., Zhu, X., Jin, F., 2016. L-Arginine supplementation inhibits the growth of breast cancer by enhancing innate and adaptive immune responses mediated by suppression of MDSCs in vivo. BMC Cancer 16, 343. https://doi.org/10.1186/s12885-016-2376-0

Carman, C.V., Springer, T.A., 2004. A transmigratory cup in leukocyte diapedesis both through individual vascular endothelial cells and between them. J Cell Biol 167, 377–388. https://doi.org/10.1083/jcb.200404129

Casanova-Acebes, M., Nicolás-Ávila, J.A., Li, J.L., García-Silva, S., Balachander, A., Rubio-Ponce, A., Weiss, L.A., Adrover, J.M., Burrows, K., A-González, N., Ballesteros, I., Devi, S., Quintana, J.A., Crainiciuc, G., Leiva, M., Gunzer, M., Weber, C., Nagasawa, T., Soehnlein, O., Merad, M., Mortha, A., Ng, L.G., Peinado, H., Hidalgo, A., 2018. Neutrophils instruct homeostatic and pathological states in naive tissues. J Exp Med 215, 2778–2795. https://doi.org/10.1084/jem.20181468

Casanova-Acebes, M., Pitaval, C., Weiss, L.A., Nombela-Arrieta, C., Chèvre, R., A-González, N., Kunisaki, Y., Zhang, D., van Rooijen, N., Silberstein, L.E., Weber, C., Nagasawa, T., Frenette, P.S., Castrillo, A., Hidalgo, A., 2013. Rhythmic modulation of the hematopoietic niche through neutrophil clearance. Cell 153, 1025–1035. https://doi.org/10.1016/j.cell.2013.04.040

Casbon, A.-J., Reynaud, D., Park, C., Khuc, E., Gan, D.D., Schepers, K., Passegué, E., Werb, Z., 2015. Invasive breast cancer reprograms early myeloid differentiation in the bone marrow to generate immunosuppressive neutrophils. Proc Natl Acad Sci U S A 112, E566-575. https://doi.org/10.1073/pnas.1424927112

Catino, S., Tutino, M., Ruggieri, S., Marinaccio, C., Giua, R., de Gennaro, G., Corsi, P., Assennato, G., Ribatti, D., 2017. Angiogenic activity *in vivo* of the particulate matter (PM10). Ecotoxicology and Environmental Safety 140, 156–161. https://doi.org/10.1016/j.ecoenv.2017.02.036

Chiba, Y., Mizoguchi, I., Hasegawa, H., Ohashi, M., Orii, N., Nagai, T., Sugahara, M., Miyamoto, Y., Xu, M., Owaki, T., Yoshimoto, T., 2018. Regulation of myelopoiesis by proinflammatory

cytokines in infectious diseases. Cell Mol Life Sci 75, 1363–1376. https://doi.org/10.1007/s00018-017-2724-5

ChooChuay, C., Pongpiachan, S., Tipmanee, D., Suttinun, O., Deelaman, W., Wang, Q., Xing, L., Li, G., Han, Y., Palakun, J., Cao, J., 2020. Impacts of PM2.5 sources on variations in particulate chemical compounds in ambient air of Bangkok, Thailand. Atmospheric Pollution Research 11, 1657–1667. https://doi.org/10.1016/j.apr.2020.06.030

Ciraolo, E., Althoff, S., Ruß, J., Rosnev, S., Butze, M., Pühl, M., Frentsch, M., Bullinger, L., Na, I.-K., 2022. Simultaneous Genetic Ablation of PD-1, LAG-3, and TIM-3 in CD8 T Cells Delays Tumor Growth and Improves Survival Outcome. Int J Mol Sci 23, 3207. https://doi.org/10.3390/ijms23063207

Colín-Val, Z., Flores-Navarro, G., Rocha-Zavaleta, L., Robledo-Cadena, D.X., Quintana-Belmares, R.O., López-Marure, R., 2024. Fine particulate matter (PM2.5) promotes chemoresistance and aggressive phenotype of A549 lung cancer cells. Toxicol Appl Pharmacol 487, 116955. https://doi.org/10.1016/j.taap.2024.116955

Condamine, T., Dominguez, G.A., Youn, J.-I., Kossenkov, A.V., Mony, S., Alicea-Torres, K., Tcyganov, E., Hashimoto, A., Nefedova, Y., Lin, C., Partlova, S., Garfall, A., Vogl, D.T., Xu, X., Knight, S.C., Malietzis, G., Lee, G.H., Eruslanov, E., Albelda, S.M., Wang, X., Mehta, J.L., Bewtra, M., Rustgi, A., Hockstein, N., Witt, R., Masters, G., Nam, B., Smirnov, D., Sepulveda, M.A., Gabrilovich, D.I., 2016. Lectin-type oxidized LDL receptor-1 distinguishes population of human polymorphonuclear myeloid-derived suppressor cells in cancer patients. Sci Immunol 1, aaf8943. https://doi.org/10.1126/sciimmunol.aaf8943

Condamine, T., Mastio, J., Gabrilovich, D.I., 2015. Transcriptional regulation of myeloid-derived suppressor cells. J Leukoc Biol 98, 913–922. https://doi.org/10.1189/jlb.4RI0515-204R

Cools-Lartigue, J., Spicer, J., Najmeh, S., Ferri, L., 2014. Neutrophil extracellular traps in cancer progression. Cell Mol Life Sci 71, 4179–4194. https://doi.org/10.1007/s00018-014-1683-3

Cooper, W.A., Lam, D.C.L., O'Toole, S.A., Minna, J.D., 2013. Molecular biology of lung cancer. J Thorac Dis 5 Suppl 5, S479-490. https://doi.org/10.3978/j.issn.2072-1439.2013.08.03

Crawford, A., Angelosanto, J.M., Kao, C., Doering, T.A., Odorizzi, P.M., Barnett, B.E., Wherry, E.J., 2014. Molecular and transcriptional basis of $CD4^+$ T cell dysfunction during chronic infection. Immunity 40, 289–302. https://doi.org/10.1016/j.immuni.2014.01.005

Czerska, M., Mikołajewska, K., Zieliński, M., Gromadzińska, J., Wąsowicz, W., 2015. Today's oxidative stress markers. Med Pr 66, 393–405. https://doi.org/10.13075/mp.5893.00137

Danesh Yazdi, M., Wang, Y., Di, Q., Wei, Y., Requia, W.J., Shi, L., Sabath, M.B., Dominici, F., Coull, B.A., Evans, J.S., Koutrakis, P., Schwartz, J.D., 2021. Long-Term Association of Air Pollution and Hospital Admissions Among Medicare Participants Using a Doubly Robust Additive Model. Circulation 143, 1584–1596. https://doi.org/10.1161/CIRCULATIONAHA.120.050252

den Hartigh, L.J., Lamé, M.W., Ham, W., Kleeman, M.J., Tablin, F., Wilson, D.W., 2010. Endotoxin and polycyclic aromatic hydrocarbons in ambient fine particulate matter from Fresno, California initiate human monocyte inflammatory responses mediated by reactive oxygen species. Toxicol In Vitro 24, 1993–2002. https://doi.org/10.1016/j.tiv.2010.08.017

Devarakonda, S., Li, Y., Martins Rodrigues, F., Sankararaman, S., Kadara, H., Goparaju, C., Lanc, I., Pepin, K., Waqar, S.N., Morgensztern, D., Ward, J., Masood, A., Fulton, R., Fulton, L., Gillette, M.A., Satpathy, S., Carr, S.A., Wistuba, I., Pass, H., Wilson, R.K., Ding, L., Govindan, R., 2021. Genomic Profiling of Lung Adenocarcinoma in Never-Smokers. J Clin Oncol 39, 3747–3758. https://doi.org/10.1200/JCO.21.01691

Eash, K.J., Greenbaum, A.M., Gopalan, P.K., Link, D.C., 2010. CXCR2 and CXCR4 antagonistically regulate neutrophil trafficking from murine bone marrow. J Clin Invest 120, 2423–2431. https://doi.org/10.1172/JCI41649

Engblom, C., Pfirschke, C., Zilionis, R., Da Silva Martins, J., Bos, S.A., Courties, G., Rickelt, S., Severe, N., Baryawno, N., Faget, J., Savova, V., Zemmour, D., Kline, J., Siwicki, M., Garris, C., Pucci, F., Liao, H.-W., Lin, Y.-J., Newton, A., Yaghi, O.K., Iwamoto, Y., Tricot, B., Wojtkiewicz, G.R., Nahrendorf, M., Cortez-Retamozo, V., Meylan, E., Hynes, R.O., Demay, M., Klein, A., Bredella, M.A., Scadden, D.T., Weissleder, R., Pittet, M.J., 2017. Osteoblasts remotely supply lung tumors with cancer-promoting SiglecF ^{high} neutrophils. Science 358, eaal5081. https://doi.org/10.1126/science.aal5081

Ermert, D., Urban, C.F., Laube, B., Goosmann, C., Zychlinsky, A., Brinkmann, V., 2009. Mouse neutrophil extracellular traps in microbial infections. J Innate Immun 1, 181–193. https://doi.org/10.1159/000205281

European Commission, n.d. Emissions in the automotive sector [WWW Document]. European Commission. URL https://single-market-economy.ec.europa.eu/sectors/automotive-industry/environmental-protection/emissions-automotive-sector_en (accessed 8.11.25).

Fedak, E.A., Adler, F.R., Abegglen, L.M., Schiffman, J.D., 2021. ATM and ATR Activation Through Crosstalk Between DNA Damage Response Pathways. Bull Math Biol 83, 38. https://doi.org/10.1007/s11538-021-00868-6

Feng, B., Song, X., Dan, M., Yu, J., Wang, Q., Shu, M., Xu, H., Wang, T., Chen, J., Zhang, Y., Zhao, Q., Wu, R., Liu, S., Yu, J.Z., Wang, T., Huang, W., 2019. High level of source-specific particulate matter air pollution associated with cardiac arrhythmias. Sci Total Environ 657, 1285–1293. https://doi.org/10.1016/j.scitotenv.2018.12.178

Feng, S., Cheng, X., Zhang, L., Lu, Xuemin, Chaudhary, S., Teng, R., Frederickson, C., Champion, M.M., Zhao, R., Cheng, L., Gong, Y., Deng, H., Lu, Xin, 2018. Myeloid-derived suppressor cells inhibit T cell activation through nitrating LCK in mouse cancers. Proc Natl Acad Sci U S A 115, 10094–10099. https://doi.org/10.1073/pnas.1800695115

Fenwick, C., Joo, V., Jacquier, P., Noto, A., Banga, R., Perreau, M., Pantaleo, G., 2019. T-cell exhaustion in HIV infection. Immunol Rev 292, 149–163. https://doi.org/10.1111/imr.12823

Filippone, A., Lanza, M., Mannino, D., Raciti, G., Colarossi, C., Sciacca, D., Cuzzocrea, S., Paterniti, I., 2022. PD1/PD-L1 immune checkpoint as a potential target for preventing brain tumor progression. Cancer Immunol Immunother 71, 2067–2075. https://doi.org/10.1007/s00262-021-03130-z

Flannagan, R.S., Jaumouillé, V., Grinstein, S., 2012. The cell biology of phagocytosis. Annu Rev Pathol 7, 61–98. https://doi.org/10.1146/annurev-pathol-011811-132445

Fu, J., Yu, A., Xiao, X., Tang, J., Zu, X., Chen, W., He, B., 2020. CD4+ T cell exhaustion leads to adoptive transfer therapy failure which can be prevented by immune checkpoint blockade. Am J Cancer Res 10, 4234–4250.

Garcia, E., Rice, M.B., Gold, D.R., 2021. Air pollution and lung function in children. J Allergy Clin Immunol 148, 1–14. https://doi.org/10.1016/j.jaci.2021.05.006

García-Ortiz, A., Serrador, J.M., 2018. Nitric Oxide Signaling in T Cell-Mediated Immunity. Trends Mol Med 24, 412–427. https://doi.org/10.1016/j.molmed.2018.02.002

Glodde, N., Bald, T., van den Boorn-Konijnenberg, D., Nakamura, K., O'Donnell, J.S., Szczepanski, S., Brandes, M., Eickhoff, S., Das, I., Shridhar, N., Hinze, D., Rogava, M., van der Sluis, T.C., Ruotsalainen, J.J., Gaffal, E., Landsberg, J., Ludwig, K.U., Wilhelm, C., Riek-Burchardt, M., Müller, A.J., Gebhardt, C., Scolyer, R.A., Long, G.V., Janzen, V., Teng, M.W.L., Kastenmüller, W., Mazzone, M., Smyth, M.J., Tüting, T., Hölzel, M., 2017. Reactive Neutrophil Responses Dependent on the Receptor Tyrosine Kinase c-MET Limit Cancer Immunotherapy. Immunity 47, 789-802.e9. https://doi.org/10.1016/j.immuni.2017.09.012

Guaita, R., Pichiule, M., Maté, T., Linares, C., Díaz, J., 2011. Short-term impact of particulate matter (PM(2.5)) on respiratory mortality in Madrid. Int J Environ Health Res 21, 260–274. https://doi.org/10.1080/09603123.2010.544033

Gungabeesoon, J., Gort-Freitas, N.A., Kiss, M., Bolli, E., Messemaker, M., Siwicki, M., Hicham, M., Bill, R., Koch, P., Cianciaruso, C., Duval, F., Pfirschke, C., Mazzola, M., Peters, S., Homicsko, K., Garris, C., Weissleder, R., Klein, A.M., Pittet, M.J., 2023. A neutrophil response linked to tumor control in immunotherapy. Cell 186, 1448-1464.e20. https://doi.org/10.1016/j.cell.2023.02.032

Guo, X., Zhang, Y., Zheng, L., Zheng, C., Song, J., Zhang, Q., Kang, B., Liu, Z., Jin, L., Xing, R., Gao, R., Zhang, L., Dong, M., Hu, X., Ren, X., Kirchhoff, D., Roider, H.G., Yan, T., Zhang, Z., 2018. Global characterization of T cells in non-small-cell lung cancer by single-cell sequencing. Nat Med 24, 978–985. https://doi.org/10.1038/s41591-018-0045-3

Ha, S.Y., Choi, S.-J., Cho, J.H., Choi, H.J., Lee, J., Jung, K., Irwin, D., Liu, X., Lira, M.E., Mao, M., Kim, H.K., Choi, Y.S., Shim, Y.M., Park, W.Y., Choi, Y.-L., Kim, J., 2015. Lung cancer in never-smoker Asian females is driven by oncogenic mutations, most often involving EGFR. Oncotarget 6, 5465–5474. https://doi.org/10.18632/oncotarget.2925

Hanahan, D., 2022. Hallmarks of Cancer: New Dimensions. Cancer Discov 12, 31–46. https://doi.org/10.1158/2159-8290.CD-21-1059

Hanahan, D., Weinberg, R.A., 2011. Hallmarks of cancer: the next generation. Cell 144, 646–674. https://doi.org/10.1016/j.cell.2011.02.013

Hanahan, D., Weinberg, R.A., 2000. The Hallmarks of Cancer. Cell 100, 57–70. https://doi.org/10.1016/S0092-8674(00)81683-9

He, Y.-M., Li, X., Perego, M., Nefedova, Y., Kossenkov, A.V., Jensen, E.A., Kagan, V., Liu, Y.-F., Fu, S.-Y., Ye, Q.-J., Zhou, Y.-H., Wei, L., Gabrilovich, D.I., Zhou, J., 2018. Transitory presence of myeloid-derived suppressor cells in neonates is critical for control of inflammation. Nat Med 24, 224–231. https://doi.org/10.1038/nm.4467

Hedrick, C.C., Malanchi, I., 2022. Neutrophils in cancer: heterogeneous and multifaceted. Nat Rev Immunol 22, 173–187. https://doi.org/10.1038/s41577-021-00571-6

Heinrich, J., Schikowski, T., 2018. COPD Patients as Vulnerable Subpopulation for Exposure to Ambient Air Pollution. Curr Environ Health Rep 5, 70–76. https://doi.org/10.1007/s40572-018-0178-z

Hidalgo, A., Chilvers, E.R., Summers, C., Koenderman, L., 2019. The Neutrophil Life Cycle. Trends Immunol 40, 584–597. https://doi.org/10.1016/j.it.2019.04.013

Hill, W., Lim, E.L., Weeden, C.E., Lee, C., Augustine, M., Chen, K., Kuan, F.-C., Marongiu, F., Evans, E.J., Moore, D.A., Rodrigues, F.S., Pich, O., Bakker, B., Cha, H., Myers, R., van Maldegem, F., Boumelha, J., Veeriah, S., Rowan, A., Naceur-Lombardelli, C., Karasaki, T., Sivakumar, M., De, S., Caswell, D.R., Nagano, A., Black, J.R.M., Martínez-Ruiz, C., Ryu, M.H., Huff, R.D., Li, S., Favé, M.-J., Magness, A., Suárez-Bonnet, A., Priestnall, S.L., Lüchtenborg, M., Lavelle, K., Pethick, J., Hardy, S., McRonald, F.E., Lin, M.-H., Troccoli, C.I., Ghosh, M., Miller, Y.E., Merrick, D.T., Keith, R.L., Al Bakir, M., Bailey, C., Hill, M.S., Saal, L.H., Chen, Y., George, A.M., Abbosh, C., Kanu, N., Lee, S.-H., McGranahan, N., Berg, C.D., Sasieni, P., Houlston, R., Turnbull, C., Lam, S., Awadalla, P., Grönroos, E., Downward, J., Jacks, T., Carlsten, C., Malanchi, I., Hackshaw, A., Litchfield, K., DeGregori, J., Jamal-Hanjani, M., Swanton, C., 2023. Lung adenocarcinoma promotion by air pollutants. Nature 616, 159–167. https://doi.org/10.1038/s41586-023-05874-3

Hiscock, R., Bauld, L., Amos, A., Fidler, J.A., Munafò, M., 2012. Socioeconomic status and smoking: a review. Ann N Y Acad Sci 1248, 107–123. https://doi.org/10.1111/j.1749-6632.2011.06202.x

Hu, B., Tong, B., Xiang, Y., Li, S.-R., Tan, Z.-X., Xiang, H.-X., Fu, L., Wang, H., Zhao, H., Xu, D.-X., 2020. Acute 1-NP exposure induces inflammatory responses through activating various inflammatory signaling pathways in mouse lungs and human A549 cells. Ecotoxicol Environ Saf 189, 109977. https://doi.org/10.1016/j.ecoenv.2019.109977

Huang, C., Wang, Xuefei, Wang, Y., Feng, Y., Wang, Xiumei, Chen, Shan, Yan, P., Liao, J., Zhang, Q., Mao, C., Li, Y., Wang, L., Wang, Xinyu, Yi, W., Cai, W., Chen, Shoudeng, Hong, N., He, W., Chen, J., Jin, W., 2024. Sirpα on tumor-associated myeloid cells restrains antitumor

immunity in colorectal cancer independent of its interaction with CD47. Nat Cancer 5, 500–516. https://doi.org/10.1038/s43018-023-00691-z

IARC, 2014. Diesel and gasoline engine exhausts and some Nitroarenes. IARC Monogr Eval Carcinog Risks Hum 105, 9–699.

IQAir, 2024. World Live Air Quality Map | IQAir [WWW Document]. URL https://www.iqair.com/world-air-quality (accessed 8.8.25).

Ischenko, I., D'Amico, S., Rao, M., Li, J., Hayman, M.J., Powers, S., Petrenko, O., Reich, N.C., 2021. KRAS drives immune evasion in a genetic model of pancreatic cancer. Nat Commun 12, 1482. https://doi.org/10.1038/s41467-021-21736-w

James, P., Kaushal, D., Beaumont Wilson, R., 2024. NETosis in Surgery: Pathophysiology, Prevention, and Treatment. Ann Surg 279, 765–780. https://doi.org/10.1097/SLA.0000000000006196

Jiang, C.-L., He, S.-W., Zhang, Y.-D., Duan, H.-X., Huang, T., Huang, Y.-C., Li, G.-F., Wang, P., Ma, L.-J., Zhou, G.-B., Cao, Y., 2016. Air pollution and DNA methylation alterations in lung cancer: A systematic and comparative study. Oncotarget 8, 1369–1391. https://doi.org/10.18632/oncotarget.13622

Jiang, X., Wang, J., Deng, X., Xiong, F., Ge, J., Xiang, B., Wu, X., Ma, J., Zhou, M., Li, X., Li, Y., Li, G., Xiong, W., Guo, C., Zeng, Z., 2019. Role of the tumor microenvironment in PD-L1/PD-1-mediated tumor immune escape. Molecular Cancer 18, 10. https://doi.org/10.1186/s12943-018-0928-4

Jiang, Y., Li, Y., Zhu, B., 2015. T-cell exhaustion in the tumor microenvironment. Cell Death Dis 6, e1792. https://doi.org/10.1038/cddis.2015.162

Jilani, M.H., Simon-Friedt, B., Yahya, T., Khan, A.Y., Hassan, S.Z., Kash, B., Blankstein, R., Blaha, M.J., Virani, S.S., Rajagopalan, S., Cainzos-Achirica, M., Nasir, K., 2020. Associations between particulate matter air pollution, presence and progression of subclinical coronary and carotid atherosclerosis: A systematic review. Atherosclerosis 306, 22–32. https://doi.org/10.1016/j.atherosclerosis.2020.06.018

Jorch, S.K., Kubes, P., 2017. An emerging role for neutrophil extracellular traps in noninfectious disease. Nat Med 23, 279–287. https://doi.org/10.1038/nm.4294

Kalemkerian, G.P., Akerley, W., Bogner, P., Borghaei, H., Chow, L.Q., Downey, R.J., Gandhi, L., Ganti, A.K.P., Govindan, R., Grecula, J.C., Hayman, J., Heist, R.S., Horn, L., Jahan, T., Koczywas, M., Loo, B.W., Merritt, R.E., Moran, C.A., Niell, H.B., O'Malley, J., Patel, J.D., Ready, N., Rudin, C.M., Williams, C.C., Gregory, K., Hughes, M., National Comprehensive Cancer Network, 2013. Small cell lung cancer. J Natl Compr Canc Netw 11, 78–98. https://doi.org/10.6004/jnccn.2013.0011

Kaltenmeier, C., Yazdani, H.O., Morder, K., Geller, D.A., Simmons, R.L., Tohme, S., 2021. Neutrophil Extracellular Traps Promote T Cell Exhaustion in the Tumor Microenvironment. Front Immunol 12, 785222. https://doi.org/10.3389/fimmu.2021.785222

Khalek, I.A., Blanks, M.G., Merritt, P.M., Zielinska, B., 2015. Regulated and unregulated emissions from modern 2010 emissions-compliant heavy-duty on-highway diesel engines. J Air Waste Manag Assoc 65, 987–1001. https://doi.org/10.1080/10962247.2015.1051606

Khismatullin, D.B., Truskey, G.A., 2012. Leukocyte rolling on P-selectin: a three-dimensional numerical study of the effect of cytoplasmic viscosity. Biophys J 102, 1757–1766. https://doi.org/10.1016/j.bpj.2012.03.018

Kim, H.-B., Shim, J.-Y., Park, B., Lee, Y.-J., 2018. Long-Term Exposure to Air Pollutants and Cancer Mortality: A Meta-Analysis of Cohort Studies. Int J Environ Res Public Health 15, 2608. https://doi.org/10.3390/ijerph15112608

Kim, H.K., De La Luz Sierra, M., Williams, C.K., Gulino, A.V., Tosato, G., 2006. G-CSF down-regulation of CXCR4 expression identified as a mechanism for mobilization of myeloid cells. Blood 108, 812–820. https://doi.org/10.1182/blood-2005-10-4162

Klepac, P., Locatelli, I., Korošec, S., Künzli, N., Kukec, A., 2018. Ambient air pollution and pregnancy outcomes: A comprehensive review and identification of environmental public health challenges. Environ Res 167, 144–159. https://doi.org/10.1016/j.envres.2018.07.008

Kolaczkowska, E., Kubes, P., 2013. Neutrophil recruitment and function in health and inflammation. Nat Rev Immunol 13, 159–175. https://doi.org/10.1038/nri3399

Kruger, P., Saffarzadeh, M., Weber, A.N.R., Rieber, N., Radsak, M., von Bernuth, H., Benarafa, C., Roos, D., Skokowa, J., Hartl, D., 2015. Neutrophils: Between host defence, immune modulation, and tissue injury. PLoS Pathog 11, e1004651. https://doi.org/10.1371/journal.ppat.1004651

Kwantwi, L.B., Wang, S., Zhang, W., Peng, W., Cai, Z., Sheng, Y., Xiao, H., Wang, X., Wu, Q., 2021. Tumor-associated neutrophils activated by tumor-derived CCL20 (C-C motif chemokine ligand 20) promote T cell immunosuppression via programmed death-ligand 1 (PD-L1) in breast cancer. Bioengineered 12, 6996–7006. https://doi.org/10.1080/21655979.2021.1977102

Lahoz-Beneytez, J., Elemans, M., Zhang, Y., Ahmed, R., Salam, A., Block, M., Niederalt, C., Asquith, B., Macallan, D., 2016. Human neutrophil kinetics: modeling of stable isotope labeling data supports short blood neutrophil half-lives. Blood 127, 3431–3438. https://doi.org/10.1182/blood-2016-03-700336

Landskron, G., De la Fuente, M., Thuwajit, P., Thuwajit, C., Hermoso, M.A., 2014. Chronic inflammation and cytokines in the tumor microenvironment. J Immunol Res 2014, 149185. https://doi.org/10.1155/2014/149185

Lanigan, T.M., Rasmussen, S.M., Weber, D.P., Athukorala, K.S., Campbell, P.L., Fox, D.A., Ruth, J.H., 2020. Real time visualization of cancer cell death, survival and proliferation using fluorochrome-transfected cells in an IncuCyte® imaging system. J Biol Methods 7, e133. https://doi.org/10.14440/jbm.2020.323

Laurenti, E., Göttgens, B., 2018. From haematopoietic stem cells to complex differentiation landscapes. Nature 553, 418–426. https://doi.org/10.1038/nature25022

Lawrence, S.M., Corriden, R., Nizet, V., 2020. How Neutrophils Meet Their End. Trends Immunol 41, 531–544. https://doi.org/10.1016/j.it.2020.03.008

Lee, D.-H., Kim, S.-H., Kang, S.-H., Kwon, O.K., Park, J.-J., Yoon, C.-H., Cho, Y.-S., Heo, J., Yi, S.-M., Youn, T.-J., Chae, I.-H., 2020. Personal exposure to fine particulate air pollutants impacts blood pressure and heart rate variability. Sci Rep 10, 16538. https://doi.org/10.1038/s41598-020-73205-x

Lei, J., Li, Z., Huang, X., Li, X., Zhang, G., Kan, H., Chen, R., Zhang, Y., 2021. The Acute Effect of Diesel Exhaust Particles and Different Fractions Exposure on Blood Coagulation Function in Mice. Int J Environ Res Public Health 18, 4136. https://doi.org/10.3390/ijerph18084136

Lelieveld, J., Pozzer, A., Pöschl, U., Fnais, M., Haines, A., Münzel, T., 2020. Loss of life expectancy from air pollution compared to other risk factors: a worldwide perspective. Cardiovasc Res 116, 1910–1917. https://doi.org/10.1093/cvr/cvaa025

Leshner, M., Wang, S., Lewis, C., Zheng, H., Chen, X.A., Santy, L., Wang, Y., 2012. PAD4 mediated histone hypercitrullination induces heterochromatin decondensation and chromatin unfolding to form neutrophil extracellular trap-like structures. Front Immunol 3, 307. https://doi.org/10.3389/fimmu.2012.00307

Ley, K., Laudanna, C., Cybulsky, M.I., Nourshargh, S., 2007. Getting to the site of inflammation: the leukocyte adhesion cascade updated. Nat Rev Immunol 7, 678–689. https://doi.org/10.1038/nri2156

Li, C., Jiang, P., Wei, S., Xu, X., Wang, J., 2020. Regulatory T cells in tumor microenvironment: new mechanisms, potential therapeutic strategies and future prospects. Mol Cancer 19, 116. https://doi.org/10.1186/s12943-020-01234-1

Li, J., Wang, L., Chen, X., Li, L., Li, Y., Ping, Y., Huang, L., Yue, D., Zhang, Z., Wang, F., Li, F., Yang, L., Huang, J., Yang, S., Li, H., Zhao, X., Dong, W., Yan, Y., Zhao, S., Huang, B., Zhang, B., Zhang, Y., 2017. CD39/CD73 upregulation on myeloid-derived suppressor cells via TGF-β-mTOR-HIF-1 signaling in patients with non-small cell lung cancer. Oncoimmunology 6, e1320011. https://doi.org/10.1080/2162402X.2017.1320011

Li, K., Shi, H., Zhang, B., Ou, X., Ma, Q., Chen, Y., Shu, P., Li, D., Wang, Y., 2021. Myeloid-derived suppressor cells as immunosuppressive regulators and therapeutic targets in cancer. Signal Transduct Target Ther 6, 362. https://doi.org/10.1038/s41392-021-00670-9

Li, R., Yang, L., Jiang, N., Wang, F., Zhang, P., Zhou, R., Zhang, J., 2020. Activated macrophages are crucial during acute PM2.5 exposure-induced angiogenesis in lung cancer. Oncol Lett 19, 725–734. https://doi.org/10.3892/ol.2019.11133

Li, W., Liu, T., Xiong, Y., Lv, J., Cui, X., He, R., 2018. Diesel exhaust particle promotes tumor lung metastasis via the induction of BLT1-mediated neutrophilic lung inflammation. Cytokine 111, 530–540. https://doi.org/10.1016/j.cyto.2018.05.024

Li, X., Huang, S., Jiao, A., Yang, X., Yun, J., Wang, Y., Xue, X., Chu, Y., Liu, F., Liu, Y., Ren, M., Chen, X., Li, N., Lu, Y., Mao, Z., Tian, L., Xiang, H., 2017. Association between ambient fine particulate matter and preterm birth or term low birth weight: An updated systematic review and meta-analysis. Environ Pollut 227, 596–605. https://doi.org/10.1016/j.envpol.2017.03.055

Lin, H., Zhang, X., Feng, N., Wang, R., Zhang, W., Deng, X., Wang, Y., Yu, X., Ye, X., Li, L., Qian, Y., Yu, H., Qian, B., 2018. LncRNA LCPAT1 Mediates Smoking/ Particulate Matter 2.5-Induced Cell Autophagy and Epithelial-Mesenchymal Transition in Lung Cancer Cells via RCC2. Cell Physiol Biochem 47, 1244–1258. https://doi.org/10.1159/000490220

Lin, L.-Z., Zhan, X.-L., Jin, C.-Y., Liang, J.-H., Jing, J., Dong, G.-H., 2022. The epidemiological evidence linking exposure to ambient particulate matter with neurodevelopmental disorders: A systematic review and meta-analysis. Environ Res 209, 112876. https://doi.org/10.1016/j.envres.2022.112876

Liu, J., Li, S., Fei, X., Nan, X., Shen, Y., Xiu, H., Cormier, S.A., Lu, C., Guo, C., Wang, S., Cai, Z., Wang, P., 2022. Increased alveolar epithelial TRAF6 via autophagy-dependent TRIM37 degradation mediates particulate matter-induced lung metastasis. Autophagy 18, 971–989. https://doi.org/10.1080/15548627.2021.1965421

Liu, Y., Pan, J., Zhang, H., Shi, C., Li, G., Peng, Z., Ma, J., Zhou, Y., Zhang, L., 2019. Short-Term Exposure to Ambient Air Pollution and Asthma Mortality. Am J Respir Crit Care Med 200, 24–32. https://doi.org/10.1164/rccm.201810-1823OC

Lloyd, K.L., Kubes, P., 2006. GPI-linked endothelial CD14 contributes to the detection of LPS. Am J Physiol Heart Circ Physiol 291, H473-481. https://doi.org/10.1152/ajpheart.01234.2005

LoPiccolo, J., Gusev, A., Christiani, D.C., Jänne, P.A., 2024. Lung cancer in patients who have never smoked - an emerging disease. Nat Rev Clin Oncol 21, 121–146. https://doi.org/10.1038/s41571-023-00844-0

Lu, X., Horner, J.W., Paul, E., Shang, X., Troncoso, P., Deng, P., Jiang, S., Chang, Q., Spring, D.J., Sharma, P., Zebala, J.A., Maeda, D.Y., Wang, Y.A., DePinho, R.A., 2017. Effective combinatorial immunotherapy for castration-resistant prostate cancer. Nature 543, 728–732. https://doi.org/10.1038/nature21676

Man, K., Loudon, A., Chawla, A., 2016. Immunity around the clock. Science 354, 999–1003. https://doi.org/10.1126/science.aah4966

Manisalidis, I., Stavropoulou, E., Stavropoulos, A., Bezirtzoglou, E., 2020. Environmental and Health Impacts of Air Pollution: A Review. Front Public Health 8, 14. https://doi.org/10.3389/fpubh.2020.00014

Marchetti, S., Bengalli, R., Floris, P., Colombo, A., Mantecca, P., 2021. Combustion-derived particles from biomass sources differently promote epithelial-to-mesenchymal transition on A549 cells. Arch Toxicol 95, 1379–1390. https://doi.org/10.1007/s00204-021-02983-8

Mariathasan, S., Turley, S.J., Nickles, D., Castiglioni, A., Yuen, K., Wang, Y., Kadel, E.E., Koeppen, H., Astarita, J.L., Cubas, R., Jhunjhunwala, S., Banchereau, R., Yang, Y., Guan, Y., Chalouni, C., Ziai, J., Şenbabaoğlu, Y., Santoro, S., Sheinson, D., Hung, J., Giltnane, J.M., Pierce, A.A., Mesh, K., Lianoglou, S., Riegler, J., Carano, R.A.D., Eriksson, P., Höglund, M., Somarriba, L., Halligan, D.L., van der Heijden, M.S., Loriot, Y., Rosenberg, J.E., Fong, L., Mellman, I., Chen, D.S., Green, M., Derleth, C., Fine, G.D., Hegde, P.S., Bourgon, R., Powles, T., 2018. TGFβ attenuates tumour response to PD-L1 blockade by contributing to exclusion of T cells. Nature 554, 544–548. https://doi.org/10.1038/nature25501

Martemucci, G., Costagliola, C., Mariano, M., D'andrea, L., Napolitano, P., D'Alessandro, A.G., 2022. Free Radical Properties, Source and Targets, Antioxidant Consumption and Health. Oxygen 2, 48–78. https://doi.org/10.3390/oxygen2020006

Marvel, D., Gabrilovich, D.I., 2015. Myeloid-derived suppressor cells in the tumor microenvironment: expect the unexpected. J Clin Invest 125, 3356–3364. https://doi.org/10.1172/JCI80005

McClellan, R.O., Hesterberg, T.W., Wall, J.C., 2012. Evaluation of carcinogenic hazard of diesel engine exhaust needs to consider revolutionary changes in diesel technology. Regulatory Toxicology and Pharmacology 63, 225–258. https://doi.org/10.1016/j.yrtph.2012.04.005

McKenna, E., Mhaonaigh, A.U., Wubben, R., Dwivedi, A., Hurley, T., Kelly, L.A., Stevenson, N.J., Little, M.A., Molloy, E.J., 2021. Neutrophils: Need for Standardized Nomenclature. Front Immunol 12, 602963. https://doi.org/10.3389/fimmu.2021.602963

McLane, L.M., Abdel-Hakeem, M.S., Wherry, E.J., 2019. CD8 T Cell Exhaustion During Chronic Viral Infection and Cancer. Annu Rev Immunol 37, 457–495. https://doi.org/10.1146/annurev-immunol-041015-055318

Merk, R., Heßelbach, K., Osipova, A., Popadić, D., Schmidt-Heck, W., Kim, G.-J., Günther, S., Piñeres, A.G., Merfort, I., Humar, M., 2020. Particulate Matter (PM2.5) from Biomass Combustion Induces an Anti-Oxidative Response and Cancer Drug Resistance in Human Bronchial Epithelial BEAS-2B Cells. Int J Environ Res Public Health 17, 8193. https://doi.org/10.3390/ijerph17218193

Miller, M., McLean, S.G., Shaw, C.A., Duffin, R., Lawal, A.O., Araujo, J.A., Hadoke, P.W.F., Newby, D.E., 2015. Diesel exhaust particles impair vascular function and promote atherosclerosis through generation of oxidative stress. Atherosclerosis 241, e137–e138. https://doi.org/10.1016/j.atherosclerosis.2015.04.477

Miller, M.R., Newby, D.E., 2020. Air pollution and cardiovascular disease: car sick. Cardiovasc Res 116, 279–294. https://doi.org/10.1093/cvr/cvz228

Moldogazieva, N.T., Mokhosoev, I.M., Feldman, N.B., Lutsenko, S.V., 2018. ROS and RNS signalling: adaptive redox switches through oxidative/nitrosative protein modifications. Free Radic Res 52, 507–543. https://doi.org/10.1080/10715762.2018.1457217

Morales-Bárcenas, R., Chirino, Y.I., Sánchez-Pérez, Y., Osornio-Vargas, Á.R., Melendez-Zajgla, J., Rosas, I., García-Cuellar, C.M., 2015. Particulate matter (PM_{10}) induces metalloprotease activity and invasion in airway epithelial cells. Toxicol Lett 237, 167–173. https://doi.org/10.1016/j.toxlet.2015.06.001

Morioka, S., Maueröder, C., Ravichandran, K.S., 2019. Living on the Edge: Efferocytosis at the Interface of Homeostasis and Pathology. Immunity 50, 1149–1162. https://doi.org/10.1016/j.immuni.2019.04.018

Muralidharan, S., Mandrekar, P., 2013. Cellular stress response and innate immune signaling: integrating pathways in host defense and inflammation. J Leukoc Biol 94, 1167–1184. https://doi.org/10.1189/jlb.0313153

Niranjan, R., Mishra, K.P., Tripathi, S.N., Thakur, A.K., 2021. Proliferation of Lung Epithelial Cells Is Regulated by the Mechanisms of Autophagy Upon Exposure of Soots. Front Cell Dev Biol 9, 662597. https://doi.org/10.3389/fcell.2021.662597

Niu, B.-Y., Li, W.-K., Li, J.-S., Hong, Q.-H., Khodahemmati, S., Gao, J.-F., Zhou, Z.-X., 2020. Effects of DNA Damage and Oxidative Stress in Human Bronchial Epithelial Cells Exposed to

PM2.5 from Beijing, China, in Winter. Int J Environ Res Public Health 17, 4874. https://doi.org/10.3390/ijerph17134874

Nordenfelt, P., Tapper, H., 2011. Phagosome dynamics during phagocytosis by neutrophils. J Leukoc Biol 90, 271–284. https://doi.org/10.1189/jlb.0810457

Oberdörster, G., Sharp, Z., Atudorei, V., Elder, A., Gelein, R., Lunts, A., Kreyling, W., Cox, C., 2002. Extrapulmonary translocation of ultrafine carbon particles following whole-body inhalation exposure of rats. J Toxicol Environ Health A 65, 1531–1543. https://doi.org/10.1080/00984100290071658

O'Brien, B.J., Faraoni, E.Y., Strickland, L.N., Ma, Z., Mota, V., Mota, S., Chen, X., Mills, T., Eltzschig, H.K., DelGiorno, K.E., Bailey-Lundberg, J.M., 2023. CD73-generated extracellular adenosine promotes resolution of neutrophil-mediated tissue injury and restrains metaplasia in pancreatitis. FASEB J 37, e22684. https://doi.org/10.1096/fj.202201537R

Ogulur, I., Mitamura, Y., Yazici, D., Pat, Y., Ardicli, S., Li, M., D'Avino, P., Beha, C., Babayev, H., Zhao, B., Zeyneloglu, C., Giannelli Viscardi, O., Ardicli, O., Kiykim, A., Garcia-Sanchez, A., Lopez, J.-F., Shi, L.-L., Yang, M., Schneider, S.R., Skolnick, S., Dhir, R., Radzikowska, U., Kulkarni, A.J., Imam, M.B., Veen, W. van de, Sokolowska, M., Martin-Fontecha, M., Palomares, O., Nadeau, K.C., Akdis, M., Akdis, C.A., 2025. Type 2 immunity in allergic diseases. Cell Mol Immunol 22, 211–242. https://doi.org/10.1038/s41423-025-01261-2

Orillion, A., Hashimoto, A., Damayanti, N., Shen, L., Adelaiye-Ogala, R., Arisa, S., Chintala, S., Ordentlich, P., Kao, C., Elzey, B., Gabrilovich, D., Pili, R., 2017. Entinostat Neutralizes Myeloid-Derived Suppressor Cells and Enhances the Antitumor Effect of PD-1 Inhibition in Murine Models of Lung and Renal Cell Carcinoma. Clin Cancer Res 23, 5187–5201. https://doi.org/10.1158/1078-0432.CCR-17-0741

Pan, J., Xue, Y., Li, S., Wang, L., Mei, J., Ni, D., Jiang, J., Zhang, M., Yi, S., Zhang, R., Ma, Y., Liu, Yang, Liu, Ying, 2022. PM2.5 induces the distant metastasis of lung adenocarcinoma via promoting the stem cell properties of cancer cells. Environ Pollut 296, 118718. https://doi.org/10.1016/j.envpol.2021.118718

Panopoulos, A.D., Watowich, S.S., 2008. Granulocyte colony-stimulating factor: molecular mechanisms of action during steady state and "emergency" hematopoiesis. Cytokine 42, 277–288. https://doi.org/10.1016/j.cyto.2008.03.002

Papayannopoulos, V., Metzler, K.D., Hakkim, A., Zychlinsky, A., 2010. Neutrophil elastase and myeloperoxidase regulate the formation of neutrophil extracellular traps. J Cell Biol 191, 677–691. https://doi.org/10.1083/jcb.201006052

Parida, T., Daka, G., Murapala, D., Kolli, S.K., Malla, R.R., Namuduri, S., 2023. PM2.5: Epigenetic Alteration in Lung Physiology and Lung Cancer Pathogenesis. Crit Rev Oncog 28, 51–58. https://doi.org/10.1615/CritRevOncog.2023049651

Pelosof, L., Ahn, C., Gao, A., Horn, L., Madrigales, A., Cox, J., McGavic, D., Minna, J.D., Gazdar, A.F., Schiller, J., 2017. Proportion of Never-Smoker Non-Small Cell Lung Cancer Patients at Three Diverse Institutions. J Natl Cancer Inst 109, djw295. https://doi.org/10.1093/jnci/djw295

Petri, B., Sanz, M.-J., 2018. Neutrophil chemotaxis. Cell Tissue Res 371, 425–436. https://doi.org/10.1007/s00441-017-2776-8

Phillipson, M., Heit, B., Colarusso, P., Liu, L., Ballantyne, C.M., Kubes, P., 2006. Intraluminal crawling of neutrophils to emigration sites: a molecularly distinct process from adhesion in the recruitment cascade. J Exp Med 203, 2569–2575. https://doi.org/10.1084/jem.20060925

Pieper, C., Pieloch, P., Galla, H.-J., 2013. Pericytes support neutrophil transmigration via interleukin-8 across a porcine co-culture model of the blood-brain barrier. Brain Res 1524, 1–11. https://doi.org/10.1016/j.brainres.2013.05.047

Popovicheva, O., Engling, G., Lin, K.-T., Persiantseva, N., Timofeev, M., Kireeva, E., Völk, P., Hubert, A., Wachtmeister, G., 2015. Diesel/biofuel exhaust particles from modern

internal combustion engines: Microstructure, composition, and hygroscopicity. Fuel 157, 232–239. https://doi.org/10.1016/j.fuel.2015.04.073

Porter, M., Karp, M., Killedar, S., Bauer, S.M., Guo, J., Williams, D., Breysse, P., Georas, S.N., Williams, M.A., 2007. Diesel-enriched particulate matter functionally activates human dendritic cells. Am J Respir Cell Mol Biol 37, 706–719. https://doi.org/10.1165/rcmb.2007-0199OC

Qi, X., Yu, Y., Sun, R., Huang, J., Liu, L., Yang, Y., Rui, T., Sun, B., 2021. Identification and characterization of neutrophil heterogeneity in sepsis. Crit Care 25, 50. https://doi.org/10.1186/s13054-021-03481-0

Qin, P., Luo, X., Zeng, Y., Zhang, Y., Li, Y., Wu, Y., Han, M., Qie, R., Wu, X., Liu, D., Huang, S., Zhao, Y., Feng, Y., Yang, X., Hu, F., Sun, X., Hu, D., Zhang, M., 2021. Long-term association of ambient air pollution and hypertension in adults and in children: A systematic review and meta-analysis. Sci Total Environ 796, 148620. https://doi.org/10.1016/j.scitotenv.2021.148620

Quezada-Maldonado, E.M., Chirino, Y.I., Gonsebatt, M.E., Morales-Bárcenas, R., Sánchez-Pérez, Y., García-Cuellar, C.M., 2022. Nucleotide Excision Repair Pathway Activity Is Inhibited by Airborne Particulate Matter (PM10) through XPA Deregulation in Lung Epithelial Cells. Int J Mol Sci 23, 2224. https://doi.org/10.3390/ijms23042224

Raaschou-Nielsen, O., Andersen, Z.J., Beelen, R., Samoli, E., Stafoggia, M., Weinmayr, G., Hoffmann, B., Fischer, P., Nieuwenhuijsen, M.J., Brunekreef, B., Xun, W.W., Katsouyanni, K., Dimakopoulou, K., Sommar, J., Forsberg, B., Modig, L., Oudin, A., Oftedal, B., Schwarze, P.E., Nafstad, P., De Faire, U., Pedersen, N.L., Ostenson, C.-G., Fratiglioni, L., Penell, J., Korek, M., Pershagen, G., Eriksen, K.T., Sørensen, M., Tjønneland, A., Ellermann, T., Eeftens, M., Peeters, P.H., Meliefste, K., Wang, M., Bueno-de-Mesquita, B., Key, T.J., de Hoogh, K., Concin, H., Nagel, G., Vilier, A., Grioni, S., Krogh, V., Tsai, M.-Y., Ricceri, F., Sacerdote, C., Galassi, C., Migliore, E., Ranzi, A., Cesaroni, G., Badaloni, C., Forastiere, F., Tamayo, I., Amiano, P., Dorronsoro, M., Trichopoulou, A., Bamia, C., Vineis, P., Hoek, G., 2013. Air pollution and lung cancer incidence in 17 European cohorts: prospective analyses from the European Study of Cohorts for Air Pollution Effects (ESCAPE). Lancet Oncol 14, 813–822. https://doi.org/10.1016/S1470-2045(13)70279-1

Raaschou-Nielsen, O., Antonsen, S., Agerbo, E., Hvidtfeldt, U.A., Geels, C., Frohn, L.M., Christensen, J.H., Sigsgaard, T., Brandt, J., Pedersen, C.B., 2023. PM2.5 air pollution components and mortality in Denmark. Environment International 171, 107685. https://doi.org/10.1016/j.envint.2022.107685

Ramanathan, M., London, N.R., Tharakan, A., Surya, N., Sussan, T.E., Rao, X., Lin, S.Y., Toskala, E., Rajagopalan, S., Biswal, S., 2017. Airborne Particulate Matter Induces Nonallergic Eosinophilic Sinonasal Inflammation in Mice. Am J Respir Cell Mol Biol 57, 59–65. https://doi.org/10.1165/rcmb.2016-0351OC

Renzi, M., Stafoggia, M., Michelozzi, P., Davoli, M., Forastiere, F., Solimini, A.G., 2020. Short-term exposure to PM2.5 and risk of venous thromboembolism: A case-crossover study. Thrombosis Research 190, 52–57. https://doi.org/10.1016/j.thromres.2020.03.008

Reyes-Zárate, E., Sánchez-Pérez, Y., Gutiérrez-Ruiz, M.C., Chirino, Y.I., Osornio-Vargas, Á.R., Morales-Bárcenas, R., Souza-Arroyo, V., García-Cuellar, C.M., 2016. Atmospheric particulate matter (PM10) exposure-induced cell cycle arrest and apoptosis evasion through STAT3 activation via PKCζ and Src kinases in lung cells. Environ Pollut 214, 646–656. https://doi.org/10.1016/j.envpol.2016.04.072

Robertson, S., Miller, M.R., 2018. Ambient air pollution and thrombosis. Part Fibre Toxicol 15, 1. https://doi.org/10.1186/s12989-017-0237-x

Rocks, N., Vanwinge, C., Radermecker, C., Blacher, S., Gilles, C., Marée, R., Gillard, A., Evrard, B., Pequeux, C., Marichal, T., Noel, A., Cataldo, D., 2019. Ozone-primed neutrophils promote early steps of tumour cell metastasis to lungs by enhancing their NET production. Thorax 74, 768–779. https://doi.org/10.1136/thoraxjnl-2018-211990

Rodriguez, P.C., Ernstoff, M.S., Hernandez, C., Atkins, M., Zabaleta, J., Sierra, R., Ochoa, A.C., 2009. Arginase I-producing myeloid-derived suppressor cells in renal cell carcinoma are a subpopulation of activated granulocytes. Cancer Res 69, 1553–1560. https://doi.org/10.1158/0008-5472.CAN-08-1921

Ronchetti, L., Boubaker, N.S., Barba, M., Vici, P., Gurtner, A., Piaggio, G., 2021. Neutrophil extracellular traps in cancer: not only catching microbes. J Exp Clin Cancer Res 40, 231. https://doi.org/10.1186/s13046-021-02036-z

Rosales, C., 2018. Neutrophil: A Cell with Many Roles in Inflammation or Several Cell Types? Front Physiol 9, 113. https://doi.org/10.3389/fphys.2018.00113

Roussel, M., Le, K.-S., Granier, C., Llamas Gutierrez, F., Foucher, E., Le Gallou, S., Pangault, C., Xerri, L., Launay, V., Lamy, T., Tartour, E., Olive, D., Fest, T., 2021. Functional characterization of PD1+TIM3+ tumor-infiltrating T cells in DLBCL and effects of PD1 or TIM3 blockade. Blood Advances 5, 1816–1829. https://doi.org/10.1182/bloodadvances.2020003080

Rychlik, K.A., Secrest, J.R., Lau, C., Pulczinski, J., Zamora, M.L., Leal, J., Langley, R., Myatt, L.G., Raju, M., Chang, R.C.-A., Li, Y., Golding, M.C., Rodrigues-Hoffmann, A., Molina, M.J., Zhang, R., Johnson, N.M., 2019. In utero ultrafine particulate matter exposure causes offspring pulmonary immunosuppression. Proc Natl Acad Sci U S A 116, 3443–3448. https://doi.org/10.1073/pnas.1816103116

Ryou, H.G., Heo, J., Kim, S.-Y., 2018. Source apportionment of PM10 and PM2.5 air pollution, and possible impacts of study characteristics in South Korea. Environ Pollut 240, 963–972. https://doi.org/10.1016/j.envpol.2018.03.066

Ryzhov, S., Novitskiy, S.V., Goldstein, A.E., Biktasova, A., Blackburn, M.R., Biaggioni, I., Dikov, M.M., Feoktistov, I., 2011. Adenosinergic regulation of the expansion and immunosuppressive activity of CD11b+Gr1+ cells. J Immunol 187, 6120–6129. https://doi.org/10.4049/jimmunol.1101225

Salvi, S.S., Nordenhall, C., Blomberg, A., Rudell, B., Pourazar, J., Kelly, F.J., Wilson, S., Sandström, T., Holgate, S.T., Frew, A.J., 2000. Acute exposure to diesel exhaust increases IL-8 and GRO-alpha production in healthy human airways. Am J Respir Crit Care Med 161, 550–557. https://doi.org/10.1164/ajrccm.161.2.9905052

Santibáñez-Andrade, M., Quezada-Maldonado, E.M., Rivera-Pineda, A., Chirino, Y.I., García-Cuellar, C.M., Sánchez-Pérez, Y., 2023. The Road to Malignant Cell Transformation after Particulate Matter Exposure: From Oxidative Stress to Genotoxicity. Int J Mol Sci 24, 1782. https://doi.org/10.3390/ijms24021782

Schabath, M.B., Cote, M.L., 2019. Cancer Progress and Priorities: Lung Cancer. Cancer Epidemiol Biomarkers Prev 28, 1563–1579. https://doi.org/10.1158/1055-9965.EPI-19-0221

Schoen, J., Euler, M., Schauer, C., Schett, G., Herrmann, M., Knopf, J., Yaykasli, K.O., 2022. Neutrophils' Extracellular Trap Mechanisms: From Physiology to Pathology. Int J Mol Sci 23, 12855. https://doi.org/10.3390/ijms232112855

Shi, J., Zhao, Y., Wang, Y., Gao, W., Ding, J., Li, P., Hu, L., Shao, F., 2014. Inflammatory caspases are innate immune receptors for intracellular LPS. Nature 514, 187–192. https://doi.org/10.1038/nature13683

Shoenfelt, J., Mitkus, R.J., Zeisler, R., Spatz, R.O., Powell, J., Fenton, M.J., Squibb, K.A., Medvedev, A.E., 2009. Involvement of TLR2 and TLR4 in inflammatory immune responses induced by fine and coarse ambient air particulate matter. J Leukoc Biol 86, 303–312. https://doi.org/10.1189/jlb.1008587

Siret, C., Collignon, A., Silvy, F., Robert, S., Cheyrol, T., André, P., Rigot, V., Iovanna, J., van de Pavert, S., Lombardo, D., Mas, E., Martirosyan, A., 2019. Deciphering the Crosstalk Between Myeloid-Derived Suppressor Cells and Regulatory T Cells in Pancreatic Ductal Adenocarcinoma. Front Immunol 10, 3070. https://doi.org/10.3389/fimmu.2019.03070

Soehnlein, O., Lindbom, L., 2010. Phagocyte partnership during the onset and resolution of inflammation. Nat Rev Immunol 10, 427–439. https://doi.org/10.1038/nri2779

Soehnlein, O., Steffens, S., Hidalgo, A., Weber, C., 2017. Neutrophils as protagonists and targets in chronic inflammation. Nat Rev Immunol 17, 248–261. https://doi.org/10.1038/nri.2017.10

Steiner, S., Bisig, C., Petri-Fink, A., Rothen-Rutishauser, B., 2016. Diesel exhaust: current knowledge of adverse effects and underlying cellular mechanisms. Arch Toxicol 90, 1541–1553. https://doi.org/10.1007/s00204-016-1736-5

Stockwell, B.R., Friedmann Angeli, J.P., Bayir, H., Bush, A.I., Conrad, M., Dixon, S.J., Fulda, S., Gascón, S., Hatzios, S.K., Kagan, V.E., Noel, K., Jiang, X., Linkermann, A., Murphy, M.E., Overholtzer, M., Oyagi, A., Pagnussat, G.C., Park, J., Ran, Q., Rosenfeld, C.S., Salnikow, K., Tang, D., Torti, F.M., Torti, S.V., Toyokuni, S., Woerpel, K.A., Zhang, D.D., 2017. Ferroptosis: A Regulated Cell Death Nexus Linking Metabolism, Redox Biology, and Disease. Cell 171, 273–285. https://doi.org/10.1016/j.cell.2017.09.021

Summers, C., Rankin, S.M., Condliffe, A.M., Singh, N., Peters, A.M., Chilvers, E.R., 2010. Neutrophil kinetics in health and disease. Trends Immunol 31, 318–324. https://doi.org/10.1016/j.it.2010.05.006

Sun, H., Li, S., Wang, Q., Luo, C., Zhong, L., Wan, G., Li, Z., Zhao, G., Bu, X., Zeng, M., Feng, G., 2024. Formyl peptide enhances cancer immunotherapy by activating antitumoral neutrophils, and T cells. Biomed Pharmacother 175, 116670. https://doi.org/10.1016/j.biopha.2024.116670

Sutherland, K.D., Song, J.-Y., Kwon, M.C., Proost, N., Zevenhoven, J., Berns, A., 2014. Multiple cells-of-origin of mutant K-Ras-induced mouse lung adenocarcinoma. Proc Natl Acad Sci U S A 111, 4952–4957. https://doi.org/10.1073/pnas.1319963111

Tan, C., Lu, S., Wang, Y., Zhu, Y., Shi, T., Lin, M., Deng, Z., Wang, Z., Song, N., Li, S., Yang, P., Yang, L., Liu, Y., Chen, Z., Xu, K., 2017. Long-term exposure to high air pollution induces cumulative DNA damages in traffic policemen. Sci Total Environ 593–594, 330–336. https://doi.org/10.1016/j.scitotenv.2017.03.179

Taş, İ., Zhou, R., Park, S.-Y., Yang, Y., Gamage, C.D.B., Son, Y.-J., Paik, M.-J., Kim, H., 2019. Inflammatory and tumorigenic effects of environmental pollutants found in particulate matter on lung epithelial cells. Toxicol In Vitro 59, 300–311. https://doi.org/10.1016/j.tiv.2019.05.022

Tavazoie, M.F., Pollack, I., Tanqueco, R., Ostendorf, B.N., Reis, B.S., Gonsalves, F.C., Kurth, I., Andreu-Agullo, C., Derbyshire, M.L., Posada, J., Takeda, S., Tafreshian, K.N., Rowinsky, E., Szarek, M., Waltzman, R.J., Mcmillan, E.A., Zhao, C., Mita, M., Mita, A., Chmielowski, B., Postow, M.A., Ribas, A., Mucida, D., Tavazoie, S.F., 2018. LXR/ApoE Activation Restricts Innate Immune Suppression in Cancer. Cell 172, 825-840.e18. https://doi.org/10.1016/j.cell.2017.12.026

Teijeira, Á., Garasa, S., Gato, M., Alfaro, C., Migueliz, I., Cirella, A., de Andrea, C., Ochoa, M.C., Otano, I., Etxeberria, I., Andueza, M.P., Nieto, C.P., Resano, L., Azpilikueta, A., Allegretti, M., de Pizzol, M., Ponz-Sarvisé, M., Rouzaut, A., Sanmamed, M.F., Schalper, K., Carleton, M., Mellado, M., Rodriguez-Ruiz, M.E., Berraondo, P., Perez-Gracia, J.L., Melero, I., 2020. CXCR1 and CXCR2 Chemokine Receptor Agonists Produced by Tumors Induce Neutrophil Extracellular Traps that Interfere with Immune Cytotoxicity. Immunity 52, 856-871.e8. https://doi.org/10.1016/j.immuni.2020.03.001

Thandra, K.C., Barsouk, Adam, Saginala, K., Aluru, J.S., Barsouk, Alexander, 2021. Epidemiology of lung cancer. Contemp Oncol (Pozn) 25, 45–52. https://doi.org/10.5114/wo.2021.103829

Thangavel, P., Park, D., Lee, Y.-C., 2022. Recent Insights into Particulate Matter (PM2.5)-Mediated Toxicity in Humans: An Overview. International Journal of Environmental Research and Public Health 19, 7511. https://doi.org/10.3390/ijerph19127511

Thieblemont, N., Witko-Sarsat, V., Ariel, A., 2018. Regulation of macrophage activation by proteins expressed on apoptotic neutrophils: Subversion towards autoimmunity by proteinase 3. Eur J Clin Invest 48 Suppl 2, e12990. https://doi.org/10.1111/eci.12990

Umansky, V., Blattner, C., Gebhardt, C., Utikal, J., 2016. The Role of Myeloid-Derived Suppressor Cells (MDSC) in Cancer Progression. Vaccines (Basel) 4, 36. https://doi.org/10.3390/vaccines4040036

Umansky, V., Sevko, A., 2013. Tumor microenvironment and myeloid-derived suppressor cells. Cancer Microenviron 6, 169–177. https://doi.org/10.1007/s12307-012-0126-7

Ünal, E., Özdemir, A., Khanjani, N., Dastoorpoor, M., Özkaya, G., 2022. Air pollution and pediatric respiratory hospital admissions in Bursa, Turkey: A time series study. Int J Environ Health Res 32, 2767–2780. https://doi.org/10.1080/09603123.2021.1991282

Ural, B.B., Caron, D.P., Dogra, P., Wells, S.B., Szabo, P.A., Granot, T., Senda, T., Poon, M.M.L., Lam, N., Thapa, P., Lee, Y.S., Kubota, M., Matsumoto, R., Farber, D.L., 2022. Inhaled particulate accumulation with age impairs immune function and architecture in human lung lymph nodes. Nat Med 28, 2622–2632. https://doi.org/10.1038/s41591-022-02073-x

van der Vliet, A., O'Neill, C.A., Cross, C.E., Koostra, J.M., Volz, W.G., Halliwell, B., Louie, S., 1999. Determination of low-molecular-mass antioxidant concentrations in human respiratory tract lining fluids. Am J Physiol 276, L289-296. https://doi.org/10.1152/ajplung.1999.276.2.L289

van Meerbeeck, J.P., Franck, C., 2021. Lung cancer screening in Europe: where are we in 2021? Transl Lung Cancer Res 10, 2407–2417. https://doi.org/10.21037/tlcr-20-890

Van Opdenbosch, N., Lamkanfi, M., 2019. Caspases in Cell Death, Inflammation, and Disease. Immunity 50, 1352–1364. https://doi.org/10.1016/j.immuni.2019.05.020

Veglia, F., Hashimoto, A., Dweep, H., Sanseviero, E., De Leo, A., Tcyganov, E., Kossenkov, A., Mulligan, C., Nam, B., Masters, G., Patel, J., Bhargava, V., Wilkinson, P., Smirnov, D., Sepulveda, M.A., Singhal, S., Eruslanov, E.B., Cristescu, R., Loboda, A., Nefedova, Y., Gabrilovich, D.I., 2021. Analysis of classical neutrophils and polymorphonuclear myeloid-derived suppressor cells in cancer patients and tumor-bearing mice. Journal of Experimental Medicine 218, e20201803. https://doi.org/10.1084/jem.20201803

Veglia, F., Perego, M., Gabrilovich, D., 2018. Myeloid-derived suppressor cells coming of age. Nat Immunol 19, 108–119. https://doi.org/10.1038/s41590-017-0022-x

Vijayan, D., Young, A., Teng, M.W.L., Smyth, M.J., 2017. Targeting immunosuppressive adenosine in cancer. Nat Rev Cancer 17, 765. https://doi.org/10.1038/nrc.2017.110

Vilas-Boas, V., Chatterjee, N., Carvalho, A., Alfaro-Moreno, E., 2024. Particulate matter-induced oxidative stress – Mechanistic insights and antioxidant approaches reported in in vitro studies. Environmental Toxicology and Pharmacology 110, 104529. https://doi.org/10.1016/j.etap.2024.104529

Vincent, J., Mignot, G., Chalmin, F., Ladoire, S., Bruchard, M., Chevriaux, A., Martin, F., Apetoh, L., Rébé, C., Ghiringhelli, F., 2010. 5-Fluorouracil selectively kills tumor-associated myeloid-derived suppressor cells resulting in enhanced T cell-dependent antitumor immunity. Cancer Res 70, 3052–3061. https://doi.org/10.1158/0008-5472.CAN-09-3690

Wang, G., Lu, X., Dey, P., Deng, P., Wu, C.C., Jiang, S., Fang, Z., Zhao, K., Konaparthi, R., Hua, S., Zhang, J., Li-Ning-Tapia, E.M., Kapoor, A., Wu, C.-J., Patel, N.B., Guo, Z., Ramamoorthy, V., Tieu, T.N., Heffernan, T., Zhao, D., Shang, X., Khadka, S., Hou, P., Hu, B., Jin, E.-J., Yao, W., Pan, X., Ding, Z., Shi, Y., Li, L., Chang, Q., Troncoso, P., Logothetis, C.J., McArthur, M.J., Chin, L., Wang, Y.A., DePinho, R.A., 2016. Targeting YAP-Dependent MDSC Infiltration Impairs Tumor Progression. Cancer Discov 6, 80–95. https://doi.org/10.1158/2159-8290.CD-15-0224

Wang, J., Huang, J., Wang, L., Chen, C., Yang, D., Jin, M., Bai, C., Song, Y., 2017. Urban particulate matter triggers lung inflammation via the ROSMAPK- NF-κB signaling pathway. Journal of Thoracic Disease 9. https://doi.org/10.21037/jtd.2017.09.135

Wang, L., Luo, D., Liu, X., Zhu, J., Wang, F., Li, B., Li, L., 2021. Effects of PM2.5 exposure on reproductive system and its mechanisms. Chemosphere 264, 128436. https://doi.org/10.1016/j.chemosphere.2020.128436

Wang, M., Kim, R.Y., Kohonen-Corish, M.R.J., Chen, H., Donovan, C., Oliver, B.G., 2025. Particulate matter air pollution as a cause of lung cancer: epidemiological and experimental evidence. Br J Cancer 1–11. https://doi.org/10.1038/s41416-025-02999-2

Wang, X., Ricciuti, B., Nguyen, T., Li, X., Rabin, M.S., Awad, M.M., Lin, X., Johnson, B.E., Christiani, D.C., 2021. Association between Smoking History and Tumor Mutation Burden in Advanced Non–Small Cell Lung Cancer. Cancer Research 81, 2566–2573. https://doi.org/10.1158/0008-5472.CAN-20-3991

Wei, H., Liang, F., Cheng, W., Zhou, R., Wu, X., Feng, Y., Wang, Y., 2017. The mechanisms for lung cancer risk of PM2.5 : Induction of epithelial-mesenchymal transition and cancer stem cell properties in human non-small cell lung cancer cells. Environ Toxicol 32, 2341–2351. https://doi.org/10.1002/tox.22437

WHO, 2025. Air pollution [WWW Document]. Air pollution. URL https://www.who.int/health-topics/air-pollution (accessed 8.8.25).

WHO, 2021. Thoracic tumours, 5th ed, World health organization classification of tumours. International agency for research on cancer, Lyon.

Xia, C., Yin, S., To, K.K.W., Fu, L., 2023. CD39/CD73/A2AR pathway and cancer immunotherapy. Molecular Cancer 22, 44. https://doi.org/10.1186/s12943-023-01733-x

Xia, T., Zhu, Y., Mu, L., Zhang, Z.-F., Liu, S., 2016. Pulmonary diseases induced by ambient ultrafine and engineered nanoparticles in twenty-first century. Natl Sci Rev 3, 416–429. https://doi.org/10.1093/nsr/nww064

Xu, H., Jiao, X., Wu, Y., Li, S., Cao, L., Dong, L., 2019. Exosomes derived from PM2.5-treated lung cancer cells promote the growth of lung cancer via the Wnt3a/β-catenin pathway. Oncol Rep 41, 1180–1188. https://doi.org/10.3892/or.2018.6862

Xue, Q., Yan, Y., Zhang, R., Xiong, H., 2018. Regulation of iNOS on Immune Cells and Its Role in Diseases. Int J Mol Sci 19, 3805. https://doi.org/10.3390/ijms19123805

Yang, B., Chen, D., Zhao, H., Xiao, C., 2016. The effects for PM2.5 exposure on non-small-cell lung cancer induced motility and proliferation. Springerplus 5, 2059. https://doi.org/10.1186/s40064-016-3734-8

Yang, B., Xiao, C., 2018. PM2.5 exposure significantly improves the exacerbation of A549 tumor-bearing CB17-SCID mice. Environ Toxicol Pharmacol 60, 169–175. https://doi.org/10.1016/j.etap.2018.04.025

Yang, D., Ma, M., Zhou, W., Yang, B., Xiao, C., 2017. Inhibition of miR-32 activity promoted EMT induced by PM2.5 exposure through the modulation of the Smad1-mediated signaling pathways in lung cancer cells. Chemosphere 184, 289–298. https://doi.org/10.1016/j.chemosphere.2017.05.152

Yang, Y.-S., Pei, Y.-H., Gu, Y.-Y., Zhu, J.-F., Yu, P., Chen, X.-H., 2022. Association between short-term exposure to ambient air pollution and heart failure: An updated systematic review and meta-analysis of more than 7 million participants. Front Public Health 10, 948765. https://doi.org/10.3389/fpubh.2022.948765

Yipp, B.G., Kubes, P., 2013. NETosis: how vital is it? Blood 122, 2784–2794. https://doi.org/10.1182/blood-2013-04-457671

Zarbock, A., Ley, K., McEver, R.P., Hidalgo, A., 2011. Leukocyte ligands for endothelial selectins: specialized glycoconjugates that mediate rolling and signaling under flow. Blood 118, 6743–6751. https://doi.org/10.1182/blood-2011-07-343566

Zea, A.H., Rodriguez, P.C., Culotta, K.S., Hernandez, C.P., DeSalvo, J., Ochoa, J.B., Park, H.-J., Zabaleta, J., Ochoa, A.C., 2004. L-Arginine modulates CD3zeta expression and T cell function in activated human T lymphocytes. Cell Immunol 232, 21–31. https://doi.org/10.1016/j.cellimm.2005.01.004

Zelenay, S., van der Veen, A.G., Böttcher, J.P., Snelgrove, K.J., Rogers, N., Acton, S.E., Chakravarty, P., Girotti, M.R., Marais, R., Quezada, S.A., Sahai, E., Reis e Sousa, C., 2015. Cyclooxygenase-Dependent Tumor Growth through Evasion of Immunity. Cell 162, 1257–1270. https://doi.org/10.1016/j.cell.2015.08.015

Zhang, F., Xia, Y., Su, J., Quan, F., Zhou, H., Li, Q., Feng, Q., Lin, C., Wang, D., Jiang, Z., 2024. Neutrophil diversity and function in health and disease. Signal Transduct Target Ther 9, 343. https://doi.org/10.1038/s41392-024-02049-y

Zhang, H., Wang, Y., Onuma, A., He, J., Wang, H., Xia, Y., Lal, R., Cheng, X., Kasumova, G., Hu, Z., Deng, M., Beane, J.D., Kim, A.C., Huang, H., Tsung, A., 2021. Neutrophils Extracellular Traps Inhibition Improves PD-1 Blockade Immunotherapy in Colorectal Cancer. Cancers (Basel) 13, 5333. https://doi.org/10.3390/cancers13215333

Zhao, Y., Rahmy, S., Liu, Z., Zhang, C., Lu, X., 2020. Rational targeting of immunosuppressive neutrophils in cancer. Pharmacol Ther 212, 107556. https://doi.org/10.1016/j.pharmthera.2020.107556

Zheng, L., Dong, H., Zhao, W., Zhang, X., Duan, X., Zhang, H., Liu, S., Sui, G., 2019. An Air-Liquid Interface Organ-Level Lung Microfluidics Platform for Analysis on Molecular Mechanisms of Cytotoxicity Induced by Cancer-Causing Fine Particles. ACS Sens 4, 907–917. https://doi.org/10.1021/acssensors.8b01672

Zheng, W., Zhu, Y., Chen, X., Zhao, J., 2021. CD73 expression in myeloid-derived suppressor cells is correlated with clinical stages in head and neck squamous cell carcinomas. Ann Transl Med 9, 1148. https://doi.org/10.21037/atm-21-2589

Zheng, Y., Sanchez-Guerra, M., Zhang, Z., Joyce, B.T., Zhong, J., Kresovich, J.K., Liu, L., Zhang, W., Gao, T., Chang, D., Osorio-Yanez, C., Carmona, J.J., Wang, S., McCracken, J.P., Zhang, X., Chervona, Y., Díaz, A., Bertazzi, P.A., Koutrakis, P., Kang, C.-M., Schwartz, J., Baccarelli, A.A., Hou, L., 2017. Traffic-derived particulate matter exposure and histone H3 modification: A repeated measures study. Environ Res 153, 112–119. https://doi.org/10.1016/j.envres.2016.11.015

Zhou, J., Nefedova, Y., Lei, A., Gabrilovich, D., 2018. Neutrophils and PMN-MDSC: Their biological role and interaction with stromal cells. Semin Immunol 35, 19–28. https://doi.org/10.1016/j.smim.2017.12.004

Zhou, W., Tian, D., He, J., Wang, Y., Zhang, Lijun, Cui, L., Jia, L., Zhang, Li, Li, L., Shu, Y., Yu, S., Zhao, J., Yuan, X., Peng, S., 2016. Repeated PM2.5 exposure inhibits BEAS-2B cell P53 expression through ROS-Akt-DNMT3B pathway-mediated promoter hypermethylation. Oncotarget 7, 20691–20703. https://doi.org/10.18632/oncotarget.7842

Zhu, Y.P., Padgett, L., Dinh, H.Q., Marcovecchio, P., Blatchley, A., Wu, R., Ehinger, E., Kim, C., Mikulski, Z., Seumois, G., Madrigal, A., Vijayanand, P., Hedrick, C.C., 2018. Identification of an Early Unipotent Neutrophil Progenitor with Pro-tumoral Activity in Mouse and Human Bone Marrow. Cell Rep 24, 2329-2341.e8. https://doi.org/10.1016/j.celrep.2018.07.097

Zilionis, R., Engblom, C., Pfirschke, C., Savova, V., Zemmour, D., Saatcioglu, H.D., Krishnan, I., Maroni, G., Meyerovitz, C.V., Kerwin, C.M., Choi, S., Richards, W.G., De Rienzo, A., Tenen, D.G., Bueno, R., Levantini, E., Pittet, M.J., Klein, A.M., 2019. Single-Cell Transcriptomics of Human and Mouse Lung Cancers Reveals Conserved Myeloid Populations across Individuals and Species. Immunity 50, 1317-1334.e10. https://doi.org/10.1016/j.immuni.2019.03.009

ANNEXES

ANNEXES

Annex 1

National Institute of Standards & Technology

Certificate of Analysis

Standard Reference Material® 1650b

Diesel Particulate Matter

This Standard Reference Material (SRM) is intended for use in evaluating analytical methods for the determination of selected polycyclic aromatic hydrocarbons (PAHs) and nitro-substituted PAHs (nitro-PAHs) in diesel particulate matter and similar matrices. In addition to certified and non-certified values for selected PAHs and nitro-PAHs, non-certified values are provided for percent extractable mass, particle-size distribution, and specific surface area; supplemental information on mutagenic activity is also provided. All of the chemical constituents for which certified and non-certified values are provided are naturally present in the diesel particulate material. SRM 1650b was prepared from the same bulk diesel particulate material that was issued in 1985 as SRM 1650 [1] and in 2000 as SRM 1650a [2–4]. A unit of SRM 1650b consists of a bottle containing approximately 200 mg of diesel particulate material.

Certified Mass Fraction Values: Certified values are provided for PAHs in Table 1. The certified values for the PAHs are based on the agreement of results obtained at NIST from two or more independent analytical methods [5]. A NIST certified value is a value for which NIST has the highest confidence in its accuracy, in that all known or suspected sources of bias have been investigated or taken into account [5]. Metrological traceability is to the International System of Units (SI) unit of mass expressed as derived unit of mass fraction.

Non-Certified Values: Non-certified mass fraction values are provided for nitro-PAHs in Table 2, additional PAHs in Table 3, for PAHs of molecular mass 302 in Table 4, and for additional nitro-PAHs for specific method conditions in Table 5. In Tables 3 and 5, the non-certified mass fraction values for some PAHs and nitro-PAHs, respectively, are listed more than once depending on the extraction conditions that are used (see "Preparation and Analysis"). A non-certified value for percent extractable mass is provided in Table 6. Non-certified values for specific surface area, as determined by N_2 gas adsorption, and particle-size characteristics are provided in Table 7. Non-certified values are the best estimate of the true value; however, the values do not meet the NIST criteria for certification and are provided with associated uncertainties that may reflect only measurement precision, may not include all sources of uncertainty, or may reflect a lack of sufficient statistical agreement among multiple analytical methods [5]. Non-certified values are traceable to the measurement processes and standards used by NIST.

Period of Validity: SRM 1650b is valid, with the measurement uncertainty specified, until **01 May 2031**, provided the SRM is handled and stored in accordance with instructions given in this certificate (see "Instructions for Use"). The value assignments are nullified if the SRM is damaged, contaminated, or otherwise modified.

Maintenance of SRM Certification: NIST will monitor this SRM over the period of its validity. If substantive technical changes occur that affect the certification before the expiration of this certificate, NIST will notify the purchaser. Registration (see attached sheet or register online) will facilitate notification.

Coordination of the technical measurements leading to the certification of SRM 1650b was under the leadership of S.A. Wise of the NIST Chemical Sciences Division and M.M. Schantz, formerly of NIST.

Statistical consultation was provided by N.A. Heckert of the NIST Statistical Engineering Division and S.D. Leigh, formerly of NIST.

Analytical measurements for the certification of SRM 1650b were performed by D.L. Poster of the NIST Material Measurement Laboratory Office and H.A. Bamford, B.J. Porter, M.M. Schantz, P. Schubert, and R. Zeisler, formerly of NIST. Analytical measurements for PAHs and nitro-PAHs were also provided by C. Chiu of the Environmental Technology Centre, Environment Canada (Ottawa, Canada). Specific surface area and porosity measurements and confirmation measurements for 1-nitropyrene were provided by P. Scheepers of the Department of Epidemiology at Katholieke Universiteit Nijmegen (Nijmegen, The Netherlands).

Support aspects involved in the issuance of this SRM were coordinated through the NIST Office of Reference Materials.

INSTRUCTIONS FOR HANDLING, STORAGE, AND USE

Handling: This material is a naturally occurring diesel particulate material and contains constituents of known and unknown toxicities and mutagenicities; therefore, extreme caution and care should be exercised during its handling and use.

Storage: Store SRM 1650b in its original bottle at approximately 25 °C (room temperature) and keep away from direct sunlight.

Use: Prior to removal of subsamples for analysis, the contents of the bottle should be mixed thoroughly. The recommended minimum sample size is 50 mg, although smaller sample sizes have been evaluated. The evaluation of the homogeneity of SRM 1650b, at small sample sizes for PAHs, is described in "Homogeneity Assessment for PAHs" and in further detail in reference 6.

PREPARATION AND ANALYSIS[(1)]

Sample Collection and Preparation: The diesel particulate material used for the preparation of SRM 1650b was the same bulk diesel particulate material used for the preparation of SRM 1650 and SRM 1650a. This material was obtained through the Coordinating Research Council, Inc. (Atlanta, GA). The particulate material was collected from the heat exchangers of a dilution tube facility following 200 engine hours of particulate accumulation. Several direct injection four-cycle diesel engines, operating under a variety of conditions were used to generate this particulate material. Therefore, while the sample is not intended to be representative of any particular diesel engine operating under any specific conditions, it should be representative of heavy-duty diesel engine particulate emissions.

Relationship Among SRM 1650, SRM 1650a, and SRM 1650b: SRM 1650b was prepared from the same bulk diesel particulate matter used for preparation of SRM 1650; the bulk material had been stored at –20 °C since the preparation of SRM 1650 in 1984. SRM 1650b was analyzed as described below to confirm that the bulk diesel particulate matter was the same as the material used for SRM 1650 and SRM 1650a. The analyses of SRM 1650b confirmed that the material was the same and that the mass fractions of PAHs and nitro-PAHs had not significantly changed. The results of these analyses were then used to assign new certified and non-certified mass fractions and to increase again the number of PAHs and nitro-PAHs with values assigned. However, measurements for some properties (e.g., percent extractable mass and pore size) and some PAHs (selected methyl- and dimethyl-substituted PAHs) were not repeated on SRM 1650b; instead it was determined that the information values from SRM 1650a are applicable to SRM 1650b.

Polycyclic Aromatic Hydrocarbons (PAHs)

The general approach used for the value assignment of the PAHs in SRM 1650b consisted of pressurized fluid extraction (PFE) using dichloromethane (DCM), toluene, or a toluene/methanol mixture at two extraction temperatures (100 °C and 200 °C), cleanup of the extracts using solid phase extraction (SPE), and analysis by using gas chromatography/mass spectrometry (GC/MS) on three stationary phases of different selectivity [i.e., a relatively nonpolar phase, a 50 % (mole fraction) phenyl-substituted methylpolysiloxane phase, and a dimethyl 50 % (mole fraction) polysiloxane liquid crystalline stationary phase]. PFE was the only extraction method used at NIST; previous studies indicated that conventional Soxhlet extraction was not as effective as PFE in the removal of higher relative molecular mass PAHs [7]. Results were also obtained from Environment Canada as described in "GC/MS
(Environment Canada)".

[(1)]Certain commercial equipment, instruments or materials are identified in this certificate to adequately specify the experimental procedure. Such identification does not imply recommendation or endorsement by the National Institute of Standards and Technology, nor does it imply that the materials or equipment identified are necessarily the best available for the purpose.

Multiple sets of GC/MS results performed by the NIST Chemical Sciences Division, designated as GC/MS (Ia and Ib), GC/MS (IIa and IIb), GC/MS (IIIa and IIIb), GC/MS (IVa and IVb), GC/MS (Va and Vb),
GC/MS (VIa and VIb), GC/MS (VII), GC/MS (VIII) and GC/MS (Environment Canada), were obtained using three columns with different selectivities for the separation of PAHs. For all PAH analyses, the mass spectrometer was operated using electron impact ionization.

GC/MS (Ia and Ib): For GC/MS (I) analyses, duplicate subsamples of 50 mg from six bottles of SRM 1650b were mixed with Hydromatrix (Isco, Lincoln, NE) and extracted with toluene using PFE at 100 °C and 13.8 MPa as described by Schantz et al. [7]. The extracts were concentrated to about 0.5 mL, solvent exchanged to hexane, placed on an aminopropylsilane SPE cartridge, and eluted with 20 mL of 2 % DCM in hexane (volume fraction). The eluant was concentrated and then analyzed by using GC/MS with a 0.25 mm i.d. × 60 m fused silica capillary column with a relatively nonpolar phase (0.25 µm film thickness; DB-XLB, J&W Scientific, Folsom, CA) and these results are denoted as GC/MS (Ia). Concentrated eluants were also analyzed on a 50 % phenyl-substituted methylpolysiloxane stationary phase (0.25 mm i.d. × 60 m, 0.25 µm film thickness; DB-17MS, J&W Scientific), and these results are designated as GC/MS (Ib).

GC/MS (IIa and IIb): For the GC/MS (IIa and IIb) analyses, 50 mg samples from six bottles of SRM 1650b were extracted with toluene using PFE at 200 °C and 13.8 MPa. The extracts were processed and analyzed as described above for GC/MS (Ia) and GC/MS (Ib) and the results are designated GC/MS (IIa) and GC/MS (IIb), respectively.

GC/MS (IIIa and IIIb): For GC/MS (IIIa and IIIb) analyses, subsamples of 50 mg to 100 mg from six bottles of SRM 1650b were mixed with clean sodium sulfate and extracted with DCM using PFE at 100 °C and 13.8 MPa. The extracts were processed as described above for GC/MS (Ia and Ib) and then analyzed by using GC/MS on fused silica capillary columns with a 50 % phenyl-substituted methylpolysiloxane stationary phase (0.25 mm i.d. × 60 m, 0.25 µm film thickness), designated as GC/MS (IIIa), and on a dimethyl 50 % polysiloxane liquid crystalline stationary phase (0.25 mm i.d. × 15 m, 0.25 µm film thickness; LC-50, J&K Environmental, Milton, Ontario, Canada), designated as GC/MS (IIIb).

GC/MS (IVa and IVb): For GC/MS (IVa and IVb) analyses, subsamples of 50 mg to 100 mg from six bottles of SRM 1650b were extracted with DCM using PFE at 200 °C and 13.8 MPa. The extracts were processed and analyzed by using GC/MS on the two columns as described above for GC/MS (IIIa and IIIb).

GC/MS (Va and Vb) and GC/MS (VIa and VIb): Additional extractions and analyses were performed in the same manner as for GC/MS (IIIa and IIIb) and GC/MS (IVa and IVb) to obtain concentrations for selected methylated PAHs. These data sets are designated as GC/MS (Va and Vb) and GC/MS (VIa and VIb).

GC/MS (VII): For the relative molecular mass (M_r) 276 and higher PAHs, additional extractions and analyses were performed in a similar manner as for GC/MS (Ib) except that the PAHs of interest were eluted from the aminopropylsilane SPE cartridge using 40 mL of 10 % DCM in hexane (volume fraction). These data are designated as GC/MS (VII).

GC/MS (VIIIa through VIIId): The effect of increasing the temperature and pressure used for PFE on the extraction efficiency for PAHs was evaluated. The solvent used was toluene, although a 9:1 toluene:methanol (volume fraction) was also evaluated. The PFE conditions used included: 100 °C with 13.8 MPa; 100 °C with 20.7 MPa; 200 °C with 13.8 MPa; and 200 °C with 20.7 MPa, methods GC/MS (VIIIa) through GC/MS (VIIId), respectively. Following an SPE step similar to that of method I above, the processed extracts were analyzed using a non-polar, extra-low bleed phase (0.25 mm i.d. × 60 m, 0.25 µm film thickness).

GC/MS Internal Standards: For all GC/MS measurements described above, except GC/MS (VIa and VIb), selected perdeuterated PAHs were added to the diesel particulate matter prior to extraction for use as internal standards for quantification purposes. For GC/MS (VIa and VIb), fluorinated PAHs were added to the diesel particulate matter prior to extraction for use as internal standards for quantification purposes.

GC/MS (Environment Canada): For PAH measurements at Environment Canada, subsamples of approximately 10 mg from each of four bottles of SRM 1650b were extracted with DCM or hexane/acetone (1:1 volume fraction) using microwave-assisted extraction at 100 °C for 20 min. The extract was filtered through sodium sulfate and concentrated to a few milliliters by rotary evaporation, solvent exchanged to cyclohexane, and then divided into two portions; one portion was processed for PAH measurements and the other portion was processed for nitro-PAH measurements (see below). The PAH fraction was isolated from the extract by using open-column chromatography on silica, with hexane followed by benzene as the mobile phase. The PAH fraction was then analyzed by using GC/MS on a DB-XLB column (0.25 mm i.d. × 30 m, 0.25 µm film thickness). Selected perdeuterated PAHs were added to the diesel particulate matter prior to extraction for use as internal standards for quantification purposes.

PAH Isomers of Relative Molecular Mass (M_r) *302*: For the determination of the relative molecular mass (M_r) 302 isomers, the method used was similar to that described by Schubert et al. [8]. Two sets of samples (one set of three subsamples and one set of six subsamples) of approximately 50 mg each were extracted using PFE at 100 °C and 13.8 MPa with DCM. The extracts were then concentrated, solvent exchanged to hexane, passed through an aminopropylsilane SPE cartridge, and eluted with 40 mL of 10 % DCM in hexane (volume fraction). The processed extract was then analyzed by GC/MS using a 0.25 mm i.d. × 60 m fused silica capillary column with a 50 % phenyl-substituted methylpolysiloxane phase (0.25 µm film thickness; DB-17MS). Perdeuterated dibenzo[*a,i*]pyrene was added to the diesel particulate matter, prior to extraction, for use as an internal standard.

Homogeneity Assessment for PAHs: The homogeneity of SRM 1650b was assessed by analyzing duplicate samples of 50 mg from six bottles selected by stratified random sampling. Samples were processed and analyzed as described above for GC/MS (I). No statistically significant differences among bottles were observed for the PAHs at the 50 mg sample size. The relative homogeneity of trace levels of PAHs in SRM 1650b in the milligram sampling range was also evaluated. The subsampling contribution to the overall uncertainty varies with PAH considered. Using pyrene as an example, the subsampling error for a 10 mg sample size of SRM 1650b is 2 %, while the subsampling error for a 50 mg sample of SRM 1650b is 0.9 %. A more extensive evaluation of the homogeneity of SRM 1650b, at small sample sizes for PAHs, is described in reference 6.

Nitro-Substituted Polycyclic Aromatic Hydrocarbons (Nitro-PAHs)

SRM 1650b was analyzed at NIST and Environment Canada for the determination of nitro-PAHs. The general procedure for determination of nitro-PAHs at NIST utilizes GC with negative ion chemical ionization mass spectrometry (GC/NICI-MS) [9,10] and high-resolution mass spectrometry using negative chemical ionization (GC/NCI-HRMS). Mass fraction values for nitro-PAHs are provided in Tables 2 and 5.

GC/NICI-MS (I): Subsamples of approximately 50 mg from each of six bottles of SRM 1650b were mixed with Hydromatrix (Isco, Lincoln, NE) and extracted with DCM using PFE at 100 °C and 13.8 MPa. The extracts were concentrated to about 0.5 mL, solvent exchanged to hexane, placed on an aminopropylsilane SPE cartridge, and eluted with 40 mL of 20 % DCM in hexane (volume fraction). To isolate the nitro-PAH fraction, the concentrated eluant was analyzed by normal-phase liquid chromatography (LC) using a semi-preparative amino/cyano phase

column with a mobile phase of 20 % DCM in hexane [10]. The nitro-PAH fraction was analyzed by GC with GC/NICI-MS using a 0.25 mm i.d. × 30 m fused silica capillary column containing a 50 % phenyl-substituted methylpolysiloxane stationary phase (0.25 µm film thickness), and the results are designated as GC/NICI-MS (I).

GC/NICI-MS (II): A second set of four subsamples of SRM 1650b was processed and analyzed at a different time using the same procedures described above and the results are denoted as GC/NICI-MS (II).

GC/NICI-MS (IIIa through IIId): The effect of increasing the temperature and pressure used for PFE on the extraction efficiency for nitro-PAHs was evaluated. The solvent used was toluene, although a 9:1 toluene:methanol (volume fraction) was also evaluated. The PFE conditions used included: 100 °C with 13.8 MPa; 100 °C with 20.7 MPa; 200 °C with 13.8 MPa; and 200 °C with 20.7 MPa [methods GC/NICI-MS (IIIa) through GC/NICI-MS (IIId), respectively]. Following an SPE step similar to that of method I above, the processed extracts were analyzed using a non-polar, extra-low bleed proprietary phase (0.25 mm i.d. × 60 m, 0.25 µm film thickness).

GC/NCI-HRMS: For the Environment Canada measurements of nitro-PAHs, five subsamples of SRM 1650b were extracted as described above for PAH measurements. The second portion of the extract was taken to dryness and then redissolved in 1 mL of dimethyl sulfoxide (DMSO). The nitro-PAH fraction was isolated by using a liquid-liquid partition scheme involving hexane extraction of the DMSO to remove aliphatic hydrocarbons, followed by dilution of the DMSO with water and extraction of the polar fraction into cyclohexane. The nitro-PAHs were then isolated by using normal-phase LC on a silica column with a solvent gradient from 5 % DCM in hexane (volume fraction) to 100 % DCM. The nitro-PAH fraction was collected from 60 % DCM in hexane to 100 % DCM, concentrated, and analyzed by using GC on a 30 m 5 % phenyl-substituted methylpolysiloxane column (0.25 mm i.d., 0.25 µm film thickness) with detection by high-resolution mass spectrometry using negative chemical ionization (GC/NCI-HRMS).

GC/NICI-MS and GC/NCI-HRMS Internal Standards: For the GC/NICI-MS and GC/NCI-HRMS measurements described above, perdeuterated nitro-PAHs were added to the diesel particulate matter, prior to extraction, for use as internal standards for quantification purposes.

Value Assignment for PAHs and Nitro-PAHs

The value assignment of PAHs and nitro-PAHs in SRM 1650b is based on the measurements used when SRM 1650b was issued in 2003 and on recent additional measurements using different extraction temperatures. Recent studies on the extraction of PAHs and nitro-PAHs from diesel particulate matter [11–13] have shown that using PFE at 200 °C removes higher quantities of some PAHs and nitro-PAHs than using PFE at 100 °C. As a result of these studies, value assignment for specific PAHs and nitro-PAHs in SRM 1650b is based on measurements using PFE at both 100 °C and 200 °C. In cases where the quantities of the individual PAHs and nitro-PAHs do not change with the PFE temperature, the measurements were combined and the resulting values are denoted as certified values and non-certified values in Tables 1 and 2, respectively. When different results are obtained at 100 °C and 200 °C, the values are reported for both temperatures, and they are denoted as non-certified values in Tables 3 and 5. These non-certified values should be considered "method dependent" values, because they are dependent on the extraction method and temperature.

Percent Extractable Mass

For the determination of percent extractable mass, six subsamples of approximately 200 mg were extracted using Soxhlet extraction for 18 h with DCM. The extract was concentrated to approximately 20 mL and then filtered to remove particulate matter. Aliquots of 100 µL to 150 µL were placed in tared aluminum foil pans; the DCM was evaporated until constant mass was obtained, and then the mass of the residue remaining was determined. The percent extractable mass non-certified value for SRM 1650a is applicable to SRM 1650b and provided in Table 6.

Particle Size Information, Specific Surface Area, and Porosity

Particle-size distribution measurements for SRM 1650b were carried out using a laser diffraction instrument (Mastersizer 2000, Malvern Instruments, Southborough, MA) set at a refractive index of 1.5 and absorption index of 0.1 and the liquid suspension method with the instrument manufacturer's small volume sample dispersion unit (Hydro 2000 SM). A suspension of 0.1 % (mass fraction) of SRM 1650b in distilled water with 0.001 % Triton (volume fraction) was prepared by ultra-sonication for 1 h and 24 h. After the recording of the background, a

portion of the suspension was added to the measurement cell to achieve an obscuration of 5 %. Three passes of the sample solution were recorded and averaged. Results were calculated using the General Purpose Model provided by the instrument manufacturer; the results obtained for the two sonication periods are shown in Figure 1. The diesel particulate matter, as-received, does not have a stable particle size because of agglomeration which is evident, as the particle-size distribution for SRM 1650b measured after the 1 h sonication period did not show a typical profile for a material from a combustion process. The subsequent 24 h sonication broke up most agglomerates, and the size distribution shows a profile typical for combustion engine emissions (see Table 7).

The specific surface area and porosity were determined based on N_2 gas adsorption measurements [14]. The gas adsorption measurements were performed on a NOVA-1200 instrument (Quantachrome Corp., Boynton Beach, FL) at 77 K after the samples were outgassed for 24 h at 120 °C under vacuum. The N_2 isotherms were analyzed using the Brunauer-Emmet-Teller (BET) equation [15] to obtain the surface area (Table 7) and the Barrett-Joyner-Halenda (BJH) method [16] to obtain the porosity. Based on the BJH method, SRM 1650b shows a wide distribution of mesopores, but with substantial outer area. The pore diameter of the particles in SRM 1650b ranges from 4 nm to 45 nm with a mean at about 25 nm.

Supplemental Information for SRM 1650b

Because SRM 1650, SRM 1650a, and SRM 1650b were all prepared from the same bulk diesel particulate matter, some measurements reported for the previous two materials have not been duplicated for SRM 1650b and the previous results are transferable to the current SRM 1650b. In addition, because SRM 1650 and SRM 1650a have been available since 1985, a considerable amount of information on the characterization of these materials has been published. A summary of some of the studies reporting characterization of this diesel particulate matter SRM is provided in Poster et al [3,4]. A description of the mutagenicity assay is provided below as supplemental information for SRM 1650b.

Mutagenicity Activity: Non-certified values for the mutagenic activity of a dichloromethane extract of SRM 1650 were determined as part of an international collaborative study in 1989 sponsored by the International Programme on Chemical Safety (IPCS) and supported and technically coordinated by the U.S. Environmental Protection Agency's (EPA) Office of Health Research. Twenty laboratories from North America, Europe, and Japan participated in the study for which a complete summary has been published [17,18]. Mutagenicity data were provided by J. Lewtas and L.D. Claxton of the National Health and Environmental Effects Research Laboratory, U.S. EPA (Research
Triangle Park, NC).

Table 1. Certified Mass Fraction Values for PAHs in SRM 1650b

PAH	Mass Fraction[(a)] (mg/kg)					
Phenanthrene[(b,c,d,e,f,g,h,i,j,k)]	65.6	±	3.6	1-Methylphenanthrene[(b,c,d,e,k,l,m)]	32.1	± 1.4
2-Methylphenanthrene[(b,c,d,e,k,l,m)]	72.3	±	1.2			
3-Methylphenanthrene[(b,c,d,e,k,l,m)]	56.7	±	1.9			
9-Methylphenanthrene[(b,c,d,e,k,l,m)]	36.6	±	1.6			
Fluoranthene[(b,c,d,e,f,g,h,i,j,k)]	48.1	±	1.1[(n)]			
Pyrene[(b,c,d,e,f,g,h,i,j,k)]	44.1	±	1.2			
Benzo[*ghi*]fluoranthene[(c,e,f,g,h,i,j,k)]	11.1	±	0.7			
Benzo[*c*]phenanthrene[(b,c,d,e,f,g,h,i,k)]	2.65	±	0.24	Benz[*a*]anthracene[(b,c,d,e,f,g,h,i,j,k)]	6.45	± 0.39
Chrysene[(b,d,g,o)]	13.4	±	0.6			
Triphenylene[(b,d,g,o)]	9.49	±	0.63			
Benzo[*a*]fluoranthene[(b,c,d,e,f,h,k)]	0.384	±	0.023			
Benzo[*b*]fluoranthene[(c,e,f,g,h,i)]	6.77	±	0.92			
Benzo[*j*]fluoranthene[(c,e,f,h)]	3.24	±	0.50[(n)]			
Benzo[*k*]fluoranthene[(b,c,d,e,f,g,h,i,j,k)]	2.30	±	0.18[(n)]			
Benzo[*e*]pyrene[(b,c,d,e,f,g,h,i,j,k)]	6.36	±	0.37	Benzo[*a*]pyrene[(b,c,d,e,f,g,h,i,j,k)]	1.25	± 0.12

Perylene[c,d,e,k]		0.167 ± 0.019[n]	
Indeno[1,2,3-*cd*]pyrene[b,c,d,e,f,g,h,i,j,k,o]	4.48 ± 0.21	Benzo[*ghi*]perylene[b,c,d,e,f,g,h,i,j,k,o]	6.04 ± 0.30
Dibenz[*a,c*]anthracene[c,e,f,g,h,i]	0.439 ± 0.048	Dibenz[*a,h*]anthracene[c,e,g,i]	0.365 ± 0.082
Dibenz[*a,j*]anthracene[c,e,g,i]	0.387 ± 0.068[n]	Benzo[*b*]chrysene[b,c,d,e,f,g,h,i,k]	0.301 ± 0.019[n]
Picene[b,c,d,e,f,g,h,i,k]		0.506 ± 0.058[n]	

[a] The certified mass fraction values, unless otherwise footnoted, are weighted means of the mass fractions from multiple analytical methods [19]. The uncertainty listed with each value is an expanded uncertainty about the mean [19,20] with coverage factor, $k = 2$, calculated by combining within-method variances with a between-method variance [21] following the ISO/JCGM Guide [22,23].

[b] GC/MS (Ia) on a proprietary relatively nonpolar phase after PFE at 100 °C and 13.8 MPa with toluene.

[c] GC/MS (Ib) on 50 % phenyl-substituted methylpolysiloxane phase, same extract as GC/MS (Ia).

[d] GC/MS (IIa) on a proprietary relatively nonpolar phase after PFE at 200 °C and 13.8 MPa with toluene.

[e] GC/MS (IIb) on 50 % phenyl-substituted methylpolysiloxane phase same extract as GC/MS (IIa).

[f] GC/MS (IIIa) on 50 % phenyl-substituted methylpolysiloxane phase after PFE at 100 °C and 13.8 MPa with DCM.

[g] GC/MS (IIIb) on dimethyl 50 % polysiloxane liquid crystalline stationary phase with same extract as GC/MS (IIIa).

[h] GC/MS (IVa) on 50 % phenyl-substituted methylpolysiloxane phase after PFE at 200 °C and 13.8 MPa with DCM.

[i] GC/MS (IVb) on dimethyl 50 % polysiloxane liquid crystalline stationary phase with same extract as GC/MS (IVa).

[j] GC/MS (Environment Canada) on a proprietary relatively nonpolar phase.

[k] GC/MS (VIII) on non-polar extra low bleed proprietary phase after PFE with toluene at 100 °C with 13.8 MPa; 100 °C with
20.7 MPa; 200 °C with 13.8 MPa; and 200 °C with 20.7 MPa.

[l] GC/MS (Va) on 50 % phenyl-substituted methylpolysiloxane phase after PFE at 100 °C and 13.8 MPa with DCM.

[m] GC/MS (VIa) on 50 % phenyl-substituted methylpolysiloxane phase after PFE at 200 °C and 13.8 MPa with DCM.

[n] The certified value is a weighted mean of average mass fractions, with one average from each of two or more analytical methods [19,20]. The expanded uncertainty is the half width of a symmetric 95 % parametric bootstrap confidence interval [24] which is consistent with the ISO/JCGM Guide [22,23] with an effective coverage factor, *k*, equals 2.

[o] GC/MS (VII) on 50 % phenyl-substituted methylpolysiloxane phase after PFE at 100 °C with DCM.

Table 2. Non-Certified Mass Fraction Values for Nitro-PAHs in SRM 1650b

Nitro-PAH	Mass Fraction[a] (µg/kg)
9-Nitrophenanthrene[b,c,d,e]	539 ± 24
3-Nitrophenanthrene[b,c,e]	4250 ± 50[f]
2-Nitrofluoranthene[b,c,e]	217 ± 15
3-Nitrofluoranthene[b,c,e]	65.1 ± 1.1
1-Nitropyrene[b,c,e,g]	18400 ± 300
7-Nitrobenz[*a*]anthracene[b,c,e]	943 ± 22[f]
6-Nitrochrysene[b,c,e]	46.6 ± 1.1[f]

[a] The non-certified mass fraction values, unless otherwise footnoted, are weighted means of the mass fractions from multiple analytical methods [19]. The uncertainty listed with each value is an expanded uncertainty about the mean [19,20] with coverage factor, $k = 2$, calculated by combining within-method variances with a between-method variance [21] following the ISO/JCGM Guide [22,23].

[b] GC/NICI-MS (I) on 50 % phenyl-substituted methylpolysiloxane stationary phase.

[c] GC/NICI-MS (II) on 50 % phenyl-substituted methylpolysiloxane stationary phase.

[d] GC/NCI-HRMS on 5 % phenyl-substituted methylpolysiloxane stationary phase.

[e] GC/NICI-MS (III) on 50 % phenyl-substituted methylpolysiloxane phase after PFE with toluene at two temperatures and two pressures (100 °C with 13.8 MPa; 100 °C with 20.7 MPa; 200 °C with 13.8 MPa; and 200 °C with 20.7 MPa).

[f] The non-certified value is a weighted mean of average mass fractions, with one average from each of two or more analytical methods [19,20]. The expanded uncertainty is the half width of a symmetric 95 % parametric bootstrap confidence interval [24], which is consistent with the ISO/JCGM Guide [22,23] with an effective coverage factor, *k*, equals 2.

[g] Non-certified value for 1-nitropyrene confirmed original SRM 1650 certified value, which included measurements by two other independent techniques [2,25].

Table 3. Non-Certified Mass Fraction Values for PAHs in SRM 1650b Based on Extraction Method and Conditions

Extraction Conditions	Mass Fractions (mg/kg)[a]
PFE at temperatures between 100 °C and 200 °C	
1-Methylnaphthalene[b,c,d,e,f]	1.71 ± 0.26[g]
2-Methylnaphthalene[b,c,d,e,f]	3.71 ± 0.21
Acenaphthene[c,e,f,h]	0.233 ± 0.021
1,7-Dimethylphenanthrene[e,f,i,j]	17.2 ± 0.7
4H-Cyclopenta[*def*]phenanthrene[e,f]	3.35 ± 0.18
Cyclopenta[*def*]phenanthrone[k,l]	15.6 ± 0.8
Cyclopenta[*cd*]pyrene[b,h]	0.349 ± 0.068
1-Methylfluoranthene[e,f,i,j,m]	3.17 ± 0.11
3-Methylfluoranthene[e,f,i,j,m]	6.09 ± 0.83
1-Methylpyrene[e,f,i,j]	2.05 ± 0.14
3-Methylchrysene[e,f,i,j,n,o]	2.17 ± 0.10
6-Methylchrysene[e,f,i,j,n,o]	1.57 ± 0.04[g]
Coronene[e,f,p]	9.48 ± 0.28

Extraction Conditions	Mass Fractions (mg/kg)[a]
PFE at 100 °C	
Naphthalene[e,h,q]	5.16 ± 0.48[g]
Biphenyl[e,h,k,q]	0.965 ± 0.035
Acenaphthylene[c,e,q]	0.365 ± 0.019
Fluorene[e,h,k,q]	0.762 ± 0.029
Anthracene[e,h,k,q,r,s]	1.56 ± 0.20[g]
2-Methylanthracene[h,q]	0.60 ± 0.11
Dibenzothiophene[e,h,q]	9.54 ± 0.56
1,2-Dimethylphenanthrene[t]	6.3 ± 0.5
1,6-, 2,5-, and 2,9-Dimethylphenanthrene[t]	38 ± 3
1,8-Dimethylphenanthrene[t]	4.5 ± 0.5
2,6-Dimethylphenanthrene[t]	29 ± 2
2,7-Dimethylphenanthrene[t]	20 ± 2
3,6-Dimethylphenanthrene[t]	23 ± 2
8-Methylfluoranthene[i,j]	3.60 ± 0.12[g]
2-Methylpyrene[i,j,n,o]	5.8 ± 1.4
4-Methylpyrene[i,j,n]	5.14 ± 0.63
1-Methylchrysene[n,o]	1.46 ± 0.05
2-Methylchrysene[i,j,n,o]	2.50 ± 0.26[g]
1-Methylbenz[*a*]anthracene[o]	0.355 ± 0.010
2-Methylbenz[*a*]anthracene[i,j]	0.43 ± 0.19
6-Methylbenz[*a*]anthracene[o]	5.28 ± 0.17
9- and 3-Methylbenz[*a*]anthracene[i,j]	0.61 ± 0.17
11-Methylbenz[*a*]anthracene[i,j]	0.36 ± 0.15
PFE at 200 °C	
Naphthalene[f]	7.29 ± 0.38
Biphenyl[b,c,f,l]	3.47 ± 0.17

Acenaphthylene[b,c,d,f]	1.36 ± 0.04
Fluorene[b,c,d,f]	1.27 ± 0.04
Anthracene[b,c,d,f,m]	7.58 ± 0.35
2-Methylanthracene[b,c]	5.88 ± 0.46
Dibenzothiophene[f,l,m]	20.9 ± 1.5

[a] The non-certified values, unless otherwise footnoted, are weighted means of the mass fractions from multiple analytical methods [19]. The uncertainty listed is an expanded uncertainty about the mean [19,20], with coverage factor, k = 2, calculated by combining within-method variances with a between-method variance [21] following the ISO/JCGM Guide [22,23].

[b] GC/MS (IIa) on a proprietary relatively nonpolar phase after PFE at 200 °C and 13.8 MPa with toluene.

[c] GC/MS (IIb) on 50 % phenyl-substituted methylpolysiloxane phase same extract as GC/MS (IIa).

[d] GC/MS (IVa) on 50 % phenyl-substituted methylpolysiloxane phase after PFE at 200 °C and 13.8 MPa with DCM.

[e] GC/MS (VIII) on non-polar extra low bleed proprietary phase after PFE with toluene at 100 °C and two pressures (13.8 MPa and 20.7 MPa).

[f] GC/MS (VIII) on non-polar extra low bleed proprietary phase after PFE with toluene at 200 °C and two pressures (13.8 MPa and 20.7 MPa).

[g] The non-certified value is a weighted mean of average mass fractions, with one average from each of two or more analytical methods [19,20]. The expanded uncertainty is the half width of a symmetric 95 % parametric bootstrap confidence interval [24], which is consistent with the ISO/JCGM Guide [22,23]. The effective coverage factor, k, = 2.

[h] GC/MS (Ia) on a proprietary relatively nonpolar phase after PFE at 100 °C and 13.8 MPa with toluene.

[i] GC/MS (Va) on 50 % phenyl-substituted methylpolysiloxane phase after PFE at 100 °C with DCM.

[j] GC/MS (VIa) on 50 % phenyl-substituted methylpolysiloxane phase after PFE at 100 °C with DCM.

[k] GC/MS (IIIa) on 50 % phenyl-substituted methylpolysiloxane phase after PFE at 100 °C and 13.8 MPa with DCM.

[l] GC/MS (IVa) on 50 % phenyl-substituted methylpolysiloxane phase after PFE at 200 °C and 13.8 MPa with DCM.

[m] GC/MS (IVb) on dimethyl 50 % polysiloxane liquid crystalline stationary phase with same extract as GC/MS (IVa).

[n] GC/MS (VIb) on dimethyl 50 % polysiloxane liquid crystalline stationary phase with same extract as GC/MS (VIa).

[o] GC/MS (Vb) on dimethyl 50 % polysiloxane liquid crystalline stationary phase with same extract as GC/MS (Va).

[p] GC/MS (VII) on 50 % phenyl-substituted methylpolysiloxane phase after PFE at 100 °C with DCM.

[q] GC/MS (Ib) on 50 % phenyl-substituted methylpolysiloxane phase same extract as GC/MS (Ia).

[r] GC/MS (Environment Canada) on a proprietary relatively nonpolar phase.

[s] GC/MS (IIIb) on dimethyl 50 % polysiloxane liquid crystalline stationary phase with same extract as GC/MS (IIIa).

[t] Non-certified values based on GC/MS analyses on 5 % and/or 50 % phenyl-substituted methylpolysiloxane phase after PFE at

100 °C and 13.8 MPa with DCM from SRM 1650a.

Table 4. Non-Certified Mass Fraction Values for PAHs of Relative Molecular Mass 302 in SRM 1650b

PAH	Mass Fractions[a,b] (mg/kg)
Dibenzo[*b,e*]fluoranthene	0.375 ± 0.034
Naphtho[1,2-*b*]fluoranthene and Naphtho[2,3-*j*]fluoranthene	2.31 ± 0.21
Naphtho[1,2-*k*]fluoranthene	1.71 ± 0.17
Naphtho[2,3-*b*]fluoranthene	0.427 ± 0.048
Dibenzo[*b,k*]fluoranthene	1.68 ± 0.17
Dibenzo[*a,k*]fluoranthene	0.148 ± 0.009
Dibenzo[*j,l*]fluoranthene	1.31 ± 0.09
Dibenzo[*a,l*]pyrene	0.137 ± 0.024
Naphtho[2,3-*e*]pyrene	0.770 ± 0.073
Dibenzo[*a,e*]pyrene	1.13 ± 0.049
Naphtho[2,1-*a*]pyrene	0.818 ± 0.052
Dibenzo[*e,l*]pyrene	0.770 ± 0.095
Benzo[*b*]perylene	0.125 ± 0.013

[a] The non-certified values are weighted means of the mass fractions from multiple analytical methods [19]. The uncertainty listed with each value is an expanded uncertainty about the mean [19,20], with coverage factor, k = 2, calculated by combining within-method variances with a between-method variance [21] following the ISO/JCGM Guide [22,23].

[b] GC/MS on 50 % phenyl-substituted methylpolysiloxane phase after PFE at 100 °C and 13.8 MPa with DCM.

Table 5. Non-Certified Mass Fraction Values for Selected Nitro-PAHs in SRM 1650b Based on Extraction Method and Conditions

Extraction Conditions	Mass Fractions[a] (µg/kg)
PFE at temperatures between 100 °C and 200 °C	
1-Nitronaphthalene[b,c,d,e]	85.6 ± 1.1
2-Nitronaphthalene[b,c,d,e]	236 ± 5
2-Nitrobiphenyl[b,c,d,e]	16.1 ± 0.7[f]
3-Nitrobiphenyl[b,c,d,e]	57.3 ± 1.6
5-Nitroacenaphthene[b,c,d,e]	36.8 ± 0.6[f]
2-Nitrofluorene[b,c,d,e]	46.0 ± 1.5
PFE at 100 °C	
9-Nitroanthracene[b,c,d,g]	5940 ± 90[f]
4-Nitrophenanthrene[b,c]	152 ± 3
1-Nitrofluoranthene[b,c]	272 ± 4[f]
8-Nitrofluoranthene[b,c]	112 ± 6[f]
4-Nitropyrene[b,c]	137 ± 4[f]
6-Nitrobenzo[*a*]pyrene[b,c,g]	1420 ± 26[f]
3-Nitrobenzo[*e*]pyrene[b,c]	79.8 ± 6.7[f]
1,3-Dinitropyrene[b,c,g]	45.5 ± 1.6[f]
1,6-Dinitropyrene[b,c]	83.3 ± 2.3[f]
PFE at 200 °C	
9-Nitroanthracene[e]	6930 ± 210[f]

[a] The non-certified values, unless otherwise footnoted, are weighted means of the mass fractions from multiple analytical methods [19]. The listed uncertainty is an expanded uncertainty about the mean [19,20], with coverage factor, $k = 2$, calculated by combining within-method variances with a between-method variance [21] following the ISO/JCGM Guide [22,23].

[b] GC/NICI-MS (I) on 50 % phenyl-substituted methylpolysiloxane stationary phase.

[c] GC/NICI-MS (II) on 50 % phenyl-substituted methylpolysiloxane stationary phase.

[d] GC/NICI-MS (III) on 50 % phenyl-substituted methylpolysiloxane phase after PFE with toluene at 100 °C and two pressures (13.8 MPa and 20.7 MPa).

[e] GC/NICI-MS (III) on 50 % phenyl-substituted methylpolysiloxane phase after PFE with toluene at 200 °C and two pressures (13.8 MPa and 20.7 MPa).

[f] The non-certified value is a weighted mean of the average mass fractions, with one average from each of two or more analytical methods [19,20]. The expanded uncertainty is the half width of a symmetric 95 % parametric bootstrap confidence interval [24], which is consistent with the ISO/JCGM Guide [22,23] with an effective coverage factor, *k*, equals 2.

[g] GC/NCI-HRMS on 5 % phenyl-substituted methylpolysiloxane stationary phase.

Table 6. Non-Certified Value for Percent Extractable Mass for SRM 1650b[a]

	Mass Fractions[b] (%)
Percent Extractable Mass	20.2 ± 0.4

[a] Non-certified value for percent extractable mass reported for SRM 1650a is applicable to SRM 1650b.

[b] Non-certified value is the mean of results obtained using one analytical technique. The expanded uncertainty, U, is calculated as $U = ku_c$, where u_c is one standard deviation of the analyte mean, and the coverage factor, $k = 2$, is determined from the Student's *t*-distribution corresponding to the associated degrees of freedom and 95 % confidence level for each analyte.

Table 7. Non-Certified Values for Particle-Size Characteristics and Specific Surface Area for SRM 1650b[a]

Mean Particle Diameter, d(0.5)[b]	0.18 µm	
Particle Diameter, d(0.1)[c]	0.12 µm	
Particle Diameter, d(0.9)[d]	0.33 µm	
Volume Weighted Mean[e]	0.22 µm	
Specific Surface Area (S)[f]	108	m^2/g

[a] These values are provided for informational purposes only. The values have not been confirmed by an independent analytical technique as required for certification. See Figure 1 for particle-size distribution for SRM 1650b after 1 h and 24 h sonication.
[b] d(0.5) is the particle-size distribution parameter indicating the particle size below which 50 % of the volume is present.
[c] d(0.1) is the particle-size distribution parameter indicating the particle size below which 10 % of the volume is present.
[d] d(0.9) is the particle-size distribution parameter indicating the particle size below which 90 % of the volume is present.
[e] The volume weighted mean is the particle size in a uniform distribution.
[f] Specific surface area determined by multi-point N_2 gas adsorption BET equation [15].

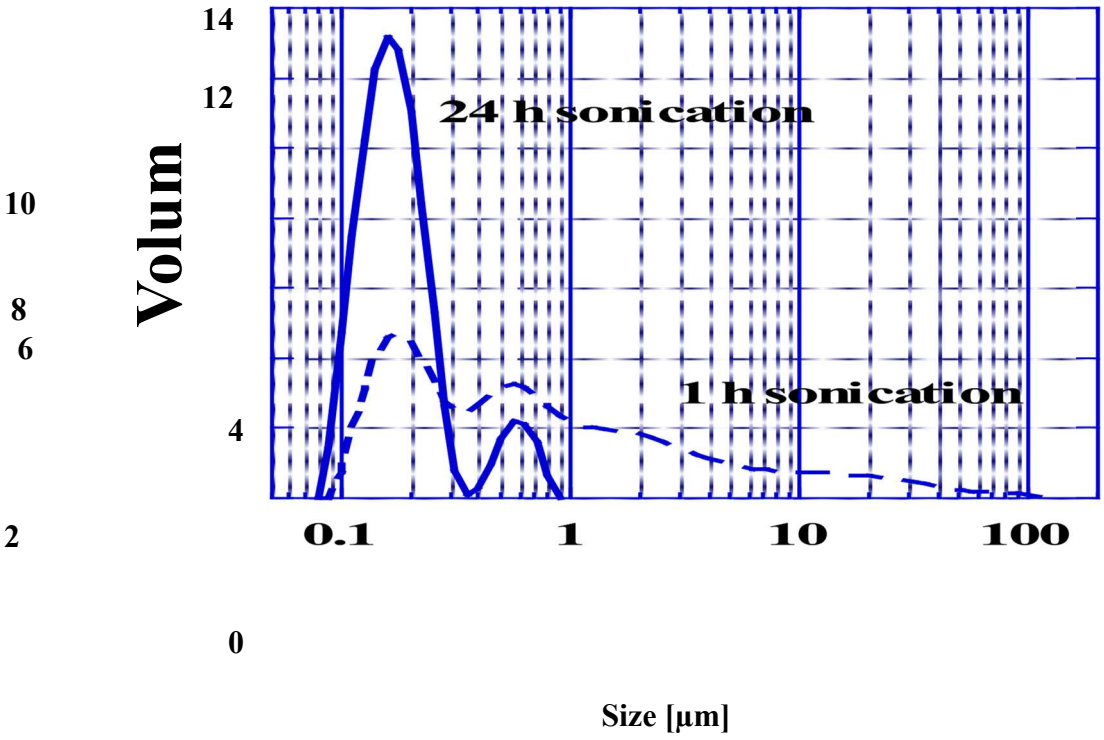

Figure 1. Particle-size distribution for SRM 1650b after 1 h and 24 h sonication.
See “Particle Size Information, Specific Surface Area, and Porosity” section for additional information.

REFERENCES

[1] SRM 1650; *Diesel Particulate Matter*; National Institute of Standards and Technology; U.S. Department of Commerce: Gaithersburg, MD (1985).

[2] SRM 1650a; *Diesel Particulate Matter*; National Institute of Standards and Technology; Department of Commerce: Gaithersburg, MD (2000).

[3] Poster, D.L.; Lopez de Alda, M.J.; Schantz, M.M.; Sander, L.C.; Vangel, M.G.; Wise, S.A.; *Development and Analysis of Three Diesel Particulate-Related Standard Reference Materials for the Determination of Chemical, Physical, and Biological Characteristics*; Polycyclic Aromat. Compd., Vol. 23, pp. 141–191 (2003).

[4] Poster, D.L.; Benner, B.A., Jr.; Schantz, M.M.; Sander, L.C.; Vangel, M.G.; Wise, S.A.; *Determination of Methyl-Substituted Polycyclic Aromatic Hydrocarbons in Diesel Particulate-Related Standard Reference Materials*; Polycyclic Aromat. Compd., Vol. 23, pp. 113–139 (2003).

[5] Beauchamp, C.R.; Camara, J.E.; Carney, J.; Choquette, S.J.; Cole, K.D.; DeRose, P.C.; Duewer, D.L.; Epstein, M.S.; Kline, M.C.; Lippa, K.A.; Lucon, E.; Phinney, K.W.; Polakoski, M.; Possolo, A.; Sharpless, K.E.; Sieber, J.R.; Toman, B.; Winchester, M.R.; Windover, D.; *Metrological Tools for the Reference Materials and Reference Instruments of the NIST Material Measurement Laboratory*; NIST Special Publication (NIST SP) 260-136, 2020 Edition; U.S. Government Printing Office: Washington, DC (2020); available at https://nvlpubs.nist.gov/nistpubs/SpecialPublications/NIST.SP.260-136-2020.pdf (accessed July 2021).

[6] Lippa, K.A.; Schantz, M.M.; *Microhomogeneity Evaluation of Polycyclic Aromatic Hydrocarbons in Particulate Standard Reference Materials*; Anal. Bioanal. Chem., Vol. 387, pp. 2389–2399 (2007).

[7] Schantz, M.M.; Nichols, J.J.; Wise, S.A.; *Evaluation of Pressurized Fluid Extraction for the Extraction of Environmental Matrix Reference Materials*; Anal. Chem., Vol. 69, pp. 4210–4219 (1997).

[8] Schubert, P.; Schantz, M.M.; Sander, L.C.; Wise, S.A.; *Determination of Polycyclic Aromatic Hydrocarbons with Molecular Mass 300 and 302 in Environmental-Matrix Standard Reference Materials by Gas Chromatography-Mass Spectrometry*; Anal. Chem., Vol. 75, pp. 234–246 (2003).

[9] Bezabeh, D.Z.; Bamford, H.A.; Schantz, M.M.; Wise, S.A.; *Determination of Nitrated Polycyclic Aromatic Hydrocarbons in Diesel Particulate-Related Standard Reference Materials by Using Gas Chromatography/Mass Spectrometry With Negative Ion Chemical Ionization*; Anal. Bioanal. Chem., Vol. 375, pp. 381–388 (2003).

[10] Bamford, H.A.; Bezabeh, D.Z.; Schantz, M.M.; Wise, S.A.; Baker, J.E.; *Determination and Comparison of Nitrated-Polycyclic Aromatic Hydrocarbons Measured in Air and Diesel Particulate Reference Materials*; Chemosphere, Vol. 50, pp. 575–587 (2003).

[11] Schantz, M.M.; McGaw, E.; Wise, S.A.; *Pressurized Liquid Extraction of Diesel and Air Particulate Standard Reference Materials: Effects of Extraction Temperature and Pressure*; Anal. Chem., Vol. 84, pp. 8222–8231 (2012).

[12] Bergvall, C.; Westerholm, R.; *Determination of 252–302 Da and Tentative Identification of 316–376 Da Polycyclic Aromatic Hydrocarbons in Standard Reference Materials 1649a Urban Dust and 1650b and 2975*

Diesel Particulate Matter by Accelerated Solvent Extration — HPLC-GC-MS; Anal. Bioanal. Chem., Vol. 391, pp. 2235–2248 (2008).

[13] Masala, S.; Ahmed, T.; Bergvall, C.; Westerholm, R.; *Improved Efficiency of Extraction of Polycyclic Aromatic Hydrocarbons (PAHs) from the National Institute of Standards and Technology (NIST) Standard Reference Material Diesel Particulate Matter (SRM 2975) using Accelerated Solvent Extraction*; Anal. Bioanal. Chem., Vol. 401, pp. 3305–3315 (2011).

[14] Gregg, S.J.; Sing, K.S.W.; *Adsorption, Surface Area and Porosity*; 2nd, Academic Press, London (1982).

[15] Brunauer, S.; Emmett, P.; Teller, E.; *Adsorption of Gases in Multimolecular Layers*; J. Am. Chem. Soc., Vol. 60, pp. 309–319 (1938).

[16] Barrett, E.P.; Joyner, L.G.; Halenda, P.P.; *The Determination of Pore Volume and Area Distributions in Porous Substances. I. Computations for Nitrogen Isotherms*; J. Am. Chem. Soc., Vol. 73, pp. 373–380 (1951).

[17] Lewtas, J.; Claxton, L.D.; Rosenkranz, H.S.; Schuetzle, D.; Shelby, M.; Matsushita, H.; Wurgler, F.E.; Zimmermann, F.K.; Lofroth, G.; May, W.E.; Krewski, D.; Matsushima, T.; Ohnishi, Y.; Gopalan, H.N.G.; Sarin, R.; Becking, G.C.; *Design and Implementation of a Collaborative Study of the Mutagenicity of Complex Mixtures in Salmonella typhimurium*; Mutat. Res., Vol. 276, pp. 3–9 (1992).

[18] Claxton, L.D.; Douglas, G.; Krewski, D.; Lewtas, J.; Matsushita, H.; Rosenkranz, H.; *Overview, Conclusions, and Recommendations of the IPCS Collaborative Study on Complex Mixtures*; Mutat. Res., Vol. 276, pp. 61–80 (1992).

[19] DerSimonian, R.; Laird, N.; *Meta-Analysis in Clinical Trials*; Control Clin. Trials, Vol. 7, pp. 177–188 (1986). [20] Rukhin, A.L.; *Weighted Means Statistics in Interlaboratory Studies*; Metrologia, Vol. 46, pp. 323–331 (2009). [21] Horn, R.D.; Horn, R.A.; Duncan, D.B.; *Estimating Heteroscedastic Variances in Linear Models*; J. Am. Stat. Assoc., Vol. 70, pp. 380–385 (1975).

[22] JCGM 100:2008; *Evaluation of Measurement Data — Guide to the Expression of Uncertainty in Measurement* (GUM 1995 with Minor Corrections); Joint Committee for Guides in Metrology (JCGM) (2008); available at https://www.bipm.org/en/publications/guides (accessed July 2021); see also Taylor, B.N.; Kuyatt, C.E.; *Guidelines for Evaluating and Expressing the Uncertainty of NIST Measurement Results*; NIST Technical Note 1297, U.S. Government Printing Office: Washington, DC (1994); available at https://www.nist.gov/pml/nist-technical-note-1297 (accessed July 2021).

[23] JCGM 101:2008; *Evaluation of Measurement Data — Supplement 1 to the "Guide to the Expression of Uncertainty in Measurement" — Propagation of Distributions using a Monte Carlo Method*; JCGM (2008); available at https://www.bipm.org/en/publications/guides (accessed July 2021).

[24] Efron, B.; Tibshirani, R.J.; *An Introduction to the Bootstrap*; Chapman & Hall: London, UK (1993).

[25] MacCrehan, W.A.; May, W.E.; Yang, S.D.; Benner, B.A., Jr.; *Determination of Nitro Polynuclear Aromatic Hydrocarbons in Air and Diesel Particulate Matter Using Liquid Chromatography with Electrochemical and Fluorescence Detection*; Anal. Chem., Vol. 60, pp. 194–199 (1988).

Certificate Revision History: 07 July 2021 (Change of expiration date; change of nitro-PAHs certified values to non-certified values due to incomplete stability testing from lack of appropriate calibrants; all other measurands previously labeled as reference or information values were converted to non-certified values; editorial changes); 17 July 2013 (Update certified and reference values for PAHs and nitro-PAHs to address the effect of temperature used for extraction; extension of certification period; editorial changes); 27 September 2006 (Original certificate date).